DISSERTATION

IDENTIFYING MOLECULAR TARGETS FROM HERBICIDE RESISTANCE PATHWAYS FOR CROP IMPROVEMENT

Submitted by

William B. Kramer

Department of Agricultural Biology

In partial fulfillment of the requirements

For the Degree of Doctor of Philosophy

Colorado State University

Fort Collins, Colorado

Spring 2026

Doctoral Committee:

Advisor: Todd A. Gaines

Franck E. Dayan
Esten Mason
Curtis Pozniak

ABSTRACT

IDENTIFYING MOLECULAR TARGETS FROM HERBICIDE RESISTANCE PATHWAYS FOR CROP IMPOVEMENT

Herbicide resistance in weeds represents one of the greatest threats to yield stability in agricultural systems. Identifying the molecular mechanisms underlying herbicide resistance pathways provides important insight into herbicide mode of action and offers opportunities to leverage this knowledge for crop improvement. The research presented integrates physiological, transcriptomic, biochemical, and heterologous validation approaches to identify and functionally validate genes associated with herbicide resistance with the goal of identifying gene targets that can be used to enhance crop performance.

First, variation in crop safety to the Group 1 ACCase inhibiting herbicide, quizalofop-P-ethyl (QPE), was investigated in CoAXium wheat (*Triticum aestivum*), where Crescent AX (Cres) consistently shows higher levels of QPE resistance compared to AP18 AX (AP18) despite both lines carrying ACCase target site mutations that should confer high levels of resistance to QPE. Reduced accumulation of QPE in Cres suggests a greater metabolic capacity compared to AP18. To understand these differences, the herbicide safener, cloquintocet-mexyl (CM), was used as a tool to induce the expression of genes associated with herbicide metabolism. RNA sequencing revealed a more robust induction of detoxification genes in Cres when treated with CM, specifically an enrichment of tau and phi class GSTs. Based on their homology to GSTs known to metabolize Group 1 herbicides in grass weeds, two candidate genes, *TaGSTF1* and *TaGSTU1*,

were selected for functional validation. Recombinant enzyme assays confirmed both GSTs conjugate quizalofop acid to form a glutathione conjugate, and Cres displayed consistently higher expression and catalytic activity. A 115 bp deletion in the *TaGSTU1* promoter unique to Cres provides a plausible cis regulatory basis for elevated transcription. These findings link the increased safety of the CoAXium system to specific metabolic pathways, positioning *TaGSTF1* and *TaGSTU1* as key candidates for marker-assisted selection and improved herbicide resistance in future CoAXium wheat breeding programs.

Second, the molecular basis of non target site resistance to the ALS inhibitor imazamox (IM) was resolved in a feral rye population lacking ALS target site mutations. RNA sequencing of segregating resistant and susceptible F2 plants identified two cytochrome P450 candidates, *CYP81A52* and *CYP72A1365*, based on constitutive and inducible expression patterns and homology to previously validated metabolic resistance genes. Functional validation in *Arabidopsis thaliana* confirmed that both candidate CYPs reduced IM accumulation and increased the O-demethylated metabolite, supporting a conserved detoxification pathway. Additional, yeast (*Saccharomyces cerevisiae*) expression assays further supported CYP mediated IM degradation further verifying the role of CYP activity in IM metabolism. These findings establish that both *CYP81A52* and *CYP72A1365* as a major driver of IM metabolism in feral rye.

Third, resistance to the synthetic auxin herbicide dicamba was translated across species by transferring a mutant *AUX/IAA16* allele from kochia (*Bassia scoparia*) into tobacco (*Nicotiana tabacum*). Comparative sequence and phylogenetic analyses supported conservation of key AUX/IAA and TIR1/AFB components required for receptor interaction. Transgenic tobacco overexpressing the kochia *AUX/IAA16* mutant allele exhibited significantly increased dicamba

resistance without obvious vegetative growth penalties. This demonstrates that disrupting auxin signaling at the degron-based co-receptor complex is sufficient to confer resistance in a heterologous crop background.

Together, this research demonstrates that herbicide resistance pathways in weeds uncover transferable molecular targets for crop improvement. By identifying GST mediated conjugation, CYP mediated metabolism, and auxin signaling components as targets, this work delivers validated candidates and molecular resources to support the development of enhanced herbicide metabolism and more resilient cropping systems.

ACKNOWLEDGMENTS

There are many individuals who deserve acknowledgment for their support and encouragement throughout this journey. Without their guidance and belief in me, I would not be writing this section of my dissertation.

I would like to start off with thanking my advisor, Dr. Todd Gaines, for agreeing to take me on as a student and for his continued mentorship. Your guidance has been invaluable, contributing significantly to both my scientific and personal growth. I am especially grateful for your ability to provide steady advice during challenging times; your ability for finding the positive in difficult results consistently made the research process feel less daunting and kept me motivated. I am deeply grateful for your support and mentorship, and I look forward to continuing to work with you in the future. I would also like to thank the rest of my committee members, Dr. Franck Dayam, Dr. Esten Mason, and Dr. Curtis Pozniak. Your direction and advice throughout my degree were important in my progress toward achieving my final goal.

I would like to thank my family for their continued encouragement throughout my educational journey. I am grateful for the time you have all spent being my hype team and reminding me that I can accomplish anything I set my mind to. I would not have made it to the end of this degree without your encouragement and acceptance of who I am. I am also thankful that you have always embraced my big and sometimes crazy ideas, whether that meant moving across the country, relocating to a neighboring country, or now moving across the world. I especially want to thank my mom, Bonnie, for everything she has done for me. Her constant strength in my life has inspired me to be a better person every day. To all my nieces and nephews, it means so much to have my very own cheerleading team that I can lean on when I need a laugh or a distraction

from grad school. I would also like to thank my Grandma Kramer for all of her kind words and positivity. I will always smile when I hear you proudly introducing me to strangers as 'a doctor', followed by my quick reminder that I am not a *medical* doctor, and that I should definitely not be consulted for medical advice.

I would like to thank my lab mates for their guidance throughout this experience. I began my PhD without a background in molecular biology or bioinformatics, which made for a steep learning curve, and I am grateful for the patience and generosity of those who helped me along the way. Dr. Jake Montgomery was quick to guide me through the RNA sequencing process and taught me a lot about bioinformatics, always taking the time to explain concepts clearly and thoughtfully. Dr. Crystal Sparks taught me a lot about molecular biology and was always willing to troubleshoot experiments, answer questions, and share her expertise, which greatly increased my confidence in the lab. Dr. Sarah Morran helped create a welcoming and positive lab environment that truly felt like a family, making even the most challenging days more enjoyable. Andre, Sofia, Amber, and Fatemeh, thank you for your camaraderie and willingness to serve as a sounding board for ideas that provided valuable insights to research questions. A special thanks to Catherine Traxler, who has become one of my best friends throughout this degree. Starting graduate school at the same time made this journey especially meaningful, as it gave me an incredible friend to lean on and learn from along the way. Through these shared experiences, you have taught me so much about myself, lessons that extend far beyond science and into what truly matters.

Finally, I would like to thank Colorado Wheat and the Sakata Family for their generous financial support. I would also like to acknowledge Dr. Corey Broeckling and the Analytical

Research Core for providing access to LC–MS instrumentation and for assistance with data acquisition and processing.

TABLE OF CONTENTS

CHAPTER I - CLOQUINTOCET-MEXYL ENHANCES GLUTATHIONE-S-TRANSFERASE MEDIATED HERBICIDE METABOLISM IN WINTER WHEAT

SUMMARY

Quizalofop-P-ethyl (QPE) resistant CoAXium™ wheat has improved chemical control options for winter annual grasses; however, variation in crop safety among wheat varieties have been reported, suggesting that factors beyond the ACCase target site mutation influence herbicide response. Field observations indicate that Crescent AX (Cres) exhibits consistently higher resistance to QPE compared to AP18 AX (AP18). As herbicide metabolism is a key determinant of crop selectivity, this study investigated whether differences in herbicide metabolic capacity underlie the differences in wheat variety response. Cloquintocet-mexyl (CM), a safener known to activate detoxification pathways, was used to evaluate metabolic differences among wheat genotypes through measurements of glutathione S-transferase (GST) activity, endogenous glutathione (GSH) pools, transcriptional induction, and in-vitro QPE metabolism. Cres retained less quizalofop acid (QZA) than AP18 following QPE treatment, indicating enhanced metabolic detoxification. CM further reduced QZA levels in all lines, but Cres showed an increased reduction and the strongest activation of safener-responsive genes. RNA-seq revealed extensive CM-induced transcriptional response, with Cres displaying higher basal expression and greater differential upregulation of GST genes. Two GST homologs, *TaGSTF1* and *TaGSTU1*, identified based on homology to Group 1 herbicide-metabolizing genes in grass weeds, were functionally validated. Recombinant enzyme assays confirmed both proteins conjugated QZA to form CQX-GSH, and Cres showed consistently higher expression and GST catalytic activity than AP18. A 115-bp deletion in the *TaGSTU1* promoter unique to Cres suggests a cis-regulatory basis for elevated transcription. Cres also maintained the highest endogenous GSH pools, supporting sustained

conjugation capacity under herbicide load. Together, these results demonstrate that observed enhanced resistance in Cres is linked to integrated metabolic advantages including elevated basal detoxification capacity, stronger safener induced gene activation, enhanced GST-mediated conjugation with GSH, and beneficial promoter architecture. This work identifies *TaGSTF1* and *TaGSTU1* as key metabolic candidates for Group 1 herbicide detoxification in wheat and provides molecular markers for future CoAXium wheat breeding programs.

INTRODUCTION

Common wheat (*Triticum aestivum L.)* is one of the world's most important cereal crops, providing approximately 20% of global dietary protein and calories (Shiferaw et al., 2013). Among the biotic stresses that threaten wheat production, weed competition is the most impactful, accounting for an estimated 45% of potential yield loss annually (Lehoczky and Reisinger, 2003), which surpasses losses caused by disease and insect pests. To mitigate these impacts, herbicide resistant cropping systems have been established to enhance efficacy of chemical weed management and minimize yield reductions associated with early-season weed crop competition. The CoAXium™ wheat system was introduced as an alternative to the Clearfield wheat (Newhouse et al., 1992), offering producers an additional mode of action for managing problematic winter annual grass weeds. CoAXium™ wheat was derived from a mutagenesis project that resulted in a target site mutation in the acetyl-CoA carboxylase (ACCase) gene resulting in resistance to the Group 1 herbicide quizalofop-P-ethyl (QPE) (Ostlie et al., 2015). Since its release, CoAXium™ wheat has been adopted across 2 million acres throughout the Western United States. However, as the system expands into new regions and environmental conditions, variability in QPE crop safety has been reported. The most pronounced differences occur among individual wheat varieties. Field observations indicate that some CoAXium lines,

such as AP18 AX (AP18), experience reduced crop safety and greater QPE-induced injury under certain environmental conditions, whereas other varieties, including Crescent AX (Cres), consistently maintain high levels of crop safety (Carnahan, 2020). The reported variation in QPE crop safety suggests that factors beyond the shared target-site mutation in the ACCase gene contribute to the overall herbicide response. Although the underlying basis for these differences remains unclear, variation in herbicide metabolic capacity may play a critical role in explaining the observed differences among varieties.

The addition of herbicide safeners provides a valuable tool for investigating differences in herbicide metabolism among wheat genotypes. More than twenty safeners have been successfully commercialized to mitigate herbicide toxicity in monocot crops such as corn, rice, sorghum, wheat, barley, and rye (Jia et al., 2022). In cereals, safeners such as cloquintocet-mexyl (CM) enhance crop safety to herbicides by activating pathways that are involved in herbicide metabolism. Various research studies have demonstrated that CM induces the transcription of genes involved in the three phases of herbicide metabolism (Landau et al., 2025; Riechers et al., 2010; Taylor et al., 2013). This includes induction of Phase I cytochrome P450 monooxygenases (CYPs), Phase II conjugating enzymes such as glutathione S-transferases (GSTs), and UDP-dependent glycosyltransferases (UGTs), and Phase III ATP-binding cassette (ABC) transporters responsible for vacuolar sequestration of conjugated metabolites (Gaines et al., 2020; Jugulam and Shyam, 2019; Rigon et al., 2020). Collectively, these enzymes function to facilitate herbicide oxidation, conjugation to endogenous molecules such as glutathione or sugars, and subsequent sequestration into the vacuole for further detoxification or compartmentalization (Brazier-Hicks et al., 2022; Rea, 2007). CM specifically, has been shown to upregulate members of the CYP and GST gene families, both of which are central contributors to metabolic or non-target site herbicide resistance

(NTSR) mechanisms (Délye, 2013; Zhao et al., 2023). The induction of these detoxification enzymes by CM highlights its critical role in enhancing herbicide metabolism to ACCase-inhibiting herbicides such as QPE. Despite the evidence that CM activates detoxification pathways in wheat, the specific genes directly responsible for safener induced metabolism of QPE remains unclear.

To address this knowledge gap, recent advancements in weed genomics (Montgomery et al., 2024; Montgomery et al., 2025a), have provided key insights into understanding the molecular basis of metabolic herbicide resistance. Previous studies have identified and functionally validated detoxification genes capable of metabolizing a wide range of herbicides (Abdollahi et al., 2021; Dimaano et al., 2020a; Goldberg-Cavalleri et al., 2025; Iwakami et al., 2019; Pan et al., 2022; Parcharidou et al., 2023; Yao et al., 2024), providing gene candidates to better understanding herbicide metabolism in crops. Leveraging these weed-evolved mechanisms offers a significant opportunity for crop improvement. Specifically, identifying the orthologous counterparts of known weed resistance genes within the wheat genome provides the framework for enhancing endogenous metabolic pathways to improve herbicide safety in wheat. To explore this possibility, previously characterized GST genes from grass weeds known to metabolize Group 1 herbicides were used as query sequences to identify functional orthologs within the wheat genome. A phi class GST (*PfGSTF2*) from *Polypogon fugax* and a phi class GST (*AmGSTF1*) from *Alopecurus myosuroides* were identified as reference genes of interest (Chen et al., 2025; Cummins et al., 2009; Cummins et al., 1999; Cummins et al., 2013). Using these validated GSTs provided the foundation for a comparative transcriptomic analysis aimed at identifying the metabolic variation between CoAXium™ wheat lines.

The first objective of this study was to investigate the molecular basis underlying the reported phenotypic differences in QPE resistance between the two CoAXium™ wheat lines AP18 and Cres, although both lines have ACCase target site mutations in two subgenomes (B&D in AP18; A&D in Cres). Byrd (Haley et al., 2012) was included as a susceptible control, as it carries no ACCase target-site mutation and is a parental line for both AP18 and Cres. To understand the mechanisms contributing to variations in safener response and herbicide resistance among each wheat genotype, three objectives were considered. First, whole plant transcriptional characterization to CM using RNA sequencing was utilized to identify safener induced genes, with particular emphasis on genes involved in herbicide metabolism. Second, examination of the glutathione (GSH) detoxification pathway, given its function in GST-mediated conjugation of QPE and related herbicides. This included quantifying GST induction at the transcriptional level using RNA seq, assessing total GST catalytic activity through whole-plant enzyme assays, and measuring endogenous GSH concentrations to determine whether baseline GSH availability differed among genotypes. Finally, the third objective was to leverage previously reported cases of GST mediated Group 1 herbicide metabolism (Chen et al., 2025; Cummins et al., 2013) in weed species and identify the closest wheat ortholog. These candidates were then utilized for functional validation through in vitro metabolism assays to determine whether they exhibit similar conjugation activity toward QPE and respond to CM. Together, these complementary approaches were designed to connect whole-plant responses, transcriptional activation, enzyme activity, and direct biochemical function to explain genotypic differences in QPE metabolism among two CoAXium™ wheat lines and the susceptible control.

MATERIALS AND METHODS

Plant materials, growth conditions, and chemical applications:

Three different winter wheat cultivars, Crescent AX (Cres) (PVP 201900409), AP18 AX (AP18) (PVP 2020000351), and Byrd (Haley et al., 2012), were sown directly in 3.8-cm by 3.8-cm by 5.8-cm pots containing LM-HP high porosity potting mix (Lambert, Rivière-Ouelle, QC, Canada). The pots were moved to a greenhouse and grown for two weeks under ambient temperature that was maintained within a range of 22–24 °C. Supplemental illumination from liquid halogen grow lights was used to sustain a 14 h light / 10 h dark photoperiod and relative humidity of ~75%. At the two-leaf stage (approximately two weeks after emergence), wheat plants were treated with one of the following: 0.25% (v/v) non-ionic surfactant (NIS) alone (untreated); 10 g ha^{-1} cloquintocet-mexyl with 0.25% (v/v) NIS (CM); 96 g ha^{-1} quizalofop with 0.25% (v/v) NIS (QPE); or 96 g ha^{-1} quizalofop plus 10 g ha^{-1} cloquintocet-mexyl with 0.25% (v/v) NIS (CM + QPE). Applications were made using a calibrated single-nozzle track sprayer (DeVries Manufacturing, Hollandale, MN) delivering 187 L ha^{-1} spray volume.

Liquid chromatography mass spectrometry analysis for quizalofop acid detection

For each treatment, three plants were grown per pot and pooled as one biological replicate; three biological replicates were used, and the entire experiment was repeated twice. Plants tissue sprayed with the above treatments were sampled 4 d after application and washed with 20% (v/v) of acetone for 1 min before being snap frozen in liquid nitrogen and stored in the -80ºC until further processing. Frozen tissue was ground in liquid nitrogen using a mortar and pestle. Ten ml of water and 10 ml of acetonitrile + 0.1% (v/v) formic acid was added to the ground tissue before homogenizing. Samples were shaken at room temperature for 20 min at 250 rpm and then centrifuged (Sorvall X1, with TX400 rotor, Thermo Scientific, Waltham, MA, USA) for 10 min at 3,800 x g. The supernatant was collected and cleaned with the addition of 1 package of

QuEChERS (1 g NACl and 4 g $MgSO_4$) (Phenomenex, Torrance, CA, USA), vortexed for 15 sec, and centrifuged for 10 min at 3,800 x g. The supernatant was collected and filtered through 13 mm by 0.2 µm nylon (Econofltr Nyln, Agilent Technologies, Santa Clara, CA, USA) and injected into the liquid chromatography-tandem mass spectrometry (LC-MS/MS) instrument. Quizalofop acid (QZA), the active hydrolyzed form of QPE, was measured per milligram of plant fresh weight, as it represents the bioactive structure that inhibits ACCase, the target enzyme responsible for fatty acid biosynthesis.

Quantification of QZA was performed using a Nexera X2 ultra-performance liquid chromatography system (Shimadzu, Kyoto, Japan). Chromatographic separation was achieved on a Phenomenex Kinetex C18 column (100 × 4.6 mm, 2.6 µm, 100 Å) maintained at 40 °C using a binary solvent system consisting of (A) water with 0.1% (v/v) formic acid and (B) acetonitrile with 0.1% (v/v) formic acid. The flow rate was set to 0.40 mL min^{-1}. Mass spectrometric detection was performed in positive electrospray ionization (ESI^+) mode with a nebulizing gas (He) flow of 24 mL min^{-1} and a desolvation temperature of 250 °C. The interface temperature was maintained at 400 °C. Data were acquired in multiple reaction monitoring (MRM) mode with Q1, Q2, and Q3 pre-bias voltages of −24.0 V, −21.0 V, and −21.0 V, respectively. The monitored precursor ion was m/z 345.00, and the product ion was m/z 299.00. Average retention times were 5.8 min for QZA and 6.9 min for QPE. A 10 µL sample volume was injected for each sample, and compound quantification was performed using calibration curves established from authentic standards.

Whole plant GST protein expression and glutathione quantification

To assess the difference between whole plant GST enzyme activity and gene expression in each wheat cultivar, whole wheat plants were treated with the treatments listed above and sampled at 24 h after application. Whole plant GST extraction was performed according to the methods

described by Cummins et al 2002. Briefly, 3 g of whole leaf tissue was ground to a fine powder in liquid nitrogen using a mortar and pestle. The powder was suspended in 15 mL of extraction buffer (100 mM Tris-HCl (pH 7.5), 2 mM EDTA, 1 mM dithiothreitol (DDT) and 15 g L -1 of polyvinyl-polypyrrolidone (PVPP)). Samples were gently mixed, kept on ice for 5 min, then passed through two layers of filter paper. The filtrate was centrifuged (Sorvall X1, with TX400 rotor, Thermo Scientific, Waltham, MA, USA) at 5,000 x g for 30 min and the supernatant was adjusted to 80% ammonium sulfate saturation to precipitate proteins (4 °C, 2 h). The precipitated proteins were collected by centrifugation at 5,000 x g for 30 min, resuspended in 20 mM Tris-HCl (pH 7.5) containing 1 mM DTT and desalted using G-25 Sephadex columns (Cytiva, Wilmington, DE, USA). Protein concentration was determined using Bradford methods (Gotham et al., 1988).

Extracted proteins from each wheat line under all treatments were diluted to a consistent concentration. GST activity was measured using a Glutathione S-Transferase Assay Kit (Sigma-Aldrich, Inc, St. Louis, MO, USA) according to the manufacturer's instructions. The GST activity was expressed as nmol GSH-CDNB formed s -1 mg -1 sec -1 protein (Figure S1). Protein from untreated plants was also used to measure total GSH, including reduced GSH and oxidized (GSSG), levels using a Glutathione GSH/GSSG Assay Kit (Sigma-Aldrich, Inc, St. Louis, MO, USA) according to the manufacturer's instructions. Glutathione levels were expressed as µM total GSH (GSH total).

RNA sequencing and candidate GST gene selection

Three biological replicates of tissue from each wheat line treated with CM were sampled 12 h after application, ground in liquid nitrogen using a mortar and pestle, and total RNA was extracted using the Direct-zol™ RNA Miniprep Kit (Zymo Research, Irvine, CA, USA) according to the manufacturer's instructions. RNA quality and concertation was assessed using an Invitrogen

Qubit Fluorometer (Thermo Scientific, Waltham, MA, USA). Total RNA was then used to generate paired-end cDNA Illumina libraries (Novogene, Sacramento, CA, USA). Novogene performed RNA-sequencing library preparation using standard protocols, generating approximately 20 million paired-end reads (150 bp per read) per sample on an Illumina sequencing platform. Processed sequencing data were returned as FASTQ files for downstream bioinformatic analysis. Raw sequence reads in FASTQ format were quality assessed using FastQC (Andrews et al., 2010). Low quality reads and adapters were removed using Trimmomatic (Bolger et al., 2014) with default settings. The resulting trimmed reads were aligned to the indexed *Triticum aestivum* reference genome IWGSC v2.1 (Zhu et al., 2021) using STAR v2.7.9a (Dobin et al., 2013). Alignment parameters were changed to enable two-pass mapping, produce coordinate-sort BAM files, and minimize ambiguity in multimapped reads. Such mapping parameters were selected to account for high potential for multimapping in the polypoid wheat genome, ensuring that reads that were uniquely mapped were retained. The resulting BAM files were processed using FeatureCounts v2.0.1 (Liao et al., 2013) to generate gene level count for further analysis in R (R Core Team, 2024) using the DESeq2 package (Love et al., 2014) with parameters set at Log2FC± 1 (L2FC) and adjusted p-value <0.1 Padj).

Protein-level gene annotation was performed using the UniProt Swiss-Prot protein database (Boutet et al., 2007). The Swiss-Prot FASTA file was downloaded from UniProt and used to generate a local BLAST protein database with the BLAST+ package v2.13.0. Predicted protein sequences from the wheat genome were reformatted to ensure compatibility with BLAST searches. BLASTp alignments were then conducted against the Swiss-Prot database using BLAST+ v2.13.0. Output files were filtered to retain only high-confidence matches based on bit score thresholds, with redundant hits removed. Unique UniProt gene identifiers from the filtered dataset were cross-

referenced with the UniProt ID mapping database (Pundir et al., 2017) to obtain gene names and functional descriptions, which were subsequently integrated into the RNA-seq differential expression analysis.

Genes were filtered based on differential expression analysis using adjusted L2FC± 1 and padj <0.1. The resulting gene set was cross-referenced with existing literature and functional annotations to identify a subset of genes with biochemical functions previously implicated in herbicide metabolism (Gaines et al., 2020; Nandula et al., 2019; Yu & Powles, 2014) (Table 1). Protein sequences for candidate gene selection were queried against the wheat reference genome using BLASTp (Mount, 2007), and the highest matching sequences were considered.

Validation of RNA sequencing analysis through quantitative PCR

Quantitative PCR (qPCR) was used to validate the expression of candidate GST genes identified from the RNA-seq analysis. Expression levels were assessed in wheat samples collected 12 h following the treatments listed above. Three biological replicates were sampled per treatment, and two independent experimental runs were analyzed. Total RNA was extracted from each sample, and first-strand cDNA synthesis was performed using the ProtoScript® First Strand cDNA Synthesis Kit (New England Biolabs, Ipswich, MA, USA) following the manufacturer's protocol. Subgenome-specific primers were manually designed in Geneious (Geneious 11.0.20.1) and synthesized by Integrated DNA Technologies (Owczarzy et al., 2008). Primer validation and efficiency determination were conducted according to the Bio-Rad Real-Time PCR Application Guide. qPCR reactions were performed using PerfeCTa® SYBR® Green FastMix® (Quantabio, Beverly, MA, USA) on a Bio-Rad CFX96™ Real-Time PCR Detection System (Bio-Rad, USA). The thermal cycling program consisted of an initial denaturation at 95 °C for 3 min, followed by 35 cycles of 95 °C for 10 s, 65 °C for 30 s, and 72 °C for 30 s, with a final melt curve analysis

from 65 °C to 95 °C in 0.5 °C increments held for 5 s each. Relative transcript abundance was calculated using the comparative $2^{-}\Delta Ct$ method (Livak and Schmittgen, 2001), with alpha-tubulin (TUB) (GeneBank accession number: U76558) and glyceraldehyde-3-phosphate dehydrogenase (GAPDH) (GeneBank accession number EF592180) (Dudziak et al., 2020) serving as the normalization genes.

Recombinant protein expression of GST candidates

The two candidate genes, *TaGSTF1 (TraesCS1A03G0193000)* and *TaGSTU1 (TraesCS6D03G0283500),* were selected for recombinant expression in *E. coli*. The coding sequence for both genes were synthesized and codon optimized (Azenta, Genewiz, South Plainfield, NJ, USA) for *E. coli* expression. Gene specific primers were designed (IDT, Owczarzy et al., 2008) to amplify each codon optimized gene sequence in the synthesized vectors (Table S1). Primers included sequence specific overhangs required for directional TOPO® cloning (Thermo Scientific, Waltham, MA, USA) into PET101/D-TOPO® vector with a C-terminal His-Tag. PCR amplification was performed using Phusion Green High-Fidelity Polymerase (New England Biolabs, Ipswich, MA, USA) (Table S1). PCR products were analyzed on a 1% (w/v) agarose gel and cut using a DNA Gel Extraction Kit (New England Biolabs, Ipswich, MA, USA). TOPO® cloning was performed according to the manufacturer's protocol (Champion™ pET Directional TOPO® Expression Kit). Ligated expression vectors were transformed into TOP10 Competent Cells (Thermo Scientific, Waltham, MA, USA) using heat shock methods (Chang et al., 2017) and cells were plated on LB agar plates containing ampicillin and incubated overnight at 37°C. PCR-positive colonies were grown in LB broth with ampicillin overnight at 37°C with shaking at 220 rpm. Plasmids were extracted using the ZymoPURE™ Plasmid Miniprep Kit (Zymo Research, Irvine, CA, USA) and sent for sequencing (Plasmidsaurus, Louisville, KY, USA) to confirm insert

identity and orientation. Successful plasmids were transformed into chemically competent *E. coli* BL21 cells using heat shock methods (Chang et al., 2017), plated on LB and ampicillin and single colonies were used to inoculate cultures for recombinant protein expression.

Protein expression was induced according to the manufacturer's protocol (Champion™ pET Directional TOPO® Expression Kit). Protein was purified under native conditions using QIAexpress® His-tag protein purification kit (QIAexpress Ni-NTA, Qiagen, Germantown, MD, USA). The purified proteins were concentrated using 10 kDa molecular weight ultrafiltration tubes (Sigma-Aldrich, Inc, St. Louis, MO, USA). Recombinant proteins were further quantified using Bradford methods (Gotham et al., 1988) and diluted in 50 mM PBS (pH 7.0). To confirm that the GST protein was active and in good condition, enzyme activity assays were performed using Glutathione S-Transferase Assay Kit (Sigma-Aldrich, Inc, St. Louis, MO, USA) (Supplemental Figure S1). Active candidate GST genes were used for downstream herbicide incubation studies.

***In vitro* quizalofop incubation and quizalofop metabolite detection**

After confirmation of GST activity, recombinant protein for each individual candidate gene were incubated with QZA to confirm metabolite formation using ultra-high-performance liquid chromatography with tandem mass spectrometry (UPLC-MS/MS) following a similar method described by Chen et al., 2025. Briefly, to identify QPE metabolites, recombinant protein of TaGSTF1 and TaGSTU1 were incubated in 30 µM QZA dissolved in 50 mM PBS (pH 7.0), 4 mM fresh GSH, and 5 ug of each protein in a final reaction volume of 200 µL. Four replicates of each sample include TaGSTF1, TaGSTU1, and an empty vector (EV) control were incubated at 37°C with 300 rpm of shaking for 0.5 h for one sample and 4 h for a second sample. Reactions were terminated by adding 200 µL of acetonitrile and then centrifuged at 10,000 x g for 10 min at 4°C.

The resulting supernatant was filtered through 0.22 filter paper and used for UPLC-MS/MS analysis.

UPLC-MS/MS analysis was performed on a Waters ACQUITY Classic UPLC coupled to a Waters Xevo G2-XS UPLC-MS Analysis: Aqueous Phase: Separation was achieved using an ACQUITY Premier HSS T3 column (1.7 µm, 2.1 x 100 mm), using a gradient with solvent A (Water, 0.1% formic acid) and solvent B (Acetonitrile, 0.1% formic acid). Injections were made in 1% B, held at 1% B for 1 minute, ramped 1-98% B over the next 12 minutes, then held at 98% B for 3 minutes, finally returned to starting conditions and allowed to re-equilibrate for 4 minutes, with a 0.5 mL/min constant flow rate. The column and sample compartments were held at 65°C and 6 °C, respectively. The column eluent was infused into a Waters Xevo G2-XS Q-TOF-MS with an electrospray source in positive ionization mode, scanning 50-1200 m/z at 0.1 seconds per scan, alternating between MS (6 V collision energy) and MSE mode (15-30 V ramp). Calibration was performed using sodium formate with 1 ppm mass accuracy. The capillary voltage was held at 2000 V, source temperature at 150°C, and nitrogen desolvation temperature at 600 °C with a flow rate of 1000 L/hr. Lockspray mass correction was performed every 1 min, with LeuEnk +556.2771 m/z as the calibrant.

Skyline (Adams et al., 2020) was used for data processing. Data was imported using the following transition settings for MS1: Isotope Peaks Included = 3, Precursor Mass Analyzer = Centroided, Mass Accuracy = 10 ppm. For MS/MS filtering: Acquisition Method = DIA, Product Mass Analyzer = Centroided, Mass Accuracy = 10 ppm. The following formulae were used for mass calculation. QZA (Quizalofop, C17H13ClN2O4) [M+H] = 345.0637 m/z. CQX (C8H5ClN2O) [M+H] = 181.0163 m/z. CQX-GSH (C18H20ClN5O6S) [M+H] = 470.0896 m/z.

The peak areas for the M, M+1 and M+2 ions of these species were summed for quantification (Figure S2)

Promoter sequence analysis

Genomic DNA was extracted from each wheat line using a standard CTAB-based protocol (Schenk et al., 2023). DNA quantity and quality were assessed using a Qubit Fluorometer (Thermo Fisher Scientific, Waltham, MA, USA) to ensure accurate input for downstream applications. The promoter region of *TaGSTU1* was amplified from purified genomic DNA using Q5 High-Fidelity DNA Polymerase (New England Biolabs, Ipswich, MA, USA). Primers were designed to amplify approximately 800 bp upstream of the start codon, with the reverse primer anchored within the coding sequence of the target gene (Table S2). PCR reactions were prepared according to the manufacturer's recommendations for Q5 polymerase, and thermal cycling conditions are provided (Table S2).

Amplification products were visualized by agarose gel electrophoresis, and bands corresponding to the expected amplicon size were excised and purified using the Monarch PCR DNA Cleanup Kit (New England Biolabs, Ipswich, MA, USA). Purified promoter fragments were submitted for sequencing (Plasmidsaurus, Louisville, KY, USA) to confirm sequence identity and to compare promoter variation across wheat lines. Resulting sequences were aligned and analyzed using Geneious (Geneious 11.0.20.1).

Statistical analysis

All statistical analyses were conducted in R (v4.3.2). Data were examined for normality and homogeneity of variance prior to analysis, and significance was determined at $p < 0.05$. For all experiments, data were summarized as mean ± standard error (SE), and treatment means were compared using analysis of variance (ANOVA). Two-way ANOVAs were used when both wheat

line and treatment were included as fixed factors. When significant main or interaction effects were detected, means were separated using Tukey's Honest Significant Difference (HSD) test. Compact letter displays were generated from post-hoc comparisons using the *multcomp* and *emmeans* packages to indicate statistically distinct groups.

For RNA-seq analysis, differential expression was evaluated using the DESeq2 package (Love et al., 2014). Raw count data were normalized using the median-of-ratios approach implemented in *DESeq2*, in which a virtual reference sample is generated by calculating the geometric mean of counts across all samples for each gene (Anders and Huber, 2010). Genes with fewer than 10 total reads were excluded from further analysis. Log_2fold changes were estimated using the Wald test, and shrinkage of effect sizes was applied using the lfcShrink (Zhu et al., 2018) function to improve stability and interpretability for low-abundance genes. Adjusted P-values were calculated using the Benjamini–Hochberg false discovery rate correction (Benjamini and Hochberg, 1995), with significance defined as an adjusted P value (Padj) < 0.1 and an absolute log_2fold-change ≥ 1 (L2FC). Volcano plots were generated from the normalized data to visualize transcriptional responses, where log_2fold-change and $-log_{10}$ (adjusted P-value) were plotted to highlight genes exhibiting both statistical significance and biological relevance.

RESULTS

Differential quizalofop-p-ethyl metabolism among wheat lines

Quantification of QZA was performed to assess herbicide metabolism in each wheat line 4 d after application of QPE alone or in combination with the safener (QPE + CM), at a time point previously identified as showing the greatest divergence between treatments (Pelon, 2024). Across all wheat lines, there are various differences in QZA accumulation among treatments (Figure 1).

When treated with a common field rate of QPE alone (96.3 g ha -1), AP18 accumulates the highest level of QZA, followed by Cres, and Byrd at (Figure 1A) and these differences were statistically significant ($P < 0.05$). When CM was combined with QPE there was a greater reduction in QZA accumulation in Byrd and Cres compared to AP18 ($P < 0.05$). This corresponds to a 9.0-fold reduction in Byrd, 3.9-fold reduction in AP18, and 6.5-fold reduction in Cres relative to their respective QPE only treatments. The reduction in QZA levels under QPE alone treatments observed in Cres indicate that this wheat line has a greater capacity to metabolize QPE compared to AP18. This enhanced metabolic activity is consistent with the reduced visual herbicide injury observed in Cres under field conditions. The addition of the CM further decreased QZA accumulation, resulting a minor observable herbicide injury phenotype across all lines compared to QPE alone treatments Figure (Figure 1B). This outcome aligns with the increased reduction in QZA levels detected under QPE + CM treatments. Although all genotypes exhibited decreased QZA content in the presence of CM, Cres demonstrated a more pronounced reduction compared to AP18.

Whole plant GST enzyme activity in response to quizalofop and cloquintocet-mexyl

GST activity varied greatly among wheat lines and treatments (Figure 2). Under untreated conditions, all wheat lines exhibited comparable baseline enzymatic activity (2.86 μmol min $^{-1}$ mg $^{-1}$ protein Byrd, 2.88 μmol min $^{-1}$ mg $^{-1}$ protein in AP18, and 3.32 μmol min $^{-1}$ mg $^{-1}$ protein in Cres). Applications of QPE and CM alone increased GST activity relative to untreated plants, whereas the combined QPE + CM treatment produced the highest level of GST activity.

In the sensitive parental line, Byrd (Figure 2A), GST activity increased moderately following herbicide (3.06 μmol min $^{-1}$ mg $^{-1}$ protein) and CM (3.21 μmol min $^{-1}$ mg $^{-1}$ protein)

applications. The highest response was observed in the combined QPE + CM treatment (5.04 µmol min $^{-1}$ mg $^{-1}$ protein) showing approximately 1.8-fold increase compared to the untreated control.

AP18 (Figure 2B) displayed a similar trend in GST activity across treatments compared to Byrd. The untreated samples increased from 2.88 µmol min $^{-1}$ mg $^{-1}$ protein to 5.49 µmol min $^{-1}$ mg $^{-1}$ protein under the QPE + CM, representing approximately a 1.9-fold increase. Although GST activity in AP18 was increased in all treatments, mean values did not differ statistically from those observed in Byrd. Applications of CM alone (4.69 µmol min $^{-1}$ mg $^{-1}$ protein) and QPE alone (3.62 µmol min $^{-1}$ mg $^{-1}$ protein) also produced a moderate increase in activity relative to Byrd, indicating a limited but measurable capacity to induce GST activity in response to both safener and herbicide applications.

By contrast, Cres (Figure 2C) exhibited the strongest induction of GST activity across all treatments. GST activity increased from 3.32 µmol min $^{-1}$ mg $^{-1}$ protein in untreated plants to 4.72 µmol min^{-1} mg^{-1} protein with QPE alone, 5.57 µmol min^{-1} mg^{-1} protein with CM alone and reached a maximum of 7.22 µmol min^{-1} mg^{-1} protein under the combined QPE + CM treatment. The QPE + CM treatment represented approximately a 2.2-fold increase relative to untreated Crescent plants. This level of activity was significantly greater ($p < 0.05$) than that observed in Byrd but not AP18 under the same treatment. Among the individual applications, CM alone and QPE alone produced the highest GST activity in Cres compared to the other lines, indicating a strong safener induced response in this wheat line.

Collectively, these results demonstrate that all three wheat lines responded to CM and QPE treatments with increased GST activity, but the magnitude of induction varied among genotypes. Cres exhibited the greatest inducibility of GST activity, whereas AP18 showed a weaker response, although not always statistically different.

Glutathione levels comparison among untreated wheat lines

Total GSH content was quantified across each wheat line to evaluate baseline differences. Mean GSH concentrations varied among each wheat genotype (Figure 3). Byrd exhibited the lowest glutathione level, 14.6 uM. AP18 showed a moderately higher level of 16.7 uM. Whereas Cres had the highest total glutathione concentration, 21.9 uM, approximately 1.5-fold higher than Byrd and 1.3-fold higher than AP18. The elevated basal GSH levels in Cres could contribute to improved stress tolerance and field performance following QPE applications.

Transcriptional response of wheat to cloquintocet-mexyl

Raw sequencing reads with removed adapters and low-quality bases from each wheat sample were used for downstream analyses. Quality metrics, including GC content and Q30 values indicated high-quality sequencing across all wheat samples, with an average Q30 value exceeding 92%. A total of approximately 20 million paired end reads were generated per wheat sample, of which 86-89% were successfully mapped to annotated gene features, indicating efficient alignment across all wheat lines. The remaining reads included approximately 10% that did not map to annotated genes and about 3% that were either unmapped or multi-mapped (Table S3).

The differential expression results from the RNA seq experiment revealed that a 10 g ha^{-1} application of CM induced clear transcriptional changes in all three wheat lines (Figure 4). The number of differentially expressed genes (DEGs) varied among wheat lines, indicating a line specific response to CM treatments. DEGs were defined as genes with a L2FC greater than 1 (upregulated) or less than -1 (downregulated) and an Padj of <0.1. In Byrd, 8,684 genes were significantly upregulated and 3,724 were downregulated (Figure 4A) following treatment. AP18 exhibited 6,114 upregulated and 2,667 downregulated genes (Figure 4B), while Cres showed 7,334 upregulated and 5,232 downregulated genes (Figure 4C). When comparing CM responsive DEGs

among the three wheat lines, Byrd exhibited 2,707 genes that were uniquely upregulated relative to AP18 and Cres. AP18 showed 1,045 specific inducible genes, while Cres displayed 2,044 unique CM responsive genes not detected in the other wheat lines (Figure 5). The gene cohorts uniquely upregulated in each wheat line highlight distinct, genotype-specific components of the CM-induced transcriptional response passed the defined thresholds. These non-overlapping gene sets reveal that while each wheat line responds to the safener, the underlying molecular pathways could be divergent. A comparison of untreated samples between Cres and AP18 was conducted to determine whether Cres exhibited higher baseline transcriptional activity before CM treatment. This analysis proved that 319 DEGs with higher constitutive expression in Cres relative to AP18, whereas AP18 showed only 101 DEGs with higher expression than Cres under untreated conditions (Figure S2; Table S4).

To further refine the analysis of upregulated DEGs, a subset of gene families previously reported to be involved in the three phases of herbicide metabolism (Gaines et al., 2020; Rigon et al., 2020) were examined. Table 1 summarizes the upregulated NTSR related genes in response to CM that met the expression thresholds for each wheat line. Byrd exhibited 146 genes annotated as CYPs, 96 as GSTs, 59 as UDP-glycosyltransferases (UGTs), and 81 as ATP-binding cassette (ABC) transporters. AP18 showed 97 CYPs, 86 GSTs, 18 UGTs, and 73 ABC transporters. Cres displayed 111 CYPs, 102 GSTs, 90 UGTs, and 92 ABC transporters (Table 1). Under untreated conditions, Cres exhibited higher baseline expression for several of the herbicide metabolism related gene families, including 5 GSTs, 7 CYPs, 5 UGTs, and 1 ABC transporter (Figure S2; Table S4). In contrast, AP18 showed elevated constitutive expression for only 1 GST, 0 CYPs, 2 UGTs, and 2 ABC transporters (Figure S2; Table S4).

Identification of key genes involved in herbicide metabolism that respond to cloquintocet applications

Although various herbicide metabolism genes responded to CM, functional validation of each individual gene was beyond the scope of this study. Insights from previously characterized cases of NTSR in weed species aided in further refining this list of detoxification genes to identify potential candidates involved in QPE metabolism. A gene previously reported to confer QPE resistance in *Polypogon fugax* populations from China (*PfGSTF2*; (Chen et al., 2025)) was used as a query for BLAST analysis against the wheat reference genome (IWGSC RefSeq v2.1). This search identified *TraesCS1A03G0193000* as the closest wheat homolog, sharing 87 % nucleotide sequence identity with *PfGSTF2* (Figure S3). Additionally, *AmGSTF1* from *Alopecurus myosuroides* that is involved in the metabolism of fenoxaprop-p-ethyl shared 88% homology with the same gene (*TraesCS1A03G0193000*) (Cummins et al., 2009; Cummins et al., 1999; Cummins et al., 2013) (Figure S3). *TraesCS1A03G0193000* was annotated as a phi class GST (GSTF) (Figure S4) and was designated as *TaGSTF1* for this study. Notably, *TaGSTF1* exhibited strong transcriptional activation in response to CM application in each wheat line, with L2FC of 2.2 in Byrd, 1.6 in AP18, and 2.7 in Cres (Table 2). Normalized read counts reflected a clear difference in expression magnitude among genotypes, with Cres showing the highest transcript abundance (1,283 in treated vs. 197 in untreated samples), substantially greater than that observed in Byrd (18 vs. 4) or AP18 (214 vs. 146). These results indicate that while *TaGSTF1* is induced by CM across all wheat lines, the overall expression capacity of this gene is markedly higher in Cres, consistent with its stronger metabolic and enzymatic response (Figure 1: Figure 2). Given its close homology to GSTs shown to metabolize the Group 1 herbicides fenoxaprop and QPE, and its consistent

induction across wheat lines, *TaGSTF1* was selected as a candidate for functional validation of its potential role in QPE metabolism.

Another GST previously characterized in wheat, *TaGSTU4-4*, has been shown to respond to the herbicide safener fenchlorazole-ethyl and to metabolize the group 1 herbicide fenoxaprop-p-ethyl (Thom et al., 2002). Due to the structural similarity between fenoxaprop and QPE, the enzymatic activity of *TaGSTU4-4* toward QPE was evaluated. This gene, corresponding to *TraesCS6D03G0283500* in the IWGSC RefSeq v2.1 assembly, was identified as a tau class GST (GSTF) (Figure S4) and is hereafter referred to as *TaGSTU1*. Applications of CM show an induction of *TaGSTU1* across all wheat lines, showing L2FC of 2.7 in Byrd, 4.6 in AP18, and 4.9 in Cres (Table 2). Normalized read counts further emphasize this differential response, increasing from 56 to 95 in Byrd, 3 to 64 in AP18, and 8 to 248 in Cres. The magnitude of induction in Cres suggests a markedly higher transcriptional capacity and stronger safener response compared with the other lines. Based on the induction by CM and the previous report of fenoxaprop metabolism in wheat, *TaGSTU1* was selected as the second candidate for functional validation. Together, *TaGSTF1* and *TaGSTU1* represent key candidates for further downstream functional characterization to confirm the role in QPE metabolism.

Recombinant TaGSTF1 and TaGSTU1 catalyze the formation of the quizalofop metabolite CQX-GSH

Recombinant TaGSTF1 and TaGSTU1 proteins were successfully expressed and purified under native conditions. Although there was no significant decrease in the amount of parent structure of QZA across samples, both TaGSTF1 and TaGSTU1 showed a gradual reduction in QZA quantity over time, suggesting enzymatic conversion was occurring. Both recombinant proteins did produce distinct peaks with a *m/z* of 470.089, corresponding to the glutathione-

conjugated product of QPE (CQX-GSH). The amount of CQX-GSH increased with incubation time, showing approximately a 3-fold and 2-fold increase for TaGSTF1 and TaGSTU1, respectively, after 4 h compared to with the 0.5-h incubation (Figure 6). Minor quantities of CQX-GSH were also detected in the empty vector control, consistent with previous reports of spontaneous glutathione conjugation with QZA (Bakkali et al., 2007; Chen et al., 2025). The present increase in conjugated product observed in the GST reactions relative to the control confirms that both *TaGSTF1* and *TaGSTU1* actively catalyze the conjugation of QZA with GSH, supporting their functional roles in herbicide detoxification pathways.

Differential transcriptional activation of *TaGSTF1* in response to QPE and CM treatment

Expression of the phi class GST (*TaGSTF1*) candidate gene, previously identified from the RNA seq analysis and confirmed to metabolize QZA, was quantified in each wheat line following the same previously listed treatments (Figure 7). Relative transcript abundance was calculated as 2^(–ΔCt), normalized to the reference genes described above. These values represent relative gene expression levels across treatments and varieties. Under untreated conditions, all varieties exhibited comparable basal expression, indicating no constitutive upregulation of *TaGSTF1* in the absence of treatment. In Cres, the combined QPE + CM treatment produced the highest transcript abundance compared to all other wheat lines; however, this was not statistically different than AP18 and Byrd under the same treatment ($p<0.05$). AP18 exhibited a similar but weaker trend, with QPE + CM treatment inducing a moderate increase in GST expression relative to Cres. Byrd exhibited only a slight elevation in *TaGSTF1* expression under QPE + CM relative to QPE or CM alone, and all remained within the lower statistical grouping. Overall, these results demonstrate that the GST candidate gene is induced by combined herbicide and safener application, particularly

in Cres, which exhibited the greatest response. The weaker induction observed in AP18 and Byrd suggests reduced activation of this TaGSTF1 under herbicide treatments. Collectively, these data indicate that *TaGSTF1* is transcriptionally induced by the combined QPE + CM treatment, with the strongest response observed in Cres. Based on the complexity of designing subgenome specific primers in hexaploidy species, further works is necessary to measure the relative expression in the second GST candidate (*TaGSTU1*).

Promoter sequence variation

The promoter sequence of the *TaGSTU1* candidate gene was analyzed to determine whether structural variation upstream of the coding region could account for the differences in gene expression observed among wheat genotypes (Table 2). Of the two GST candidates, *TaGSTU1* was selected for promoter characterization based on previous evidence of structural variation across whole genome sequencing of multiple wheat lines (data not published). A promoter fragment approximately 800 bp upstream of the translational start site was amplified and sequenced from Byrd, AP18, and Cres. Alignment of these sequences revealed a distinct deletion among lines. Cres showed a 115 bp deletion within the promoter region, whereas both Byrd and AP18 retained the full-length sequence with no detectable gaps (Figure 8). Aside from this deletion, no additional insertions, single nucleotide polymorphisms, or rearrangements were identified within the coding sequence of the candidate genes. The presence of this 115 bp promoter deletion uniquely in Cres provides a clear sequence level distinction between genotypes and establishes the structural basis for downstream analysis.

DISCUSSION

Cloquintocet mexyl acts on increasing the metabolism of quizalofop

The differential response to QPE observed among Byrd, AP18, and Cres reflects their contrasting genetic backgrounds and different resistance mechanisms. Wheat is not inherently resistant to QPE; however, the derived lines Cres and AP18 carry a mutation in the ACCase gene that confers target site resistance (Ostlie et al., 2015). In contrast, the parental line Byrd lacks the mutation and is therefore susceptible ACCase inhibiting herbicides. QPE, applied as a proherbicide, controls grass weeds postemergence by inhibiting the plastidic ACCase enzyme (Takano et al., 2020). Following foliar application, QPE penetrates the leaf cuticle and undergoes de-esterification to its acid form, QZA, within the plant tissues. This active metabolite is subsequently translocated to meristematic regions. When treated with QPE alone, the active form of the herbicide (QZA) directly binds to the ACCase enzyme in the susceptible wheat line Byrd, leading to enzyme inhibition and the formation of a herbicide enzyme complex. This binding event stops fatty acid biosynthesis, resulting in growth inhibition and visible herbicide injury (Bough and Dayan, 2022). As the bound fraction of QZA cannot be recovered during sample extraction, it remains undetectable by LC-MS, resulting in lower measurable concentrations of QZA. In Byrd, the high affinity of the sensitive ACCase enzyme for QZA facilitates this interaction, resulting in the herbicide remaining bound to the target protein rather than being recovered for quantification. This interaction is reflected in Figure 1A, where Byrd exhibits significantly lower measurable QZA accumulation compared to the resistant line AP18. In contrast, AP18 and Cres have target site mutations within the ACCase gene reduce the herbicide's binding affinity to the enzyme, limiting effective inhibition and allowing a greater proportion of the active QZA to persist within plant tissues.

Despite this, Cres accumulated significantly less QZA than AP18 ($p > 0.05$), four days after treatment (Figure 1A). This implies that Cres has an increased ability to detoxify QPE at a faster rate, likely through the coordinated activity of several metabolic pathways. Comparable trends have been reported in weed species that have target site resistance but also contain a higher capacity to metabolize herbicides, allowing for increased herbicide degradation despite reduced target inhibition (Larran et al., 2021; Torra et al., 2021).

The addition of herbicide safeners have been widely proven to enhance the metabolic capacity of crops, thereby reducing the effects of herbicide toxicity (Kraehmer et al., 2014; Landau et al., 2025; Riechers et al., 2010; Taylor et al., 2013). The results of this study further support this relationship, demonstrating that the addition of CM enhanced herbicide metabolism in each wheat line (Figure 1B). This result was evident from the large reduction in the accumulation of QZA detected four days after treatment when QPE was applied in combination with CM compared to QPE alone (Figure 1B). AP18 retained the highest residual QZA levels under this treatment and the difference relative to Cres was statistically significant ($P < 0.05$). In Byrd, this reduction is likely due to the combined effects of herbicide binding to the ACCase target site and enhanced metabolism induced by CM. In Cres, which carries target site resistance mutations, the additional reduction in QZA is likely due to the increased metabolism, as observed in the treatment with QPE alone. This pattern suggests that Cres maintains a more efficient herbicide metabolism system, allowing it to detoxify the herbicide more rapidly despite reduced target binding.

Activation of herbicide detoxification pathway in response to cloquintocet

Cytochrome P450 response

Previous studies have demonstrated CM functions by transcriptionally activating genes associated with the detoxification pathway involved in the three phases of herbicide metabolism

(Taylor et al., 2013). CM treatments have been shown to induce thirteen CYP families in wheat with members of the *CYP71*, *CYP72*, *CYP76*, and *CYP81* families displaying catalytic activity toward selective herbicides in cereal crops (Goldberg-Cavalleri et al., 2025; Landau et al., 2025). Many of these CYP families have been widely implicated in herbicide metabolism and NTSR mechanisms across multiple grass weed species (Dimaano and Iwakami, 2021; Pan et al., 2022; Takano et al., 2020; Yao et al., 2024), highlighting their function in herbicide detoxification. More specifically, CYP81A is involved in Group 1 ACCase herbicide metabolism (Guo et al., 2019; Han et al., 2021; Pan et al., 2022), although no reports to date have been linked CYP81A to QPE metabolism specifically. Importantly, Cres exhibited a stronger transcriptional response to CM compared to AP18, with a greater number of CYP genes upregulated across multiple safener responsive families (Table 1). This increased CYP activation aligns with the enhanced metabolic capacity observed in Cres and provides additional support for the conclusion that Cres possesses a more robust herbicide metabolism system relative to AP18. However, despite the increased CYP activation observed among wheat lines, CYP gene families were not considered for further functional validation based on the lack of evidence of CYPs role in QPE metabolism in the CoAXium wheat system. Furthermore, phorate and malathion treatments, which inhibit whole plant CYP activity, did not reverse QPE resistance in this wheat system (Pelon, 2024). Together, these findings suggest that CYPs may not directly contribute to QPE detoxification.

Glutathione-s-transferase response

There are over 300 genes that have been annotated as GSTs in wheat (Hao et al., 2021). GSTs are also well characterized targets of CM induction in cereals (Landau et al., 2025; Taylor et al., 2013). Numerous studies have demonstrated that CM enhances GST activity in wheat, facilitating rapid detoxification of herbicidal compounds (Landau et al., 2025; Scarponi et al.,

2006; Theodoulou et al., 2003). The results of the present study are consistent with these findings, as CM application alone greatly increased whole plant GST enzyme activity across all wheat lines (Figure 4; Table 1). Each line exhibited elevated GST activity in response to CM, though the magnitude of activity differed (Table 2). Byrd showed a moderate increase in GST activity, AP18 displayed a weaker yet measurable response, and Cres demonstrated the strongest induction overall when compared to the untreated, suggesting that the degree of safener responsiveness varies by genetic background. When CM was combined with QPE, whole plant GST enzyme activity increased across all wheat lines (Figure 2). Byrd and AP18 exhibited a moderate increase in GST activity under the CM + QPE treatment, suggesting limited responsiveness to safener mediated detoxification. In contrast, Cres displayed the greatest activation of GST activity under the CM + QPE treatment, nearly doubling relative to untreated controls. Although the difference between AP18 and Cres under this treatment was not statistically significant, the consistent upward trend suggests that Cres has a more robust herbicide metabolism system. This enhanced metabolic responsiveness may reflect greater induction of safener activated GST genes or more efficient downstream conjugation of herbicide metabolites.

The measurement of whole plant GST activity reflects the cumulative response of multiple GST classes. Previous evidence has proven that different classes in the GST gene family can vary in their degree of safener activation (Taylor et al., 2013), therefore, the total GST activity may confound more specific class level response. While certain GST isoforms may be highly induced by CM alone or in combination with QPE, others may exhibit negligible changes in expression. Characterizing these specific GST classes is therefore essential to determine if differential herbicide safety among wheat lines is driven by genotype-specific induction patterns and whether these candidates possess the enzymatic capacity to metabolize QPE. The RNA seq results

presented in this study aid in supplementing what is happening at a transcriptional level to each GST gene annotated in each wheat line.

A total of 96 total GSTs were in Byrd, 86 in AP18, and 101 in Cres were differentially overexpressed (Table 1), indicating variation in safener responsiveness among wheat genotypes. Cres showed the greatest number of GSTs responsive to CM application, indicating a broader activation of this metabolic pathway compared with Byrd and AP18. This elevated transcriptional response may reflect a more efficient safener signaling capacity or enhanced regulatory control of CM induced metabolism in Cres, resulting in an increased potential for herbicide metabolism. In addition to the strong response to CM, Cres also showed a greater number of GSTs with higher constitutive expression, suggesting that its basal metabolic capacity is more active even without the addition of a safener (Table S4). Among the GST gene family that have been previously reported to respond to CM, tau (GSTU), phi (GSTF), and lambda (GSTL) are the predominant classes of GSTs associated with CM application (Taylor et al., 2013) and each of these classes have been linked to herbicide metabolism (Cummins et al., 2013; Parcharidou et al., 2023; Theodoulou et al., 2003). When the GSTs that were considered differentially expressed in response to CM were classified according to the established GST families (Hao et al., 2021), Cres showed a greater number of tau and phi class GSTs relative to AP18 and Byrd (Figure S4). The enrichment of these classes, both of which have been previously linked to herbicide metabolism, suggests that Cres activates a broader subset of GST involved in herbicide metabolism after CM treatment. Notably, these same tau and phi classes of GSTs have also been associated group 1 ACCase inhibiting herbicide metabolism in both crop and weed species. For instance, in wheat the tau class GST (*TaGSTU4-4*) has been shown to conjugate fenoxaprop (Thom et al., 2002), while the phi class from black-grass (*Alopecurus myosuroides*) performs a similar function (Cummins et al.,

2013). Likewise, *PfGSTF1* from Asian minor bluegrass (*Polypogon fugax*) has been proven to metabolize QPE (Chen et al., 2025). Consequently, the identification of wheat orthologs with high sequence similarity to these characterized GST enzymes provides the basis for functional validation assays.

Candidate GST response to cloquintocet-mexyl and functional validation

The expression patterns of *TaGSTF1* and *TaGSTU1* varied across wheat lines, reflecting a genotype specific response to treatments. Following CM treatments, RNA seq analysis showed strong induction of both candidate genes in Cres compared to AP18 and Byrd (Figure 4). This indicates that Cres exhibits a more robust transcriptional response to safener treatment, which aligns with the enhanced herbicide metabolism. qPCR validation of *TaGSTF1* further supports this trend (Figure 7). While CM alone elicited only moderate changes in transcript abundance across genotypes consistent with the RNA seq results, the combined QPE + CM treatment produced the strongest induction overall. Cres displayed the highest expression level difference, whereas AP18 and Byrd showed a weaker response. Although these differences were not statistically significant, the pattern aligns with the enzyme activity and metabolic data presented throughout this study, where Cres shows consistently higher GST activity and reduced QZA accumulation. Collectively, these findings reinforce the mechanistic link between safener induced transcriptional activation, elevated GST enzyme activity, and improved QZA metabolism in Cres compared with Byrd and AP18.

Analysis of the TaGSTU1 promoter provides a plausible mechanistic explanation for the expression differences observed among wheat lines (Table 2). Cres contains a 115 bp deletion in the promoter region of this gene that is absent in AP18 and Byrd (Figure 8). Motif analysis revealed that this variation includes a MYB-binding site, a regulatory element previously associated with

transcriptional control under stress conditions. MYB motifs have been shown to recruit either activating or repressing MYB transcription factors, and several of the repressors are known to modulate metabolic pathways through direct promoter binding. In particular, MYB repressors like R2R3-MYB and R3-MYB are involved in the down regulation of target genes involved in phenylpropanoid, flavonoid, and general stress response pathways (Ma and Constabel, 2019; Ma et al., 2018). Often their activity is influenced by co-repressors, signaling proteins, or environmental cues. Therefore, the absence of the MYB-binding motif in Cres may limit repressor recruitment to *TaGSTU1* promoter, allowing increased transcriptional activation compared to AP18. This structural variation may also provide a mechanistic basis for the higher expression observed in various herbicide metabolism genes that show greater activity in response to CM in Cres compared to AP18. Whole genome sequencing of these lines would help to resolve the sequence differences and investigate other genomic variants that may further modulate herbicide metabolism gene expression. Once the sequence difference has been confirmed, evaluating the promoter differences in a protoplast transient expression system would enable direct measurement of its transcriptional output (He et al., 2025; Wilson and Schwessinger, 2025). This would offer a controlled system to test whether the deletion drives the expression differences observed between Cres and AP18.

Basal glutathione levels among wheat lines

GSH plays a crucial role in maintaining cellular redox balance and protecting plants against oxidative stress (Hasanuzzaman et al., 2017). Its role in mitigating plant damage caused by abiotic stress has been well described (Ahmad et al., 2023; Nemat Alla et al., 2008; Suliman et al., 2024). As an antioxidant, GSH directly detoxifies reactive oxygen species (ROS), including hydrogen peroxide, singlet oxygen, superoxide, and hydroxyl radicals, and participates in the glutathione-

ascorbate cycle to regenerate other antioxidants (Hasanuzzaman et al., 2017; Traxler et al., 2023). GSH also plays a key role in the detoxification of herbicide (Nemat Alla et al., 2008). Increased herbicide tolerance has been linked to elevated GSH concentrations and the activity of GSH-associated enzymes. In many cases of NTSR, herbicide detoxification occurs through the conjugation of the herbicide molecule with GSH, a reaction catalyzed by GSTs (Chen et al., 2025; Cummins et al., 2013). The formation of GSH-herbicide conjugates enhances its solubility and facilitates subsequent vacuolar sequestration, thereby reducing the likelihood of the herbicide reaching the target site and causing damage (Dixon et al., 2002; Katerova and Miteva, 2010). Through this function, GSTs contribute both to the direct detoxification of herbicides and to the mitigation of oxidative stress, reinforcing GSH's central role in protecting plant cells when applied with herbicides.

In untreated samples, AP18 and Byrd exhibited significantly lower GSH levels compared to Cres (Figure 3) ($p<0.05$), indicating that Cres maintains a higher baseline antioxidant and detoxification capacity. This trend was consistent with the RNA seq data, where Cres displayed greater constitutive expression of multiple genes involved in the GSH synthesis pathway (Table S5 & S6). The addition of CM further elevated these transcripts, suggesting an amplified transcriptional response and enhanced glutathione metabolism. Collectively, these results indicate that Crescent possesses a stronger glutathione dependent detoxification network even under limited stress conditions. Lower endogenous GSH pools in AP18 and Byrd may limit the availability of substrate for GST to conjugate with herbicide molecules, thereby reducing the capacity of these wheat lines to detoxify herbicide. In contrast, elevated basal levels of GSH in Crescent provides a greater reserve for conjugation of herbicide and enhanced protection against oxidative damage.

This difference may be further amplified under additional abiotic stress conditions such as nutrient limitations, drought, or pH variations, where GSH may be allocated for redox regulation and ROS scavenging (Hasanuzzaman et al., 2017; Noctor et al., 2012; Suliman et al., 2024). Under stress conditions, AP18 and Byrd may divert their limited GSH reserves toward general stress defense rather than herbicide detoxification, whereas Cres, with higher baseline GSH content, likely retains sufficient resources to sustain both antioxidant defense and GST mediated herbicide conjugation. This difference in GSH content could be the main driver of the increased performance observed in Cres compared to AP18.

CONCLUSION

Cres has consistently performed as an elite wheat line under field conditions, exhibiting markedly higher QPE crop safety than AP18. The results of this study provide multiple lines of evidence that help explain why this difference in crop safety is observed.

At a biochemical level, Cres metabolized QPE more efficiently than AP18, achieving QZA levels closer to those of Byrd, the susceptible line in which herbicide binding to ACCase reduces extractable QZA (Figure 1). When QPE is combined with CM there is an increase in overall QZA metabolism based on the result of CM interacting with various genes involved in herbicide metabolism (Cummins et al., 2009; Landau et al., 2025; Riechers et al., 2010; Scarponi et al., 2006; Taylor et al., 2013; Theodoulou et al., 2003). Although both wheat lines show a decrease in QZA, Cres is able to metabolize more compared to AP18 (Figure 1B). At a transcriptional level, Cres exhibited the strongest response to CM with greater number of genes involved in herbicide metabolism, specifically CYPs and GSTs (Table 1). Among this set of genes, Cres showed higher expression of tau and phi class GSTs (Figure S4), that have previously been reported to respond

to CM (Landau et al., 2025; Scarponi et al., 2006; Taylor et al., 2013; Theodoulou et al., 2003) and have been implicated in ACCase herbicide metabolism (Chen et al., 2025; Cummins et al., 2013; Thom et al., 2002). The increased expression of GSTs in Cres aids in supporting the increased metabolic response compared to AP18. This elevated transcriptional response directly translates to higher whole plant GST enzyme activity. Although not statistically significant, Cres showed a higher upward trend of activity among treatments, especially under the combined QPE + CM treatment (Figure 2). Additionally, functional validation assays confirmed that two GST genes, *TaGSTF1* and *TaGSTU1*, both capable of metabolizing QZA, were expressed at higher levels in Cres compared to AP18 (Table 2; Figure 6), consistent with the enhanced GST mediated conjugation observed in this wheat line. Combined, these results prove that Cres possesses a more efficient metabolic system for QPE metabolism compared to AP18, contributing to increased herbicide resistance.

The promoter analysis further revealed a 115 bp deletion that was unique to Cres in the *TaGSTU1* gene candidate, which removed a MYB-binding site previously linked with transcriptional repression under stress conditions (Figure 8) (Ma and Constabel, 2019; Ma et al., 2018). This structural variation provides a possible mechanistic basis for elevated expression levels of *TaGSTU1* in Cres, suggesting that cis-regulatory differences contribute to the enhanced expression and potential increased detoxification capacity of Cres.

Additionally, Cres maintained higher basal levels of GSH than AP18 and Byrd, providing a larger conjugation pool available for both plant defense and GST mediated herbicide metabolism (Figure 3). As GSH serves as the required substrate for GST catalyzed conjugation reactions, greater endogenous GSH reserves increase the plant's potential to detoxify QZA immediately following exposure. The elevated pool of GSH in Cres were further reflected at a transcriptional

level, with higher expression of genes involved in GSH biosynthesis in response to CM (Table S5 & S6), suggesting that Cres processes a more robust and responsive GSH metabolic response compared to AP18 and Byrd. Excess GSH reduces competition between herbicide and general plant stress, allowing Cres to sustain both processes simultaneously leading to less potential for QPE injury.

Together, these findings indicate that superior QPE resistance observed in Cres arises from a combination of enhanced safener responsiveness, stronger transcriptional and enzymatic detoxification capacity, advantageous promoter architecture, and elevated endogenous GSH pools. This integrated resistance profile highlights the genetic advantage observed in Cres for herbicide resistance compared to AP18. Further research will begin to identify and confirm the cis- or trans-regulatory variants driving the differences in expression observed in Cres. Such molecular markers could be utilized in future wheat breeding programs to develop varieties that have improved metabolic herbicide resistance for wheat farmers.

TABLES

Table 1. Differentially expressed genes grouped by gene families previously implicated in herbicide metabolism across wheat lines treated with CM.
Subset of overexpressed genes (log_2 fold-change > 1) in Byrd, AP18 (AP18 AX), and Cres (Crescent AX) following cloquintocet (CM) treatment, grouped by gene families previously linked to metabolic resistance.

Gene Family	Byrd	AP18	Cres
Cytochrome P450 (P450)	146	97	111
Glutathione S-transferase (GST)	96	86	102
Glucosyltransferase (UGT)	59	18	90
ABC Transporters (ABC)	81	73	92

Table 2. Normalized counts and differential expression for TaGSTF1 and TaGSTU1 plus their subsequent subgenomes across each wheat line.
Average normalized gene count, log_2foldchange (L2FC) and adjusted p-value (Padj) for two GST gene candidates (TaGSTF1 and TaGSTU1) for Byrd, AP18 (AP18 AX), and Cres (Crescent AX) including corresponding subgenome assignments.

WHEAT LINE	GENE NAME	GENE ID	L_2FC	PADJ	NORMALIZED COUNTS TREATED VS UNTREATED	
BYRD	Traes**CS1A**03G0193000	*TaGSTF1*	2.24	0.07	18	4
	TraesCS1B03G0260800		3.55	3.32×10^{-4}	332	28
	TraesCS1D03G0185900		3.71	1.49×10^{-6}	1925	147
	Traes**CS6D**03G0283500	*TaGSTU1*	2.68	0.063	40	6
	TraesCS6A03G0329800		NA	NA	4	1
	TraesCS6B03G0425400		NA	NA	95	56
AP18	Traes**CS1A**03G0193000	*TaGSTF1*	1.62	0.04	214	146
	TraesCS1B03G0260800		NA	NA	0	0
	TraesCS1D03G0185900		2.82	1.11×10^{-8}	2074	1188
	Traes**CS6D**03G0283500	*TaGSTU1*	3.43	0.004	64	3
	TraesCS6A03G0329800		NA	NA	1	0
	TraesCS6B03G0425400		NA	NA	9	1
CRES	Traes**CS1A**03G0193000	*TaGSTF1*	2.72	3.64×10^{-5}	1283	197
	TraesCS1B03G0260800		4.11	2.60×10^{-7}	480	77
	TraesCS1D03G0185900		2.91	2.30×10^{-4}	4199	1315
	Traes**CS6D**03G0283500	*TaGSTU1*	4.91	1.30×10^{-8}	248	8
	TraesCS6A03G0329800		NA	NA	8	0
	TraesCS6B03G0425400		6.35	8.46×10^{-4}	17	0

FIGURES

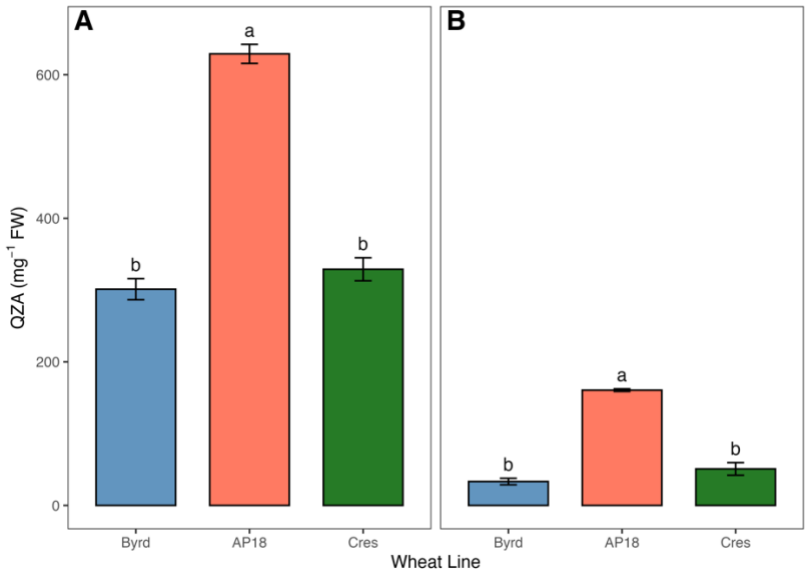

Figure 1. Quantification of QZA in each wheat line under QPE and QPE + CM treatments. QZA concertation (mg g -1 fresh weight) measured 4 days after quizlafop-p-ethyl (QPE) alone (A) or in combination with the safener cloquintocet-mexyl (CM) (B) among Byrd, AP18 (AP18 AX), and Cres (Crescent AX). Bars represent mean ± SE of biological replicates. Statistical significance among treatments and varieties was assessed using two-way ANOVA followed by Tukey's HSD ($p < 0.05$).

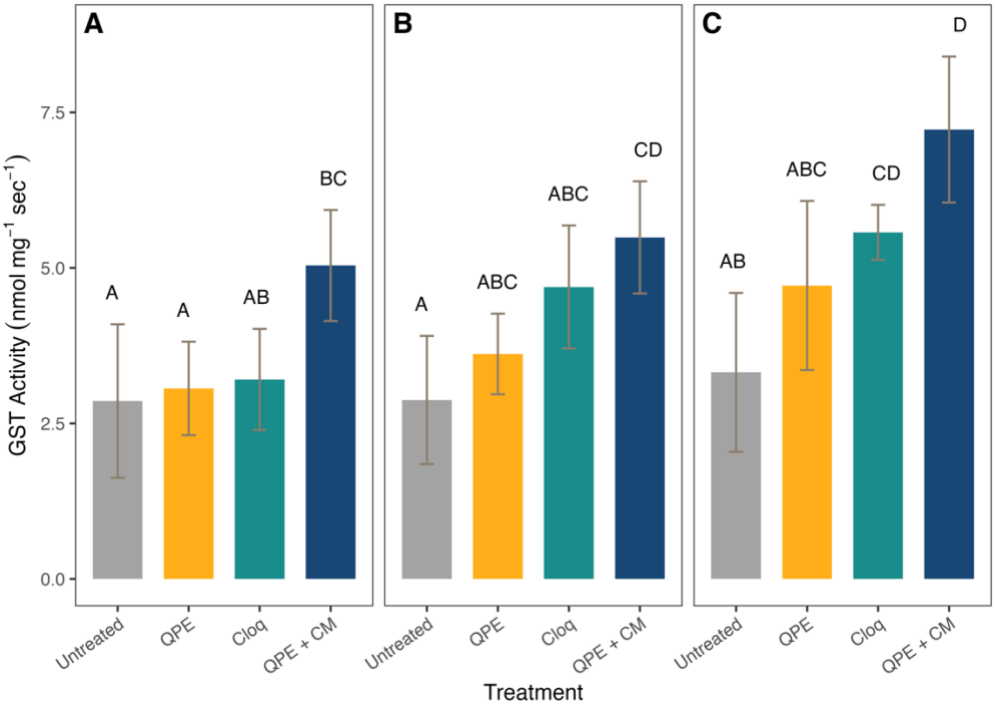

Figure 2. Whole plant GST activity following treatment across all wheat lines.
Whole-plant glutathione S-transferase (GST) activity was quantified in Byrd (A), AP18 (AP18 AX) (B), and Crescent (Crescent AX) (C) wheat lines following four treatments: untreated control (NIS only), quizalofop-p-ethyl (QPE), cloquintocet-mexyl (CM), and the combined QPE + CM application. Data represent mean ± SE of biological replicates. Statistical significance among treatments and varieties was assessed using two-way ANOVA followed by Tukey's HSD ($p < 0.05$).

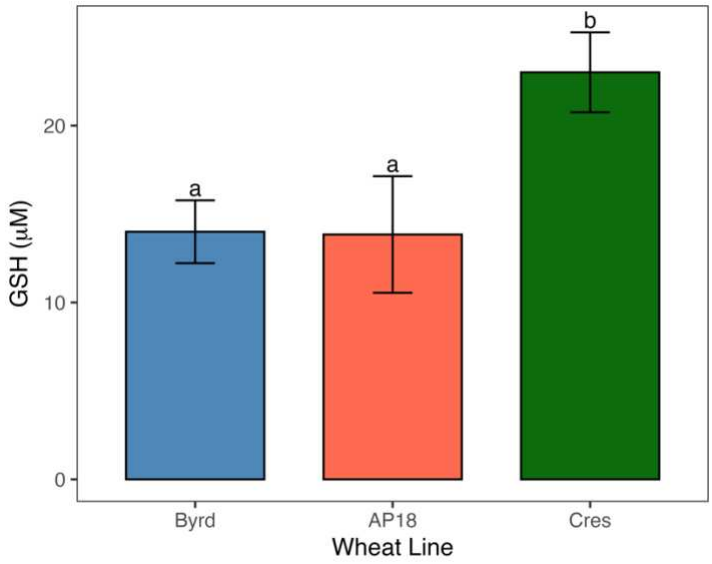

Figure 3. Basal GSH concentrations among wheat lines.
Total glutathione (GSH) content was measured in untreated two-week-old seedlings of Byrd, AP18 (AP18 AX), and Cres (Crescent AX). Values represent mean ± SE. Statistical significance among treatments and wheat lines were assessed using one-way ANOVA followed by Tukey's HSD ($p < 0.05$).

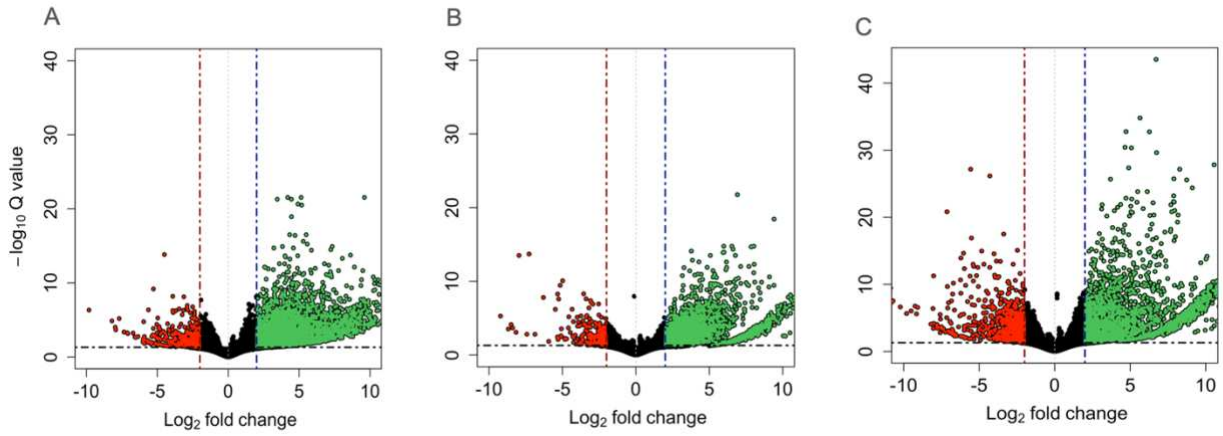

Figure 4. Differential expression profiles following CM treatment in three wheat lines. Volcano plot that represents $\log_2$ fold change (x-axis) and $-\log_{10}$ (Q value) (y-axis) for all expressed genes in (A) Byrd, (B) AP18 (AP18 AX), and (C) Cres (Crescent AX) following CM treatment relative to untreated controls. Genes meeting significance thresholds ($Q < 0.1$ and $\log_2FC > 1$) are highlighted in green (upregulated) and red (downregulated), while non-significant genes are shown in black. Vertical dashed lines indicate the ± 1 $\log_2$ fold-change cutoff, and the horizontal dashed line marks the $Q = 0.1$ threshold.

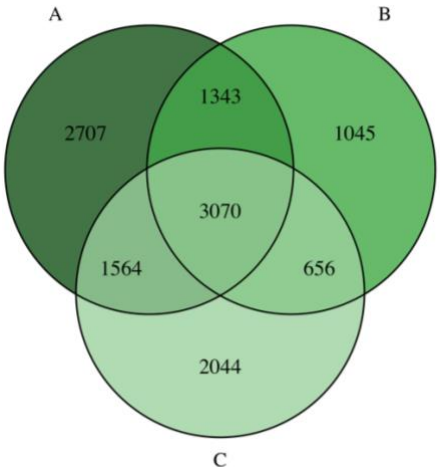

Figure 5. Differentially expressed gene comparison among wheat lines following CM treatment.

Venn diagrams summarizing the number of significantly upregulated genes in Byrd (A), AP18 AX (B), and Crescent AX (C) in response to cloquintocet-mexyl (CM) treatments. Each diagram displays the total number of differentially expressed genes unique to each wheat line as well as those shared between two or all three lines. Values reflect differential expression identified using thresholds of $padj < 0.1$ and $\log_2 FC > 1$.

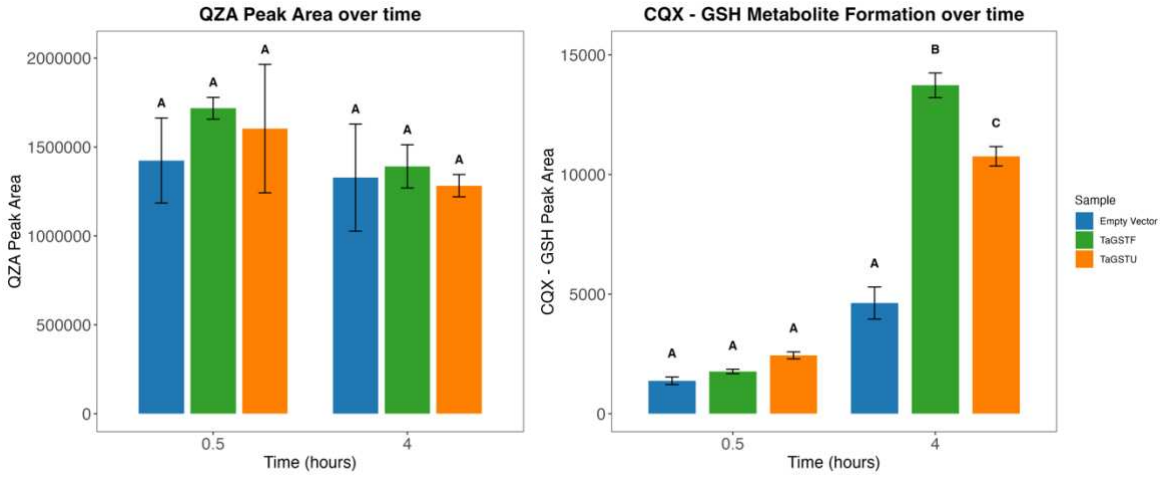

Figure 6. In vitro metabolism of quizalofop acid by recombinant wheat GSTs.
In vitro conjugation of quizalofop acid (QZA) by two recombinant candidate GSTs. Purified TaGSTF1, TaGSTU1, and an empty vector control were incubated with QZA and glutathione, and LC-MS/MS was used to quantify (a) the amount of unmetabolized QZA and (b) the accumulation of the 6-chloroquinoxalin-2-ol-glutathione (CQX-GSH) conjugate at two incubation points 0.5 h and 4 h. Differences among samples and time combinations were assessed using a linear model followed by estimated marginal means with compact letter display grouping. Different letters denote significant differences ($P < 0.05$) among treatments based on estimated marginal means.

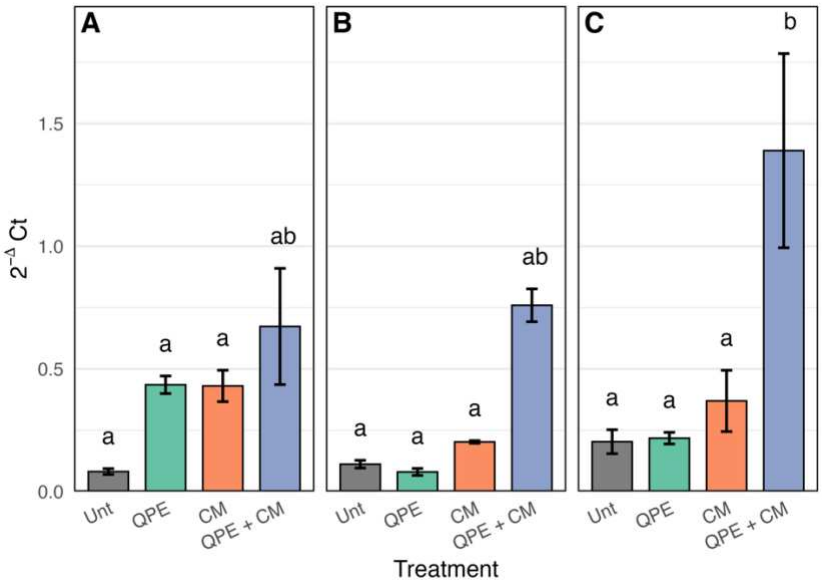

Figure 7. Relative expression of *TaGSTF* across wheat lines following herbicide and safener treatments.

Relative expression of *TaGSTF* ($2^{-}\Delta$Ct) in three wheat lines Byrd (A), AP18 (AP18 AX) (B), and Cres (Crescent AX) (C). Samples were treated with NIS (Unt), quizalofop-p-ethyl (QPE), cloquintocet-mexyl (CM), and the combined QPE + CM treatment. Bars represent mean expression ± SE (n = 3 biological replicates per treatment) ($P < 0.05$).

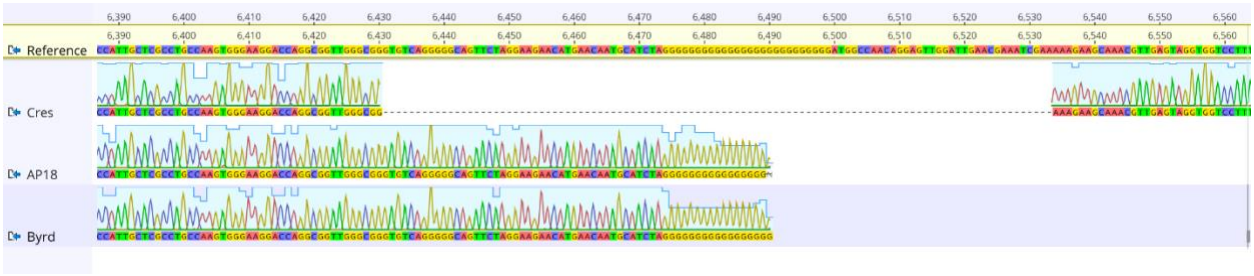

Figure 8. Promoter sequence variation in *TaGSTU1* candidate among wheat lines.
Promoter sequence comparison among three wheat lines Cres (Crescent AX), AP18 (AP18AX), and Byrd. Sequence represents 115 bp gap observed in Cres ~800 bp upstream of the start site of *TaGSTU1* gene candidate in comparison to AP18 and Byrd that show no sequence variation.

REFERENCES

1.
2. Abdollahi, Fatemeh, Mohammad Taghi Alebrahim, Chheng Ngov, Etienne Lallemand, Yongxiang Zheng, Claire Villette, Julie Zumsteg, François André, Nicolas Navrot, Danièle Werck-Reichhart and Laurence Miesch 2021. Innate promiscuity of the CYP706 family of P450 enzymes provides a suitable context for the evolution of dinitroaniline resistance in weed. New Phytologist 229: 3253–3268. doi: https://doi.org/10.1111/nph.17126
3. Adams, Kendra J., Brian Pratt, Neelanjan Bose, Laura G. Dubois, Lisa St. John-Williams, Kevin M. Perrott, Karina Ky, Pankaj Kapahi, Vagisha Sharma, Michael J. MacCoss, M. Arthur Moseley, Carol A. Colton, Brendan X. MacLean, Birgit Schilling and J. Will Thompson 2020. Skyline for Small Molecules: A Unifying Software Package for Quantitative Metabolomics. Journal of Proteome Research 19: 1447–1458. doi: 10.1021/acs.jproteome.9b00640
4. Ahmad, M., S. Ahmed, N. A. Yasin, A. Wahid and R. Sardar 2023. Exogenous application of glutathione enhanced growth, nutritional orchestration and physiochemical characteristics of Brassica oleracea L. under lead stress. Physiol Mol Biol Plants 29: 1103–1116. doi: 10.1007/s12298-023-01346-0
5. Anders, Simon and Wolfgang Huber 2010. Differential expression analysis for sequence count data. Genome Biology 11: R106. doi: 10.1186/gb-2010-11-10-r106
6. Andrews, S, A Segonds-Pichon, L Biggins, C Krueger and S Wingett 2010. FastQC: a quality control tool for high throughput sequence data. In FastQC: a quality control tool for high throughput sequence data.
7. Bakkali, Y., J. P. Ruiz-Santaella, M. D. Osuna, J. Wagner, A. J. Fischer and R. De Prado 2007. Late watergrass (Echinochloa phyllopogon): mechanisms involved in the resistance to fenoxaprop-p-ethyl. J Agric Food Chem 55: 4052–4058. doi: 10.1021/jf0624749
8. Benjamini, Yoav and Yosef Hochberg 1995. Controlling the False Discovery Rate: A Practical and Powerful Approach to Multiple Testing. Journal of the Royal Statistical Society. Series B (Methodological) 57: 289–300.
9. Bolger, Anthony M., Marc Lohse and Bjoern Usadel 2014. Trimmomatic: a flexible trimmer for Illumina sequence data. Bioinformatics 30: 2114–2120. doi: 10.1093/bioinformatics/btu170
10. Bough, Raven and Franck E. Dayan 2022. Biochemical and structural characterization of quizalofop-resistant wheat acetyl-CoA carboxylase. Scientific Reports 12: 679. doi: 10.1038/s41598-021-04280-x
11. Boutet, E., D. Lieberherr, M. Tognolli, M. Schneider and A. Bairoch 2007. UniProtKB/Swiss-Prot. Methods Mol Biol 406: 89–112. doi: 10.1007/978-1-59745-535-0_4
12. Brazier-Hicks, Melissa, Sara Franco-Ortega, Philip Watson, Blandine Rougemont, Jonathan Cohn, Richard Dale, Tim R. Hawkes, Alina Goldberg-Cavalleri, Nawaporn Onkokesung and Robert Edwards 2022. Characterization of Cytochrome P450s with Key Roles in Determining Herbicide Selectivity in Maize. ACS Omega 7: 17416–17431. doi: 10.1021/acsomega.2c01705
13. Chen, Wen, Dingyi Bai, Yuxi Liao, Qin Yu, Lianyang Bai and Lang Pan 2025. PfGSTF2 endows resistance to quizalofop-p-ethyl in *Polypogon fugax* by GSH conjugation. Plant Biotechnology Journal 23: 216–231. doi: https://doi.org/10.1111/pbi.14491

14. Cummins, I., D. N. Bryant and R. Edwards 2009. Safener responsiveness and multiple herbicide resistance in the weed black-grass (Alopecurus myosuroides). Plant Biotechnol J 7: 807–820. doi: 10.1111/j.1467-7652.2009.00445.x
15. Cummins, I., D. J. Cole and R. Edwards 1999. A role for glutathione transferases functioning as glutathione peroxidases in resistance to multiple herbicides in black-grass. Plant J 18: 285–292. doi: 10.1046/j.1365-313x.1999.00452.x
16. Cummins, I., D. J. Wortley, F. Sabbadin, Z. He, C. R. Coxon, H. E. Straker, J. D. Sellars, K. Knight, L. Edwards, D. Hughes, S. S. Kaundun, S. J. Hutchings, P. G. Steel and R. Edwards 2013. Key role for a glutathione transferase in multiple-herbicide resistance in grass weeds. Proc Natl Acad Sci U S A 110: 5812–5817. doi: 10.1073/pnas.1221179110
17. Délye, Christophe 2013. Unravelling the genetic bases of non-target-site-based resistance (NTSR) to herbicides: a major challenge for weed science in the forthcoming decade. Pest Management Science 69: 176–187. doi: https://doi.org/10.1002/ps.3318
18. Dimaano, N. G., T. Yamaguchi, K. Fukunishi, T. Tominaga and S. Iwakami 2020. Functional characterization of cytochrome P450 CYP81A subfamily to disclose the pattern of cross-resistance in Echinochloa phyllopogon. Plant Mol Biol 102: 403–416. doi: 10.1007/s11103-019-00954-3
19. Dimaano, Niña Gracel and Satoshi Iwakami 2021. Cytochrome P450-mediated herbicide metabolism in plants: current understanding and prospects. Pest Management Science 77: 22–32. doi: https://doi.org/10.1002/ps.6040
20. Dixon, D. P., A. Lapthorn and R. Edwards 2002. Plant glutathione transferases. Genome Biol 3: Reviews3004. doi: 10.1186/gb-2002-3-3-reviews3004
21. Dobin, A., C. A. Davis, F. Schlesinger, J. Drenkow, C. Zaleski, S. Jha, P. Batut, M. Chaisson and T. R. Gingeras 2013. STAR: ultrafast universal RNA-seq aligner. Bioinformatics 29: 15–21. doi: 10.1093/bioinformatics/bts635
22. Dudziak, Karolina, Magdalena Sozoniuk, Hubert Szczerba, Adam Kuzdraliński, Krzysztof Kowalczyk, Andreas Börner and Michał Nowak 2020. Identification of stable reference genes for qPCR studies in common wheat (Triticum aestivum L.) seedlings under short-term drought stress. Plant Methods 16: 58. doi: 10.1186/s13007-020-00601-9
23. Gaines, Todd A., Stephen O. Duke, Sarah Morran, Carlos A. G. Rigon, Patrick J. Tranel, Anita Küpper and Franck E. Dayan 2020. Mechanisms of evolved herbicide resistance. Journal of Biological Chemistry 295: 10307–10330. doi: https://doi.org/10.1074/jbc.REV120.013572
24. Goldberg-Cavalleri, Alina, Sara Franco-Ortega, Stewart Brown, Andrew Walker, Blandine Rougemont, John Sinclair, Melissa Brazier-Hicks, Richard Dale, Nawaporn Onkokesung and Robert Edwards 2025. Functional Characterization of Cytochromes P450 Linked to Herbicide Detoxification and Selectivity in Winter Wheat and the Problem Competing Weed Blackgrass. ACS Omega 10: 12270–12287. doi: 10.1021/acsomega.4c11069
25. Guo, Feng, Satoshi Iwakami, Takuya Yamaguchi, Akira Uchino, Yukari Sunohara and Hiroshi Matsumoto 2019. Role of CYP81A cytochrome P450s in clomazone metabolism in Echinochloa phyllopogon. Plant Science 283: 321–328. doi: https://doi.org/10.1016/j.plantsci.2019.02.010
26. Haley, Scott D., Jerry J. Johnson, Frank B. Peairs, John A. Stromberger, Emily E. Hudson, Scott A. Seifert, Rebecca A. Kottke, Victoria A. Valdez, Jeff B. Rudolph, Guihua Bai, Xianming Chen, Robert L. Bowden, Yue Jin, James A. Kolmer, Ming-Shun

Chen and Bradford W. Seabourn 2012. Registration of 'Byrd' Wheat. Journal of Plant Registrations 6: 302–305. doi: https://doi.org/10.3198/jpr2011.12.0672crc
27. Han, H., Q. Yu, R. Beffa, S. González, F. Maiwald, J. Wang and S. B. Powles 2021. Cytochrome P450 CYP81A10v7 in Lolium rigidum confers metabolic resistance to herbicides across at least five modes of action. Plant J 105: 79–92. doi: 10.1111/tpj.15040
28. Hao, Yongchao, Shoushen Xu, Zhongfan lyu, Hongwei Wang, Lingrang Kong and Silong Sun 2021. Comparative Analysis of the Glutathione S-Transferase Gene Family of Four Triticeae Species and Transcriptome Analysis of GST Genes in Common Wheat Responding to Salt Stress. International Journal of Genomics 2021: 6289174. doi: https://doi.org/10.1155/2021/6289174
29. Hasanuzzaman, M., K. Nahar, T. I. Anee and M. Fujita 2017. Glutathione in plants: biosynthesis and physiological role in environmental stress tolerance. Physiol Mol Biol Plants 23: 249–268. doi: 10.1007/s12298-017-0422-2
30. He, F., D. Du, Z. Chen, L. Ma, Y. Liu, Z. Li, L. Song, Z. Jiang, Y. Fan, Q. Sun and Z. Ni 2025. A natural variation in the promoter of TaGDSL-7D contributes to grain weight and yield in wheat. Plant Biotechnol J 23: 3851–3863. doi: 10.1111/pbi.70204
31. Iwakami, S., Y. Kamidate, T. Yamaguchi, M. Ishizaka, M. Endo, H. Suda, K. Nagai, Y. Sunohara, S. Toki, A. Uchino, T. Tominaga and H. Matsumoto 2019. CYP81A P450s are involved in concomitant cross-resistance to acetolactate synthase and acetyl-CoA carboxylase herbicides in Echinochloa phyllopogon. New Phytol 221: 2112–2122. doi: 10.1111/nph.15552
32. Jia, L., X. Y. Jin, L. X. Zhao, Y. Fu and F. Ye 2022. Research Progress in the Design and Synthesis of Herbicide Safeners: A Review. J Agric Food Chem 70: 5499–5515. doi: 10.1021/acs.jafc.2c01565
33. Jugulam, Mithila and Chandrima Shyam 2019. Non-Target-Site Resistance to Herbicides: Recent Developments. Plants 8: 417.
34. Katerova, Zornitsa and Lyuba Miteva 2010. Glutathione and Herbicide Resistance in Plants. 191–207.
35. Kraehmer, H., B. Laber, C. Rosinger and A. Schulz 2014. Herbicides as weed control agents: state of the art: I. Weed control research and safener technology: the path to modern agriculture. Plant Physiol 166: 1119–1131. doi: 10.1104/pp.114.241901
36. Landau, O. A., B. V. Jamison and D. E. Riechers 2025. Transcriptomic analysis reveals cloquintocet-mexyl-inducible genes in hexaploid wheat (Triticum aestivum L.). PLoS One 20: e0319151. doi: 10.1371/journal.pone.0319151
37. Larran, Alvaro, Valeria Palmieri, Daniel Tuesca, Hugo Permingeat and Valeria Perotti 2021. Coexistence of target-site and non-target-site mechanisms of glyphosate resistance in Amaranthus palmeri populations from Argentina. Acta Scientiarum Agronomy 44: 2022. doi: 10.4025/actasciagron.v44i1.55183
38. Lehoczky, E. and P. Reisinger 2003. Study on the weed-crop competition for nutrients in maize. Commun Agric Appl Biol Sci 68: 373–380.
39. Liao, Yang, Gordon K. Smyth and Wei Shi 2013. featureCounts: an efficient general purpose program for assigning sequence reads to genomic features. Bioinformatics 30: 923–930. doi: 10.1093/bioinformatics/btt656
40. Love, M. I., W. Huber and S. Anders 2014. Moderated estimation of fold change and dispersion for RNA-seq data with DESeq2. Genome Biol 15: 550. doi: 10.1186/s13059-014-0550-8

41. Ma, D. and C. P. Constabel 2019. MYB Repressors as Regulators of Phenylpropanoid Metabolism in Plants. Trends Plant Sci 24: 275–289. doi: 10.1016/j.tplants.2018.12.003
42. Ma, D., M. Reichelt, K. Yoshida, J. Gershenzon and C. P. Constabel 2018. Two R2R3-MYB proteins are broad repressors of flavonoid and phenylpropanoid metabolism in poplar. Plant J 96: 949–965. doi: 10.1111/tpj.14081
43. Montgomery, Jacob, Sarah Morran, Dana R. MacGregor, J. Scott McElroy, Paul Neve, Célia Neto, Martin M. Vila-Aiub, Maria Victoria Sandoval, Analia I. Menéndez, Julia M. Kreiner, Longjiang Fan, Ana L. Caicedo, Peter J. Maughan, Bianca Assis Barbosa Martins, Jagoda Mika, Alberto Collavo, Aldo Merotto, Nithya K. Subramanian, Muthukumar V. Bagavathiannan, Luan Cutti, Md Mazharul Islam, Bikram S. Gill, Robert Cicchillo, Roger Gast, Neeta Soni, Terry R. Wright, Gina Zastrow-Hayes, Gregory May, Jenna M. Malone, Deepmala Sehgal, Shiv Shankhar Kaundun, Richard P. Dale, Barend Juan Vorster, Bodo Peters, Jens Lerchl, Patrick J. Tranel, Roland Beffa, Alexandre Fournier-Level, Mithila Jugulam, Kevin Fengler, Victor Llaca, Eric L. Patterson and Todd A. Gaines 2024. Current status of community resources and priorities for weed genomics research. Genome Biology 25: 139. doi: 10.1186/s13059-024-03274-y
44. Montgomery, Jacob S., Jan E. Leach, Stephen L. Young and Todd A. Gaines 2025. Using weedy traits in crops as part of a new green revolution. New Phytologist 247: 1071–1074. doi: https://doi.org/10.1111/nph.70224
45. Nemat Alla, Mamdouh M., Abdel-Hakeem M. Badawi, Nemat M. Hassan, Zeinab M. El-Bastawisy and Enas G. Badran 2008. Herbicide tolerance in maize is related to increased levels of glutathione and glutathione-associated enzymes. Acta Physiologiae Plantarum 30: 371–379. doi: 10.1007/s11738-008-0134-x
46. Newhouse, K. E., W. A. Smith, M. A. Starrett, T. J. Schaefer and B. K. Singh 1992. Tolerance to imidazolinone herbicides in wheat. Plant Physiol 100: 882–886. doi: 10.1104/pp.100.2.882
47. Noctor, Graham, Amna Mhamdi, Sejir Chaouch, Yi Han, Jenny Neukermans, Belen Marquez-Garcia, Guillaume Queval and Christine H. Foyer 2012. Glutathione in plants: an integrated overview. Plant, Cell & Environment 35: 454–484. doi: https://doi.org/10.1111/j.1365-3040.2011.02400.x
48. Ostlie, M., S. D. Haley, V. Anderson, D. Shaner, H. Manmathan, C. Beil and P. Westra 2015. Development and characterization of mutant winter wheat (Triticum aestivum L.) accessions resistant to the herbicide quizalofop. Theor Appl Genet 128: 343–351. doi: 10.1007/s00122-014-2434-4
49. Pan, Lang, Qiushuang Guo, Junzhi Wang, Li Shi, Xiao Yang, Yaoyu Zhou, Qin Yu and Lianyang Bai 2022. CYP81A68 confers metabolic resistance to ALS and ACCase-inhibiting herbicides and its epigenetic regulation in Echinochloa crus-galli. Journal of Hazardous Materials 428: 128225. doi: https://doi.org/10.1016/j.jhazmat.2022.128225
50. Parcharidou, Evlampia, Rebecka Dücker, Peter Zöllner, Susanne Ries, Roberto Orru and Roland Beffa 2023. Recombinant glutathione transferases from flufenacet-resistant black-grass (Alopecurus myosuroides Huds.) form different flufenacet metabolites and differ in their interaction with pre- and post-emergence herbicides. Pest Management Science 79: 3376–3386. doi: https://doi.org/10.1002/ps.7523
51. Pundir, Sangya, Maria J. Martin and Claire O'Donovan 2017. UniProt Protein Knowledgebase. In Protein Bioinformatics: From Protein Modifications and Networks to

Proteomics, eds. Cathy H. Wu, Cecilia N. Arighi and Karen E. Ross, 41–55. New York, NY: Springer New York.
52. Rea, Philip A. 2007. Plant ATP-Binding Cassette Transporters. Annual Review of Plant Biology 58: 347–375. doi: https://doi.org/10.1146/annurev.arplant.57.032905.105406
53. Riechers, D. E., K. Kreuz and Q. Zhang 2010. Detoxification without intoxication: herbicide safeners activate plant defense gene expression. Plant Physiol 153: 3–13. doi: 10.1104/pp.110.153601
54. Rigon, Carlos, Todd Gaines, Anita Kuepper and Franck Dayan 2020. Metabolism-Based Herbicide Resistance, the Major Threat Among the Non-Target Site Resistance Mechanisms. Outlooks on Pest Management 31: 162–168. doi: 10.1564/v31_aug_04
55. Scarponi, Luciano, Elisa Quagliarini and Daniele Del Buono 2006. Induction of wheat and maize glutathione S-transferase by some herbicide safeners and their effect on enzyme activity against butachlor and terbuthylazine. Pest Management Science 62: 927–932. doi: https://doi.org/10.1002/ps.1258
56. Schenk, J. J., L. E. Becklund, S. J. Carey and P. P. Fabre 2023. What is the "modified" CTAB protocol? Characterizing modifications to the CTAB DNA extraction protocol. Appl Plant Sci 11: e11517. doi: 10.1002/aps3.11517
57. Shiferaw, Bekele, Melinda Smale, Hans-Joachim Braun, Etienne Duveiller, Mathew Reynolds and Geoffrey Muricho 2013. Crops that feed the world 10. Past successes and future challenges to the role played by wheat in global food security. Food Security 5: 291–317. doi: 10.1007/s12571-013-0263-y
58. Suliman, M. S. E., S. B. M. Elradi, G. Zhou, T. Meng, G. Zhu, Y. Xu, N. E. A. Nimir, A. M. I. Elsiddig, A. H. M. Awdelseid, A. Y. A. Ali, X. Guo and I. Ahmad 2024. Exogenous glutathione protected wheat seedling from high temperature and water deficit damages. Sci Rep 14: 5304. doi: 10.1038/s41598-023-47868-1
59. Takano, Hudson, Ramiro Ovejero, Gustavo Belchior, Gizella Maymone and Franck Dayan 2020. ACCase-inhibiting herbicides: mechanism of action, resistance evolution and stewardship. Scientia Agricola 78: e20190102. doi: 10.1590/1678-992X-2019-0102
60. Taylor, Victoria L., Ian Cummins, Melissa Brazier-Hicks and Robert Edwards 2013. Protective responses induced by herbicide safeners in wheat. Environmental and Experimental Botany 88: 93–99. doi: https://doi.org/10.1016/j.envexpbot.2011.12.030
61. Theodoulou, Frederica L, Ian M Clark, Xiao-Li He, Kenneth E Pallett, David J Cole and David L Hallahan 2003. Co-induction of glutathione-S-transferases and multidrug resistance associated protein by xenobiotics in wheat. Pest Management Science 59: 202–214. doi: https://doi.org/10.1002/ps.576
62. Thom, R., I. Cummins, D. P. Dixon, R. Edwards, D. J. Cole and A. J. Lapthorn 2002. Structure of a tau class glutathione S-transferase from wheat active in herbicide detoxification. Biochemistry 41: 7008–7020. doi: 10.1021/bi015964x
63. Torra, Joel, María Dolores Osuna, Aldo Merotto and Martin Vila-Aiub 2021. Editorial: Multiple Herbicide-Resistant Weeds and Non-target Site Resistance Mechanisms: A Global Challenge for Food Production. Frontiers in Plant Science Volume 12 - 2021. doi: 10.3389/fpls.2021.763212
64. Traxler, C., T. A. Gaines, A. Küpper, P. Luemmen and F. E. Dayan 2023. The nexus between reactive oxygen species and the mechanism of action of herbicides. J Biol Chem 299: 105267. doi: 10.1016/j.jbc.2023.105267

65. Wilson, S. and B. Schwessinger 2025. A Wheat Protoplast Assay for Positive Effector Screening and Investigation of Host-Pathogen Interactions. Methods Mol Biol 2898: 189–205. doi: 10.1007/978-1-0716-4378-5_11
66. Yao, Sai, Hanqi Yin, Yang Li, Qian Yang, Shuzhong Yuan and Wei Deng 2024. Cytochrome P450 CYP81A104 in Eleusine indica confers resistance to multiherbicide with different modes of action. Pest Management Science 80: 5791–5798. doi: https://doi.org/10.1002/ps.8310
67. Zhao, Yaning, Fei Ye and Ying Fu 2023. Research Progress on the Action Mechanism of Herbicide Safeners: A Review. Journal of Agricultural and Food Chemistry 71: 3639–3650. doi: 10.1021/acs.jafc.2c08815
68. Zhu, Anqi, Joseph G Ibrahim and Michael I Love 2018. Heavy-tailed prior distributions for sequence count data: removing the noise and preserving large differences. Bioinformatics 35: 2084–2092. doi: 10.1093/bioinformatics/bty895
69. Zhu, T., L. Wang, H. Rimbert, J. C. Rodriguez, K. R. Deal, R. De Oliveira, F. Choulet, G. Keeble-Gagnère, J. Tibbits, J. Rogers, K. Eversole, R. Appels, Y. Q. Gu, M. Mascher, J. Dvorak and M. C. Luo 2021. Optical maps refine the bread wheat Triticum aestivum cv. Chinese Spring genome assembly. Plant J 107: 303–314. doi: 10.1111/tpj.15289

CHAPTER II - IDENTIFICATION AND FUNCTIONAL VALIDATION OF CYTOCHROME P450S CONFERRING IMAZAMOX RESISTANCE IN FERAL RYE

SUMMARY

The increased adoption of imazamox (IM) resistant Clearfield wheat has intensified selection pressure for herbicide resistance, resulting in both target site (TSR) and non-target site resistance (NTSR) among winter annual grasses. A recent weed resistance survey identified three populations of feral rye with showing resistance to IM, including one population (population A) that lacked target site mutations in the ALS gene, suggesting metabolic resistance. This study investigates the molecular basis for IM resistance in population A through transcriptomic analyses and functional validation of cytochrome P450s (CYPs) candidates. RNA sequencing comparisons between resistant (R) and susceptible (S) F_2 plants identified two CYP candidates, CYP81A52 and CYP72A1365, based on constitutive and inducible expression patterns. Heterologous expression in *Arabidopsis thaliana* confirmed that overexpression of CYP81A52 increased IM tolerance 3.0-fold relative to WT and significantly reduced parent IM levels while increasing O-demethylated IM metabolite accumulation. Yeast metabolism assays further supported CYP-mediated IM detoxification, with both CYP81A52 and CYP72A1365 reducing IM parent levels. Collectively, these results demonstrate that both CYP81A52 and CYP72A1365 are major drivers of metabolic IM resistance in feral rye. This work expands our understanding of convergent CYP-mediated metabolic resistance mechanisms in grass weeds and highlights molecular targets that may support resistance diagnostics and inform future weed management strategies.

INTRODUCTION

Since the introduction of Clearfield wheat in 2002 (Newhouse et al., 1992), the use of imazamox (IM) has increased substantially (Heap, 2025). IM is an imidazolinone herbicide that inhibits the acetolactate synthase (ALS) enzyme, interrupting the biosynthesis of essential branched-chain amino acids and ultimately halting plant growth (Brady et al., 1998; Shaner et al., 1984). The Clearfield system provided growers with a valuable tool for managing troublesome winter annual grass weeds such as downy brome (*Bromus tectorum*), jointed goatgrass (*Aegilops cylindrica*), and feral rye (*Secale cereale*) (Carter et al., 2007; Geier et al., 2004; Pester et al., 2001; Stougaard et al., 2004). However, extensive reliance on this technology has created strong selection pressure for herbicide resistance, and both target site (TSR) and non-target site resistance (NTSR) to ALS inhibitors are now increasingly documented in weed populations across the United States (Heap, 2014; Tranel and Wright, 2002). This trend is consistent with the broader global pattern, as ALS inhibitors rank among the herbicide groups most prone to resistance evolution due to their frequent and repeated usage.

A multiyear statewide survey in Colorado was conducted to assess IM resistance in winter annual grasses, as no confirmed cases had previously been reported in in these troublesome winter annual weeds within Colorado wheat systems (Soni et al., 2022). Three feral rye populations, A, B, and C, were reported to be resistant to IM, surviving applications at the field rate of 53 g ai ha^{-1}. Of these three populations, B and C carried the target-site mutations Ser653Asn and Ser653Thr, respectively, whereas population A showed no sequence variation relative to the susceptible feral rye reference sequence, suggesting NTSR mechanism.

Among the NTSR mechanisms, enhanced metabolic resistance is the most frequently reported and arguably the most intricate. Plants decrease herbicide effects by reducing the amount

of herbicide active ingredient that reaches the target enzyme through changes in absorption, alterations in transportation, or acceleration of metabolism (Délye, 2013; Gaines et al., 2020; Jugulam and Shyam, 2019; Rigon et al., 2020). Some of the key enzyme groups involved in this process include cytochrome P450s (CYPs), glutathione S-transferases (GSTs), UDP-dependent glycosyltransferases (UGTs), and ABC transporters (ABCs). Among these enzymes, CYPs form one of the largest and functionally diverse superfamilies in plants (Werck-Reichhart and Feyereisen, 2000). Their heme-thiolate active sites enable a broad potential for oxidation, hydroxylation, O-demethylation, and other modifications that render an herbicide more soluble resulting in higher potential for further conjugation or sequestration (Brazier-Hicks et al., 2022; Dimaano and Iwakami, 2021; Werck-Reichhart, 2023). Several CYP families, including CYP71, CYP72, CYP81, and CYP709 have been implicated in metabolic resistance to ALS inhibiting herbicides (Dimaano et al., 2020b; Han et al., 2021; Saika et al., 2014; Werck-Reichhart, 2023; Xiang et al., 2006; Zhao et al., 2022). Within this group, the CYP81A subfamily has emerged repeatedly in grass weeds as a key contributor to NTSR, particularly in cases involving IM (Dimaano et al., 2020b; Yao et al., 2024). Although the diversity of CYP families and the complexity of the metabolic pathways that drive NSTR are difficult to resolve, recent advancement in genomic tools have begun to make this information more accessible to study (Montgomery et al., 2024; Montgomery et al., 2025a).

To investigate the basis of resistance in population A, assays using malathion, a known CYP inhibitor, were conducted to test for CYP involvement in NTSR (Soni et al., 2022). When applied in combination with IM, malathion reversed the resistance phenotype, indicating that CYP activity contributes to IM metabolism in this population. This provided the first direct evidence that population A relies on a NTSR mechanism that is likely driven by CYP metabolism. These

findings led to the key research question of which specific CYP genes are responsible for IM metabolism in population A and whether one or multiple CYP genes contribute to resistance within this population.

To address these questions, this research integrates transcriptomic and functional validation evidence to identify and characterize CYP enzymes involved in IM metabolism. After generating a segregating F_2 feral rye population, an RNA sequencing (RNA seq) experiment between resistant (R) and sensitive (S) F_2 plants was performed. Two CYP gene candidates, *CYP81A52* and *CYP721365*, emerged based on expression differences, and sequence homology to previously reported CYP that are involved in NTSR in ALS herbicides. To further elucidate the CYP candidate's roles in IM resistance, heterologous expression systems in *Arabidopsis thaliana (*Arabidopsis) and *Saccharomyces cerevisiae* (yeast) were utilized and combined with metabolite profiling, gene expression analysis, and sequence characterization. This combined approach provides a comprehensive foundation for determining whether one or multiple CYP pathways contribute to IM detoxification in this feral rye population.

MATERIALS AND METHODS

Establishment of homozygous F_2 feral rye lines

To generate a segregating F_2 feral rye population, controlled crosses were performed between herbicide-resistant (R) and susceptible (S) plants. Inflorescences from R plants were emasculated prior to anthesis, and pollen was collected from S plants and manually applied to the receptive stigmas of the emasculated spikes to promote cross-pollination. To confirm successful crossing, genomic DNA was extracted from R, S, and F_1 plants, and the protoporphyrinogen oxidase gene (SECCE5Rv1G0302760) was amplified through polymerase chain reaction (PCR)

and sent to sequence (Azenta, Genewiz, South Plainfield, NJ, USA). Sequence alignment and comparison of parental and F_1 alleles verified the presence of both parental genotypes in the hybrid progeny (Table S1). Confirmed F_1 hybrids from these crosses were subsequently self-pollinated to generate a F_2 generation. F_2 plants were used for downstream molecular analysis.

Plant materials, growth conditions, and chemical applications:

F_2 feral rye plants were sown directly in 3.8-cm by 3.8-cm by 5.8-cm pots containing LM-HP high porosity potting mix (Lambert, Rivière-Ouelle, QC, Canada) and grown in a greenhouse for two weeks under ambient temperature that was maintained within a range of 22–24 °C. Supplemental lighting from liquid halogen grow lights was used to sustain a 14 h light / 10 h dark photoperiod and relative humidity of ~75%. At two leaf stage, feral rye plants were treated with either 1% (v/v) methylated seed oil (MSO), and 5% (v/v) urea ammonium nitrate (UAN) (Untreated) or 36 g ha^{-1} of imazamox (IM) combined with 1% (v/v) MSO, and 5% (v/v) UAN (Treated). Applications were made using a calibrated single-nozzle track sprayer (DeVries Manufacturing, Hollandale, MN) delivering 187 L ha^{-1} spray volume.

RNA sequencing

Four biological replicates of F_2 susceptible (S) and resistant (R) feral rye plants were treated as described above. Plants were sampled zero and eight hours after application, the second fully expanded leaf was collected, snap frozen in liquid nitrogen, and stored in the -80ºC. Frozen tissue was ground to a fine powder in liquid nitrogen using a mortar and pestle, and total RNA was isolated with the Direct-zol™ RNA Miniprep Kit (Zymo Research, Irvine, CA, USA) following the manufacturer's protocol. RNA yield and purity were evaluated using a Qubit Fluorometer (Invitrogen, Thermo Scientific, Waltham, MA, USA). High-quality RNA samples were submitted to Novogene (Sacramento, CA, USA) for paired-end Illumina library preparation and sequencing.

Libraries were prepared according to standard protocols and sequenced to a depth of approximately 20 million paired-end reads (150 bp) per sample on an Illumina platform. Processed sequencing data were provided as FASTQ files for downstream analyses. Raw reads were assessed for quality using FastQC (Andrews, 2010), and adapter sequences and low-quality bases were trimmed using Trimmomatic (Bolger et al., 2014) with default parameters. Cleaned reads were aligned to the indexed cereal rye reference genome (Rabanus-Wallace et al., 2021) using STAR v2.7.9a (Dobin et al., 2013). Alignment rates averages 90-92%. Gene-level read counts were obtained with FeatureCounts v2.0.1 (Liao et al., 2014) and imported into R version 05.0+496 for differential expression analysis using the DESeq2 package (Love et al., 2014). Differential expression was defined as $\log_2$foldchange > 1 for upregulated and < -1 for downregulated, with an adjusted $P < 0.05$.

Protein-level annotation of predicted genes was conducted using the UniProt Swiss-Prot protein database. The Swiss-Prot FASTA dataset was downloaded from UniProt and formatted into a local protein database using BLAST+ v2.13.0 (Camacho et al., 2009). BLASTp alignments were performed against the Swiss-Prot database using default parameters in BLAST+, and the resulting hits were filtered to retain only high-confidence matches based on bit score criteria. Redundant alignments were removed, and unique UniProt accession identifiers from the filtered results were cross-referenced with the UniProt ID mapping database to retrieve corresponding gene names and functional annotations. These annotations were subsequently integrated with the RNA-seq differential expression dataset for downstream analyses.

Heterologous expression of CYPs in *Saccharomyces cerevisiae*

Full length coding sequence of candidate CYP genes were codon optimized for expression in *Saccharomyces cerevisiae* (Yeast) and synthesized (Azenta, Genewiz, South Plainfield, NJ,

USA). BamHI and EcoRI restriction sites were added at the 5′ and 3′ ends of the optimized gene sequence, respectively. The pUC vector and yeast expression vector pYED60 (Urban et al., 1997) was digested with 1 µL each of EcoRI and BamHI restriction enzymes in a reaction containing 500 ng of plasmid DNA, incubated at 37 °C for 1 hour. Digested products were run on a 1% agarose gel, and the target gene fragment was excised and purified using a DNA Gel Extraction Kit (New England Biolabs, Ipswich, MA, USA). A ligation reaction was performed on each CYP gene and the subsequent expression vector using T4 DNA Ligase (New England Biolabs, Ipswich, MA, USA). Ligated PCR products were transformed through heat-shock methods (Chang et al., 2017) and plated on LB agar supplemented with ampicillin. Following overnight incubation at 37 °C, PCR-positive colonies were cultured in LB broth with ampicillin at 37 °C and 220 rpm. Plasmid DNA was purified using the ZymoPURE™ Plasmid Miniprep Kit (Zymo Research, Irvine, CA, USA) and sequenced (Plasmidsaurus, Louisville, KY, USA) to confirm the correct gene insert identity and orientation. Verified constructs were then transformed into WAT11 yeast strains containing Arabidopsis genes for cytochrome P450 reductase 1 and 2 (Pompon et al., 1996; Urban et al., 1997) using the lithium acetate method (Ito et al., 1983). Successfully transformed yeast colonies were incubated with herbicide following previously described methods (Iwakami et al., 2019). Yeast transformants were first cultured in SGI medium (0.67% yeast nitrogen base without amino acids, 0.1% casamino acids, 40 µg mL^{-1} L-tryptophan, and 2% D-glucose) at 30 °C for 24 h. An aliquot from precultures was then transferred into YPD medium (1% yeast extract, 2% peptone, and 2% D-glucose) and incubated at 30 °C for another 24 h. 20% galactose was added to induce CYP expression and cultures were left to grow for an 14 h at 28ºC. Cells were collected by centrifugation for 5 min at 3000 rpm and 4ºC and resuspended in whole-cell assay buffer (100 mM potassium phosphate (pH 7.4), 7 mM magnesium sulfate, and 10 mM D-glucose). 500 µM

IM dissolved in water was added and cultures were incubated at room temperature. Samples were extracted at 0.5, 2 and 4 h of incubation and the reaction was stopped by adding 0.2% formic acid and 40% acetonitrile in water. Samples were centrifuged at 20 000 x g at 4 ºC for 5 min to separate the insoluble material. The resulting supernatant was processed by adding 5 mL of 5% acetic acid in acetonitrile along with a QuEChERS salt packet containing 1 g NaCl and 4 g $MgSO_4$ (Phenomenex, Torrance, CA, USA). The mixture was vortexed for 30 seconds to ensure thorough phase mixing and then centrifuged at 2 000 × g for 15 min. The upper layer was recovered, passed through a 13 mm × 0.2 µm nylon syringe filter (Econofltr Nyln, Agilent Technologies), and subsequently analyzed using liquid chromatography–tandem mass spectrometry (LC–MS/MS).

Heterologous expression of CYPs in *Arabidopsis thaliana*

Full length coding sequence of candidate CYP genes were synthesized (Azenta, Genewiz, South Plainfield, NJ, USA) and amplified with AscI and BamHI restriction site overhangs. The empty pFGC5941 vector was digested with same overhangs (New England Biolabs, Ipswich, MA, USA), and the CYP amplicons were ligated into the linearized vector using T4 DNA Ligase (New England Biolabs, Ipswich, MA, USA). The pFGC5941 vector drive transgene expression under the CaMV 35S promoter and terminates with OCS terminator. Ligation products were transformed into TOP10 competent *Escherichia coli* (Thermo Scientific, Waltham, MA, USA) via heat-shock transformation (Chang et al., 2017) and plated on LB agar supplemented with ampicillin. Following overnight incubation at 37 °C, PCR-positive colonies were cultured in LB broth with ampicillin at 37 °C and 220 rpm. Plasmid DNA was purified using the ZymoPURE™ Plasmid Miniprep Kit (Zymo Research, Irvine, CA, USA) and sequenced (Plasmidsaurus, Louisville, KY, USA) to confirm the correct gene insert identity and orientation. Verified constructs were then transformed into the GV3101 strain of *Agrobacterium tumefaciens* (Goldbio, St. Louis, Missouri,

USA). Colony PCR and sequencing (Plasmidsaurus, Louisville, KY, USA) confirmed the presence of the construct. Confirmed *Agrobacterium* colonies were subsequently used to transform Arabidopsis wild-type (WT) plants through floral dip methods (Clough and Bent, 1998). Arabidopsis plants were grown in a growth chamber at 22/18°C and a light intensity of 120 µE m^{-2} s^{-1} for 10/14h light/dark cycle. Transgenic T_1 seedlings were selected by spraying BASTA herbicide (BASF, Research Triangle Park, NC, USA) and confirmed with PCR for the transgene (Table S2). Selected T_1 lines were self-pollinated for two generations with BASTA selection at each generation to obtain T_3 progeny and increase homozygosity for the inserted transgene. Three independent transformation events from each construct were used for downstream characterization of IM resistance. When seedlings had four true leaves (~ 1 month) they were treated with 0.3, 0.7, 1.5, 3.0, 6.0 and 12 g ha^{-1} of IM with 1% (v/v) MSO, and 5% (v/v) UAN. Visual injury assessments were performed 14 days after treatment to evaluate resistance response. Leaf tissue was sampled 48 hours after application of 6 g ha -1 IM, washed in 20% (v/v) acetone, and ground in liquid nitrogen using a mortar and pestle. For metabolite analysis, frozen ground tissue was combined with 10 mL of water and 10 mL of acetonitrile containing 0.1% (v/v) formic acid, then homogenized thoroughly. Samples were shaken at room temperature for 20 min at 250 rpm and centrifuged (Sorvall X1 with TX400 rotor, Thermo Scientific, Waltham, MA, USA) for 10 min at 3,800 × g. The resulting supernatant was cleaned using a QuEChERS extraction packet (1 g NaCl and 4 g $MgSO_4$; Phenomenex, Torrance, CA, USA), vortexed for 15 s, and centrifuged again for 10 min at 3,800 × g. The final extract was filtered through a 13-mm, 0.2-µm nylon membrane (Econofltr Nyln, Agilent Technologies, Santa Clara, CA, USA) and injected into the LC–MS/MS system for quantification of IM and associated metabolites.

Liquid chromatography-mass spectrometry for imazamox parent and metabolite detection

A standard solution of IM (1 µg mL^{-1}) was prepared in methanol and used to generate calibration standards. Chromatographic separation and detection were performed using a Nexera X2 UPLC system equipped with two LC-30AD pumps, a SIL-30AC MP autosampler, a DGU-20A5 Prominence degasser, a CTO-30A column oven, and an SPD-M30A diode array detector coupled to an 8040 triple quadrupole mass spectrometer (Shimadzu, Kyoto, Japan). The analytical method was adapted from Demoliner et al. (2010). Samples were chromatographed on a Phenomenex Kinetex C18 column (100 × 4.6 mm, 5 µm, 100 Å; 00D-4601-E0) maintained at 40 °C. The mobile phases consisted of (A) water containing 0.1% formic acid and (B) acetonitrile with 0.1% formic acid. The gradient program was as follows: 30% B at 0 min, increased to 90% B at 4 min, held for 2 min, returned to 30% B at 6.1 min, and equilibrated at 30% B until 8 min. The flow rate was maintained at 0.4 mL min^{-1}, and samples were injected at a volume of 1 µL. Desmethyl-IM was analyzed under the same ionization and MRM settings. Representative chromatograms were obtained using a 1 ng IM standard (1 µL injection of a 1 µg mL^{-1} solution in methanol).

Statistical analysis

To assess differences between T3 transgenic Arabidopsis lines and WT plants, treatments were analyzed using a two-way analysis of variance, with Event, Treatment, and the interaction specified as fixed effects. When significant main or interaction effects were detected, estimated marginal means were calculated using the emmeans package (Lenth, 2016) in R. Pairwise comparisons were performed using Tukey's significant difference test to control for family-wise error. Compact letter displays were generated to summarize statistically distinct groups, with treatments or varieties sharing a letter not differing significantly at $P < 0.05$. All statistical analyses

were conducted in R (version 05.0+496), and assumptions of normality and homogeneity of variance were checked prior to interpretation.

Visual injury data from the IM dose response experiment were analyzed using nonlinear regression in R. Dose response curves for each Arabidopsis event were fitted using a four-parameter log-logistic model (LL.4) implemented in the drc package (Ritz et al., 2016). The LL.4 function estimates the upper limit (*d*), lower limit (*c*), slope around the inflection point (*b*), and the herbicide rate corresponding to 50% visual injury (ED_{50}). The general form of the model is:

$$Y = d/1 + \exp[b(\log X - logE)]$$

where *Y* is the observed injury response, *x* is the herbicide rate, *b* is the slope, *c* and *d* represent the lower and upper asymptotes, and ED_{50} corresponds to the imazamox rate required to cause 50% injury.

Differential expression analysis was performed using the DESeq2 pipeline in R. Raw count matrices were imported into a DESeqDataSet, with condition specified as the design factor. Genes with fewer than five total counts across all samples were removed prior to modeling to reduce noise from low abundance transcripts. Normalization and dispersion estimation were carried out using DESeq2 median-of-ratios approach, followed by fitting of negative binomial generalized linear models for each gene. The reference factor level was redefined sequentially to identify specific contrasts, including R untreated vs S untreated (RU vs. SU), S treated vs S untreated (ST vs. SU), R treated vs R untreated (RT vs. RU), and R treated vs S treated (RT vs. ST). Wald tests were used to assess differential expression, and contrasts were extracted using the results function with an alpha threshold of 0.05 or 0.1. To obtain effect-size estimates with reduced variance, $\log_2$ fold-change shrinkage was applied using the apeglm method for each comparison (Zhu et al., 2019). Shrunken estimates were used for ranking genes and determining significance thresholds.

Differentially expressed genes (DEGs) were defined based on adjusted P-values (Benjamini–Hochberg correction), with significance cutoffs of padj < 0.05. Volcano plots were generated to provide a visual summary of differential expression patterns for each contrast. For each comparison, $\log_2$ fold changes were plotted on the x-axis against the $-\log_{10}$ of the adjusted P-value on the y-axis. Reference lines were included to indicate significance thresholds (adjusted $P < 0.05$) and biologically meaningful fold-change cutoffs ($\log_2FC \geq 1$).

RESULTS

Differential gene expression patterns in resistant and susceptible feral rye following imazamox treatment

High quality reads from each R and S sample were aligned to the cereal rye reference genome (Rabanus-Wallace et al., 2021) to evaluate sequencing and mapping quality. Although this study focuses on feral rye, the *Secale cereale* reference genome was used for read alignment as it remains the only publicly available annotated genome for this species. Alignment success was high, with ~87–91% of mapped reads successfully assigned to annotated features, demonstrating strong compatibility between feral rye reads and the cereal rye reference genome (Table S3). Each library generated ~20–27 million mapped reads, and assignment rates were consistent across resistant (R) and susceptible (S) lines at both 0 h and 8 h timepoints, supporting reliable downstream differential expression analyses. Differential expression was evaluated across R and S feral rye biotypes that were untreated (U) and treated 8 h after application (T). This time point was selected based previous literature suggesting peak CYP activity is around 8 h after treatment with IM (Wright et al., 2018). The primary contrasts included treatment effects within each biotype

(RT vs. RU; ST vs. SU) and constitutive differences between biotypes under both untreated (RU vs. SU) and treated (RT vs. ST) conditions.

Constitutive gene expression differences between R and S were limited. Only 16 genes (10 upregulated and 6 downregulated) were differentially expressed in untreated samples (Figure 1C). A comparable number (12 total; 7 upregulated and 5 downregulated) were identified between R and S plants following IM treatment (Figure 1D). The limited number of constitutive DEGs in these contrasts between R and S individuals is likely due to the genetic recombination that occurred in generating the F_2, in that DEGs related to the resistance phenotype are more likely to be in common across the replicate R and S F_2 individuals. S plants were derived from F_2 individuals that did not survive IM treatment, which represents the most susceptible segregants within the same genetic background, compared to R plants that did survive IM treatment. This crossing approach minimizes background genetic variation that is commonly present when unrelated populations are compared (Keurentjes et al., 2007). Together, these results confirm that herbicide treatment induces a complex transcriptional response in both R and S phenotypes, and the untreated comparisons enable characterization of DEG responses linked to the resistance phenotype.

A clear transcriptional response to IM was observed in both R and S biotypes following treatment. Resistant plants exhibited a strong transcriptional response following IM treatment, with 2728 genes upregulated and 2726 downregulated passed the set thresholds (adjusted $p > 0.05$ and $\log_2$foldchange of $\pm$ 1) (Figure 1A.) S plants showed a similar response with 3164 genes were significantly upregulated and 3231 were downregulated (Figure 1B). These results indicate that herbicide exposure triggered widespread changes in gene expression across both R and S biotypes, consistent with the broad metabolic and stress response associated with herbicide metabolism.

Identification of candidate genes associated with imazamox resistance

To refine the list of genes potentially contributing to IM resistance, DEGs were compared across multiple treatment contrasts. Given the previously reported high constitutive expression of genes associated with NTSR in resistant plants (Aarthy et al., 2022; Giacomini et al., 2018; Zhao et al., 2022), particularly those encoding CYP450s (Dimaano et al., 2020b; Iwakami et al., 2014), a direct comparison between the R and S untreated contrast was considered (Figure 1D). Among the DEGs, only one CYP450 showed higher expression in untreated R plants compared to S (Table 1) and was annotated as *CYP81A52* (Gomes et al., 2025). Members of the CYP81A family have been proven to metabolize ALS herbicides (Han et al., 2021; Iwakami et al., 2014; Iwakami et al., 2019). Notably, *CYP81A24*, identified from a resistant population of *Echinochloa phyllopogon*, has been demonstrated to metabolize IM (Dimaano et al., 2020b). Similarly, *CYP81A104*, characterized from *Eleusine indica*, has also been demonstrated to catalyze the metabolism of imazamox (Yao et al., 2024), further supporting the involvement of the CYP81A subfamily in resistance to ALS-inhibiting herbicides, specifically IM. A BLAST search against the cereal rye genome (Rabanus-Wallace et al., 2021) revealed that the closest homolog to the previously characterized *CYP81A24* and *CYP81A104* genes is *CYP81A52* identified in the untreated contrast (Figure S1; Figure S2). Given the reported function of this gene family in *Echinochloa phyllopogon* and *Eleusine indica*, it is plausible that the corresponding *CYP81A52* gene may perform a similar role in the oxidative metabolism of IM, contributing to resistance. Examination of the RNA-seq data revealed no sequence polymorphisms between the R and S samples for this gene, suggesting that the observed differences in herbicide metabolism are likely attributable to differential gene expression rather than sequence variation. Therefore, only one sequence was considered from this candidate for further functional characterization.

Examining genes uniquely upregulated within specific contrasts helps to distinguish those directly associated with resistance from genes involved in general herbicide stress responses. A total of 335 genes were uniquely upregulated in the RT vs. RU contrast, representing transcripts induced in resistant plants following IM treatment that were not expressed in susceptible plants (Figure 2). Among this list of genes, 4 were annotated as CYPs, 1 as UGTs, no GSTs, and no ABC transporters were considered upregulated in resistant but not sensitive plants. Building on prior research in this FR population, CYPs have been established as the primary mechanism underlying resistance (Soni et al., 2022) and were considered as the primary candidate gene family for understanding the metabolism based resistance mechanism in this study. The single CYP450 identified as differentially expressed in resistant but not susceptible plants (*SECCE1Rv1G0003290*) was classified within the CYP72A gene family (Gomes et al., 2025). Members of the CYP72A subfamily in rice have previously been implicated in metabolism of bensulfuron-methyl, a sulfonylurea herbicide belonging to the ALS-inhibiting class (Saika et al., 2014). The over expression of this CYP, annotated as *CYP72A1365*, following IM treatment in resistant plants but not susceptible plants (Table 1) suggest that this enzyme may be contributing to the oxidative metabolism of IM, which would directly contribute to resistance. Analysis of RNA seq data revealed several sequence polymorphisms between R and S samples. These variants may alter the amino acid composition of the enzyme, potentially influencing the binding pocket or heme-binding domain configuration, both of which are critical for CYP450 activity (Brazier-Hicks et al., 2022; Dimaano and Iwakami, 2021). Such structural modifications could alter the herbicide binding affinity or reaction efficiency, directly influencing the potential to metabolize IM (Rigon et al., 2025; Shen et al., 2025). To evaluate this possibility, both R and S alleles of CYP72A1365

were functionally tested in heterologous systems based on their potential contribution to herbicide resistance in this study.

Functional characterization of candidate CYP450s in a transgenic *Arabidopsis* assay

T_3 transgenic Arabidopsis thaliana lines were generated for each candidate CYP gene to evaluate their potential contribution to IM resistance. Gene function was assessed using dose response experiments that included three independent transgenic events overexpressing CYP81A52, two independent transgenic events overexpressing CYP72A1365-R and CYP72A1365-S, and wild-type (WT) control plants. The dose response results demonstrate clear visual differences in IM sensitivity between WT and each CYP overexpressing lines (Figure 3, Figure S3). WT plants exhibited clear growth reduction and reached 50% injury at an ED_{50} of 0.75 g L^{-1}. In contrast, all three CYP81A52 overexpressing events showed significantly higher resistance to IM, with ED_{50} values of 2.78, 2.45, and 2.74 g L^{-1} for event #1, #2, and #3, respectively ($p < 0.05$ compared with WT). This corresponds to a 3.3- to 3.7-fold higher resistance relative to WT. Similar trends were observed for lines overexpressing CYP72A1365. WT plants again exhibited an ED50 of approximately 0.75 g L^{-1}, whereas CYP72A1365-R and CYP72A1365-S transgenic events displayed elevated tolerance to IM. The two CYP72A1365-R events reached 50% injury at ED_{50} values of 3.45 and 2.92 g L^{-1} for event #1 and #2, respectively, corresponding to approximately 3.9- to 4.6-fold higher resistance compared with WT ($p < 0.05$). The CYP72A1365-S lines also showed increased resistance, with ED50 values of 2.63 g L^{-1} for event #1 and 1.64 g L^{-1} for event #2, representing a 2.2- to 3.5-fold increase relative to WT ($p < 0.05$). Collectively, these results indicate that overexpression of both CYP72A1365 alleles confers enhanced IM resistance, although the magnitude of resistance varied among events and was generally lower for CYP72A1365-S compared with CYP72A1365-R.

To assess whether IM metabolism was enhanced in transgenic plants overexpressing CYP lines, the concentrations of IM and its O-demethylated metabolite were quantified in T_3 lines compared to WT (Figure 4). LC–MS/MS analysis revealed a significant reduction in the parent IM molecule 48 h after treatment (Figure 4A&C; Figure S4). Across the three CYP81A52 overexpressing events, parent IM levels were significantly lower than in the WT control, corresponding to a 2.4-fold reduction in CYP81A52 #1, a 1.9-fold reduction in CYP81A52 #2, and a 2.6-fold reduction in CYP81A52 #3 relative to the WT control ($p < 0.05$) (Figure 4A). Similarly, CYP72A1365 overexpressing lines exhibited reduced parent IM levels relative to the WT control (Figure 4C). CYP72A1365-R-#1 and CYP72A1365-R-#2 showed 2.1 to 2.3 fold reductions compared with WT ($p < 0.05$) and CYP72A1365-S lines also showed 1.5 and 1.7 fold reductions relative to WT. Statistical analysis indicated that CYP72A1365-R-#1, CYP72A1365-R-#2, and CYP72A1365-S-#2 accumulated significantly less parent IM than WT, while CYP72A1365-S-#1 was not significantly different compared to the WT control.

The accumulation of the O-demethylated IM metabolite was higher in CYP81A52 transgenic lines compared with the WT control (Figure 4B). Relative to WT, metabolite levels increased approximately 1.7-fold in CYP81A52-#1, 2.7-fold in CYP81A52-#2, and 2.2-fold in CYP81A52-#3. Statistical analysis indicated that CYP81A52-#2 and CYP81A52-#3 accumulated significantly higher levels of the O-demethylated IM metabolite compared with WT ($p < 0.05$), whereas CYP81A52-#1 showed an intermediate increase that was not statistically significant. Similarly, accumulation of the O-demethylated IM metabolite showed a similar trend in CYP72A1365 overexpressing lines (Figure 4D). Relative to WT, metabolite levels increased approximately 2.1-fold in CYP72A1365-R-#1, 4.0-fold in CYP72A1365-R-#2, 2.1-fold in CYP72A1365-S-#1, and 2.4-fold in CYP72A1365-S-#2. Statistical analysis indicated that both

CYP72A1365-R events accumulated significantly higher metabolite levels than WT ($p > 0.05$), whereas both CYP72A1365-S events were not significantly different from WT, despite showing increased metabolite accumulation (Figure 4D).

Functional characterization of candidate CYP450s in a Yeast metabolism assay

To investigate the ability of each candidate CYP450 to metabolize IM, recombinant proteins were expressed in a yeast system co-expressing NADPH-CYP450 reductase from Arabidopsis (Pompon et al., 1996). Yeast cells transformed with each candidate CYP were cultured following the procedures of Iwakami et al. (2019), with IM added to a final concentration of 500 μM. Cultures were sampled at 0.5 and 4 h after IM addition and analyzed by LC-MS/MS. CYP72A1365 R, CYP72A1365 S, and CYP81A52 showed a clear reduction in the parent IM signal after 4 h of incubation compared to the empty vector control that showed no reduction in parent IM over time (Figure 5). Although a clear reduction in parent IM was observed in CYP72A1365 R and CYP81A52, no detectable increase in the expected O-demethylated IM metabolite was observed in any of the yeast cultures. While O-demethylated metabolites have been reported in other in vitro yeast assays for several other ALS-inhibiting herbicides (Iwakami et al., 2014; Zhao et al., 2022), an O-demethylated derivative of IM has not previously been described. Based on the reduction in parent IM observed relative to the control, an increase in the corresponding metabolite would normally be expected; however, this was not evident in this experiment.

DISCUSSION

This research demonstrates that the feral rye population previously shown to lack ALS target-site polymorphisms (Soni et al., 2022) instead exhibits a NTSR mechanism involving IM

metabolism mediated by CYP activity. Analysis of the ALS transcripts from the transcriptomic data revealed no non-synonymous mutations in either the R or S biotypes. Consistent with Soni et al. (2022), these results exclude target-site resistance as a mechanism in these populations (Figure S5). The combined expression and functional validation data provide strong evidence that metabolic herbicide detoxification, rather than alterations at the target enzyme, underlies resistance in this population. CYPs have been shown to catalyze the metabolism of a wide range of herbicide chemistries through hydroxylation, demethylation, and other reactions that increase compound solubility and facilitate conjugation or sequestration (Abdollahi et al., 2021; Brazier-Hicks et al., 2022; Dimaano and Iwakami, 2021). Among these CYPs, members of the CYP81A and CYP72A gene families have previously reported activity against herbicides spanning multiple distinct chemical classes (Guo et al., 2019; Han et al., 2021; Iwakami et al., 2014; Rigon et al., 2025; Saika et al., 2014).

Functional and regulatory evidence supporting *CYP81A52* as a driver of imazamox metabolism

Based on the RNA seq results, *CYP81A52* emerged as a strong candidate for functional validation, given its higher constitutive expression in R relative to S plants under untreated conditions (Figure 1D). This observation is consistent with previous work demonstrating that members of the CYP81A gene family can confer resistance to multiple herbicide classes. Notably, *CYP81A52* in *E. phyllopogon* and *CYP81A104* in *E. indica* have been proven to metabolize a broad suite of ALS inhibitors, including IM (Dimaano et al., 2020b; Iwakami et al., 2019; Pan et al., 2022; Yao et al., 2024). These findings are consistent with the resistance profile observed in the feral rye population, supporting the possibility that CYP81A may contribute to similar resistance patterns across species. To further confirm this relationship and define the specific role of

CYP81A52 in IM metabolism, heterologous expression systems were employed in Arabidopsis and yeast.

Heterologous expression of CYP81A52 confirms its role in metabolic imazamox resistance

Overexpression of *CYP81A52* produced a consistent 3.3- to 3.7-fold increase in ED_{50} relative to the WT Arabidopsis (Figure 3A), demonstrating that this gene confers increased resistance in planta. The reproducibility of the resistance phenotype across three independent events indicates that the response is attributable to CYP81A52 activity rather than positional effects, supporting its role as a primary metabolic driver.

Additionally, each independent *CYP81A52* event showed degradation of IM parent (Figure 4A) in addition to the formation of the O-demethylated metabolite (Figure 4B). The detection of both IM degradation and the increased O-demethylated IM metabolite in the transgenic Arabidopsis lines provides direct evidence that the *CYP81A52* catalyzes the IM detoxification reaction. This metabolic pattern is consistent with the previously reported accumulation of O-demethylated derivatives observed in the resistant feral rye population (Soni et al., 2022), which provides enough evidence to support that *CYP81A52* gene retains its functional capacity for IM metabolism in planta and is likely contributing to metabolic resistance. Importantly, the same O-demethylated metabolite has been identified as the primary detoxification product accumulating in resistant lines in various other grass species (Dimaano et al., 2020b; Zhao et al., 2022). Together, these findings support that *CYP81A52* in feral rye operates through a conserved O-demethylation pathway shared among grass species, contributing to the enhanced metabolic detoxification and NTSR phenotype observed in resistant plants.

Evaluation of CYP81A52 catalytic activity in a yeast expression system

The yeast system also demonstrated that *CYP81A52* is capable of metabolizing IM, with a clear reduction in the parent IM structure over time (Figure 5). However, no corresponding increase in the expected O-demethylated metabolite was detected, suggesting that yeast metabolism or compound stability may influence metabolite recovery. The absence of this metabolite may be explained by several factors. The sampling times used (4 h) may have been too early to capture metabolite accumulation, or the parent compound may have already undergone further transformation into another downstream product that could not be identified due to the lack of an analytical standard. It is also possible that the O-demethylated metabolite is unstable or toxic to yeast cells, leading to its sequestration into intracellular compartments such as the vacuole or rapid conversion into less toxic conjugates, thereby reducing its detectable concentration in the extract. Additionally, the QuEChERS extraction method used may not efficiently recover partially conjugated or highly polar metabolites, resulting in their loss in the insoluble fraction and limited retention during LC-MS/MS analysis. Future experiments incorporating expanded time points and optimized extraction protocols will help determine whether the O-demethylated metabolite is transient, unstable, or further metabolized within yeast cells.

The combined results of both expression systems provide evidence that *CYP81A52* mediates the metabolism of IM. The yeast assays confirmed enzymatic activity through a measurable reduction of the parent compound, while the transgenic Arabidopsis lines demonstrated both IM degradation and accumulation of the O-demethylated metabolite.

Absence of coding variation indicates regulatory control of CYP81A52 expression

The lack of sequence variation in the CYP coding region between R and S plants suggests that the resistance phenotype is not conferred by an alteration in the enzyme catalytic function, but rather by differential gene regulation. This implies that R plants have evolved a mechanism that alters the expression of this gene and enables a more rapid detoxification response upon exposure to IM. Enhanced expression of herbicide metabolism related genes, particularly CYPs, has been reported in several grass species exhibiting NTSR. In *L. rigidum*, strong overexpression of *CYP81A10v7* has been linked with broad spectrum metabolic resistance, although the specific regulatory mechanisms driving this expression differences remain unresolved (Han et al., 2021). Similarly, in *E. phyllopogon,* multiple CYP81A genes were had high expression in resistant plants despite identical coding sequences to susceptible plants (Dimaano et al., 2020). The consistent observation of differential CYP expression among resistant populations across species indicates that transcriptional regulation likely plays a central role in the evolution of metabolic resistance. Such constitutive overexpression is typically linked with promoter sequence variation, gene duplication, or altered transcriptional regulation that results in increased basal or inducible activity (Bass and Field, 2011; Dimaano and Iwakami, 2021). This has previously been observed in *Drosophila melanogaster*, where insertion of a transposable element upstream of a CYP gene created a new enhancer sequence, resulting in elevated expression and resistance to DDT (Daborn et al., 2002). In plants, *Amaranthus palmeri* showed polymorphisms in the promoter region of *CYP72A1182* that were linked to increased expression and metabolic resistance to tembotrione, while QTL mapping suggested that trans-acting factors may also contribute to its regulation (Rigon et al., 2025). Conversely, in *Eleusine indica*, no single nucleotide polymorphisms were detected in the promoter region of *CYP81A104* between resistant and susceptible plants, indicating that overexpression of this gene is likely driven by a trans-regulatory element rather than promoter

variation (Yao et al., 2024). The expression pattern observed in the resistant feral rye population aligns with these findings, where higher constitutive expression of *CYP81A52* genes was detected in the absence of herbicide treatment. Such expression differences suggest that regulatory mechanisms, rather than sequence variation in the coding region is likely driving resistance in this population. Given this information, future work examining promoter sequence variation, gene copy number differences, and transcription factor involvement will be essential to determine whether cis- or trans-acting regulation underlies this elevated constitutive CYP activity and contributes to metabolic resistance in feral rye.

The data presented throughout this research contributes to the growing body of evidence that CYP81A gene families play a central role in metabolic based herbicide resistance across grass species. Feral rye can now be included among other resistant grass weeds, such as *E. phyllopogon*, *E. indica*, and *L. rigidum*, all of which exhibit multiple CYP81A isoforms capable of catalyzing the metabolism of ALS inhibiting herbicides (Dimaano et al., 2020b; Han et al., 2021; Iwakami et al., 2019; Pan et al., 2022; Yao et al., 2024). This reoccurring pattern further supports the previously stated concept of convergent evolution, in which distinct species that are spactially separated independently arrive at similar metabolic resistance mechanisms involving CYP81A genes (Han et al., 2021). Unlike the well documented examples of convergent evolution in TSR, where identical mutations arise in ALS target sites (Kreiner et al., 2018), NTSR represents a more complicated system involving multiple genes and elaborate regulatory systems, making it more complex to pinpoint the exact molecular convergence events. The recurring evidence of CYP81A mediated metabolic resistance across multiple grass species underscores the need to develop preemptive diagnostic tools that can provide an early warning system for the emergence of

metabolic resistance in field populations, thereby enabling more targeted and sustainable herbicide management strategies.

Functional and regulatory evidence supporting *CYP72A1365* as a driver of Imazamox metabolism

CYP72A1365 emerged as an additional candidate for functional validation due to its increased transcript abundance in R plants relative to S plants following IM treatment (Figure 1C). Members of the CYP72A family have previously been implicated in resistance to several herbicides, including sulfonylureas (Saika et al., 2014), although to our knowledge there are currently no reports directly linking this family to IM metabolism. Given the established role of CYP72A enzymes in sulfonylurea detoxification, we hypothesized that *CYP72A1365* may similarly contribute to IM metabolism. Accordingly, *CYP72A1365* was selected as a second candidate for heterologous expression to functionally evaluate its role in IM resistance.

Functional characterization of CYP72A1365 in transgenic Arabidopsis

Overexpression of *CYP72A1365* in Arabidopsis increased IM resistance, supporting its contribution to metabolic resistance in feral rye. Both R and S alleles conferred increased ED_{50} values relative to the WT control (Figure 3B), indicating that *CYP72A1365* is capable of metabolizing IM. Although both R and S alleles proved to increase resistance, the reduced ED_{50} values observed in the CYP72A1365-S events indicate functional differences between the sequences. Similarly, degradation of the IM parent compound (Figure 4C) accompanied by increased accumulation of the O-demethylated metabolite (Figure 4D) was observed in *CYP72A1365* overexpression events. This pattern was most pronounced in the R events, whereas *CYP72A1365*-S-#1 exhibited less reduction of the parent compound and lower accumulation of

the O-demethylated metabolite, consistent with its reduced resistance phenotype. The reduction in IM parent levels and increase in the O-demethylated metabolite provides further evidence that *CYP72A1365* catalyzes IM detoxification in planta. This metabolic profile confirms the accumulation of O-demethylated derivatives previously reported in resistant feral rye (Soni et al., 2022), supporting the conclusion that *CYP72A1365* retains functional capacity for IM metabolism. Moreover, the formation of the same O-demethylated metabolite observed across multiple resistant grass species suggests that *CYP72A1365* participates in a conserved oxidative detoxification pathway contributing to NTSR.

The lower resistance factor, decreased reduction parent IM, and lower accumulation of O-demethylated metabolite in S events relative to R events indicate functional divergence between the *CYP72A1365* alleles. These differences may arise from variation in gene regulation, enzyme activity, or both. This interpretation is consistent with the RNA seq results, which showed higher transcript abundance in R plants compared to S plants following IM treatment (Table 1), suggesting that regulatory differences contribute to the resistance phenotype. In addition, sequence polymorphisms identified between the R and S alleles may alter enzyme structure, substrate binding affinity, or catalytic efficiency, ultimately influencing the rate of IM metabolism. Similar allele specific effects on herbicide metabolism have been reported for CYP mediated resistance in other grass species, where coding variation or differential expression resulted in altered detoxification capacity (Dimaano et al., 2020b; Rigon et al., 2025; Yao et al., 2024). Collectively, these findings suggest that the S allele retains less baseline metabolic activity, whereas sequence or regulatory differences in the R allele enhance IM metabolic efficiency. Regardless of the precise mechanism, the data demonstrate that *CYP72A1365* contributes to IM metabolism and support the

hypothesis that multiple CYP enzymes may act together to confer NTSR in this feral rye population.

Evaluation of CYP81A52 catalytic activity in a yeast expression system

Thus far, the heterologous yeast assays indicate that both the R and S alleles of *CYP72A1365* are capable of metabolizing IM, as evidenced by the reduction in the parent compound over time (Figure 5). However, the expected O-demethylated metabolite was not detected, likely for the reasons outlined above. The reduction in the parent structure in both the R and S sequence provide a strong foundation that this gene acts in the same way as *CYP81A52*.

Next steps will involve determining whether *CYP72A1365* functions independently or in coordination with *CYP81A52* to confer resistance in this population. It remains unclear whether one of these enzymes is sufficient on its own to impart a resistant phenotype, or whether their activities are complementary, either acting on different metabolic steps or contributing additively to overall detoxification capacity. Resolving this relationship will require functional assays that test each gene individually and in combination, ideally through stacked overexpression lines or through gene editing approaches. Such work will help clarify whether resistance arises from a single dominant metabolic pathway or from a broader network of CYP mediated processes working together within this resistant feral rye population.

CONCLUSION

NTSR in feral rye is mediated by CYP dependent herbicide metabolism. Functional validation through heterologous expression demonstrated that *CYP81A52* confers resistance by catalyzing the oxidative metabolism of IM, supporting its role as a key enzyme in detoxification. The observed degradation of the parent IM structure and accumulation of the O-demethylated

metabolite in *A. thaliana* lines expressing *CYP81A52* provide direct evidence of its ability to confer resistance.

Conversely, *CYP72A1365* showed higher expression in R plants compared to S and exhibited various SNPs that may affect herbicide binding and catalytic efficiency. Although the yeast assay confirmed reduced IM parent levels in the R variant, further testing and protein modeling are required to fully define its contribution to resistance and identify key amino acid changes that could be linked to IM metabolism. Having identified *CYP81A52* and *CYP72A1365* as functional candidates, future work should investigate their potential role in cross resistance.

Collectively, this research establishes *CYP81A52* as a major determinant of metabolic resistance to imazamox in feral rye and highlights *CYP72A1365* as an additional candidate requiring further investigation. Understanding the molecular basis and regulatory control of these CYPs will be essential for developing predictive diagnostics and sustainable herbicide resistance management strategies.

TABLES

Table 1. Normalized counts and differential expression values for *CYP72A1365* and *CYP81A52*.
Log_2foldchange (L2FC), adjusted p-value (Padj), and average normalized gene count across resistant (R) and susceptible (S) plants for *CYP72A1365* and *CYP81A52.*

Gene ID	Gene Name	L2FC	Padj	R Untreated	S Untreated	R Treated	S Treated
SECCE1Rv1G0003290	*CYP72A1365*	1.37	0.033	342	599	1266	268
SECCE5Rv1G0354110	*CYP81A52*	1.48	$8.74x10^{3}$	1161	229	403	378

FIGURES

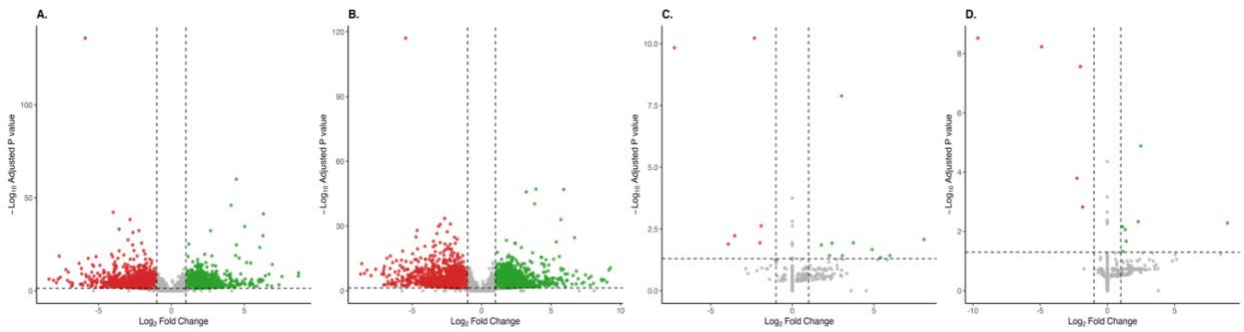

Figure 1. Differential gene expression contrasts between resistant and susceptible *S. cereale* biotypes.

Volcano plots depict transcriptomic shifts for each pairwise comparison: (A) resistant treated compared to resistant untreated, (B) susceptible treated compared to susceptible untreated, (C) resistant treated compared to susceptible treated, and (D) resistant untreated compared to susceptible untreated. Each point represents an individual gene, positioned by its $\log_2$foldchange (x-axis) and $-\log_{10}$(Q value) (y-axis). Genes surpassing significance thresholds **(**$Q < 0.05$ and log2FC > 1**)** appear as green points (upregulated) or red points (downregulated), while non-significant genes remain black. Vertical dashed lines indicate the ± 1 $\log_2$ fold-change cutoffs, and the horizontal dashed line marks the $Q = 0.05$ significance boundary.

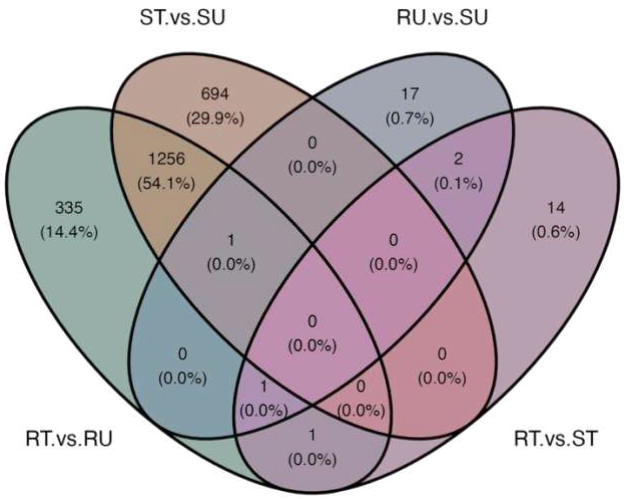

Figure 2. Overlap of differentially expressed genes among four *S. cereale* contrasts.
A four-set Venn diagram summarizing shared and unique differentially expressed genes (DEGs) among the resistant treated compared to resistant untreated (RTvsRU), susceptible treated compared to susceptible untreated (STvsSU), resistant treated compared to susceptible treated (RTvsST)**,** and resistant untreated compared to susceptible untreated (RUvsSU) contrasts. Each colored region represents DEGs unique to a specific contrast, while overlapping segments indicate genes jointly differentially expressed across multiple contrasts. Values within each segment denote the number of DEGs and their proportional contribution to the total DEG set.

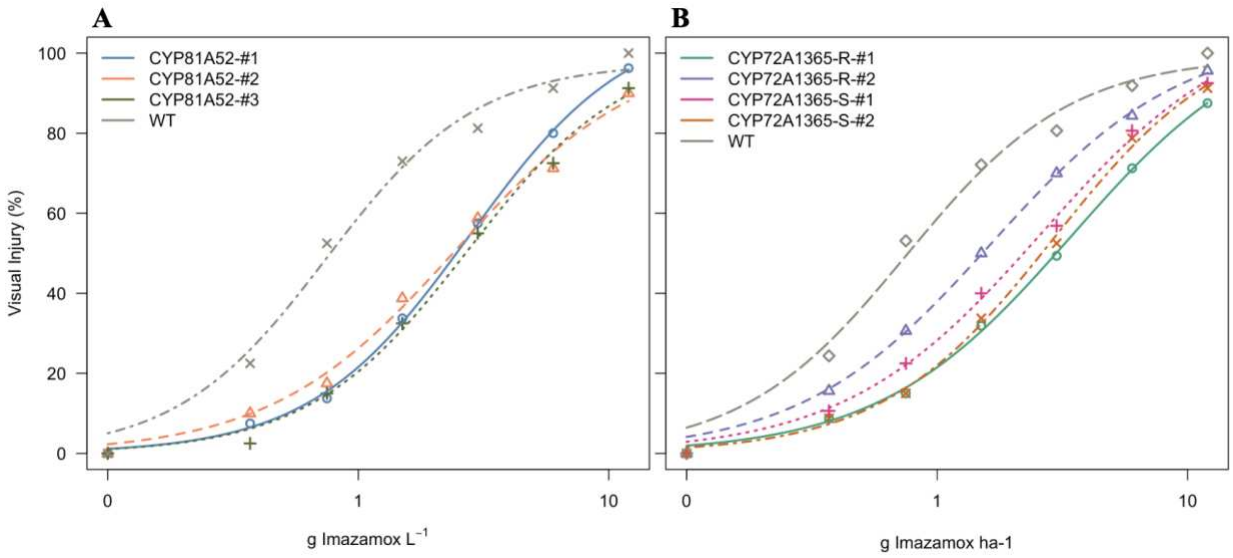

Figure 3. Dose response of wild type Arabidopsis compared with *CYP81A52* and *CYP72A1365* overexpressing lines following imazamox treatment.
Visual injury was quantified in wild type (WT) plants and transgenic lines, including (A) three independent *CYP81A52* events and (B) two resistant (R) and two sensitive (S) *CYP72A1365* events, across imazamox (IM) rates of 0.3, 0.7, 1.5, 3.0, 6.0, and 12 g ha^{-1}, applied with 1% (v/v) methylated seed oil (MSO) and 5% (v/v) urea ammonium nitrate (UAN).

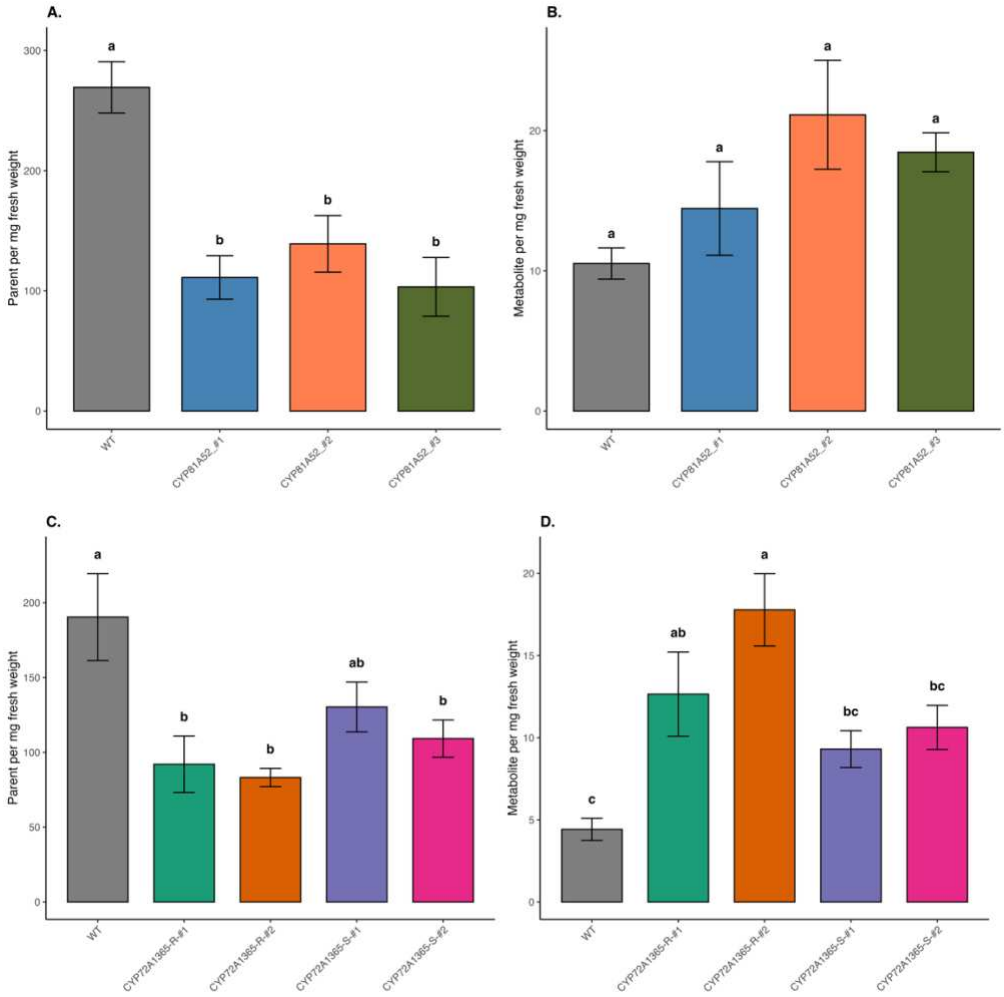

Figure 4. Concentration of parent imazamox (IM) and its O-demethylated metabolite in WT and CYP-overexpressing *Arabidopsis* lines.

(A) Concentrations of the parent imazamox (IM) and (B) its O-demethylated metabolite were measured 48 h after IM application in wild-type (WT) Arabidopsis and three independent *CYP81A52* overexpression events. (C) Concentrations of the parent IM and (D) its O demethylated metabolite were measured in WT and CYP72A1365 overexpression lines 48 h after IM treatment. Bars represent mean ± SE, and different letters denote significant differences among genotypes ($p < 0.05$).

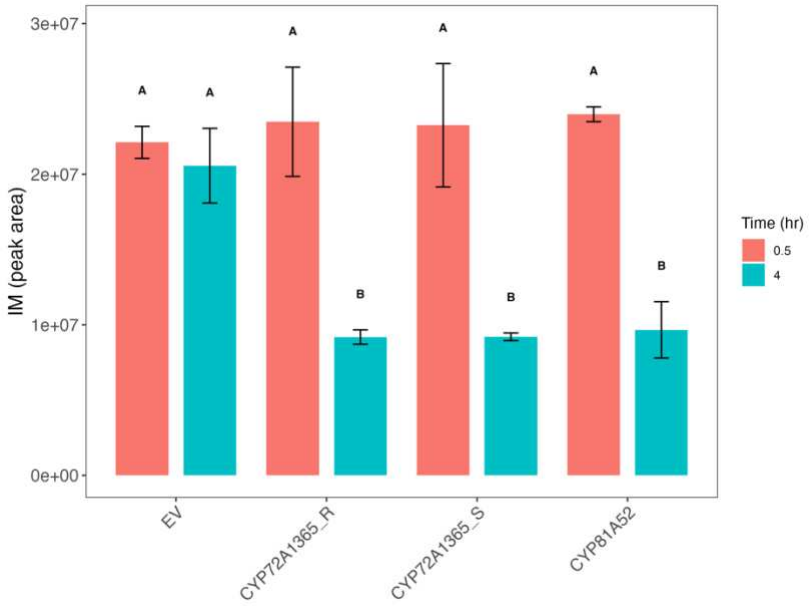

Figure 5. Relative IM accumulation in yeast expressing CYP72A1365 and CYP81A52 across two time points.

Mean IM (peak area) measured in yeast strains expressing CYP72A1365 R, CYP72A1365 S, CYP81A52, and the empty-vector control (EV) at 0.5 h and 4 h post-treatment. Bars represent the mean ± standard error.

REFERENCES

1. Aarthy, Thiagarayaselvam, Chandrima Shyam and Mithila Jugulam 2022. Rapid metabolism and increased expression of CYP81E8 gene confer high level of resistance to tembotrione in a multiple-resistant Palmer amaranth (Amaranthus palmeri S. Watson). Frontiers in Agronomy Volume 4 - 2022. doi: 10.3389/fagro.2022.1010292
2. Abdollahi, Fatemeh, Mohammad Taghi Alebrahim, Chheng Ngov, Etienne Lallemand, Yongxiang Zheng, Claire Villette, Julie Zumsteg, François André, Nicolas Navrot, Danièle Werck-Reichhart and Laurence Miesch 2021. Innate promiscuity of the CYP706 family of P450 enzymes provides a suitable context for the evolution of dinitroaniline resistance in weed. New Phytologist 229: 3253–3268. doi: https://doi.org/10.1111/nph.17126
3. Bass, C. and L. M. Field 2011. Gene amplification and insecticide resistance. Pest Manag Sci 67: 886–890. doi: 10.1002/ps.2189
4. Bolger, Anthony M., Marc Lohse and Bjoern Usadel 2014. Trimmomatic: a flexible trimmer for Illumina sequence data. Bioinformatics 30: 2114–2120. doi: 10.1093/bioinformatics/btu170
5. Brady, Thomas M., Barrington Cross, Robert F. Doehner, John Finn and David L. Ladner 1998. The Discovery of Imazamox, a New Broad-Spectrum Imidazolinone Herbicide. In Synthesis and Chemistry of Agrochemicals V, 30–37: American Chemical Society.
6. Brazier-Hicks, Melissa, Sara Franco-Ortega, Philip Watson, Blandine Rougemont, Jonathan Cohn, Richard Dale, Tim R. Hawkes, Alina Goldberg-Cavalleri, Nawaporn Onkokesung and Robert Edwards 2022. Characterization of Cytochrome P450s with Key Roles in Determining Herbicide Selectivity in Maize. ACS Omega 7: 17416–17431. doi: 10.1021/acsomega.2c01705
7. Camacho, C., G. Coulouris, V. Avagyan, N. Ma, J. Papadopoulos, K. Bealer and T. L. Madden 2009. BLAST+: architecture and applications. BMC Bioinformatics 10: 421. doi: 10.1186/1471-2105-10-421
8. Carter, Arron H., Jennifer Hansen, Thomas Koehler, Donald C. Thill and Robert S. Zemetra 2007. The Effect of Imazamox Application Timing and Rate on Imazamox Resistant Wheat Cultivars in the Pacific Northwest. Weed Technology 21: 895–899. doi: 10.1614/WT-07-025.1
9. Clough, S. J. and A. F. Bent 1998. Floral dip: a simplified method for Agrobacterium-mediated transformation of Arabidopsis thaliana. Plant J 16: 735–743. doi: 10.1046/j.1365-313x.1998.00343.x
10. Daborn, P. J., J. L. Yen, M. R. Bogwitz, G. Le Goff, E. Feil, S. Jeffers, N. Tijet, T. Perry, D. Heckel, P. Batterham, R. Feyereisen, T. G. Wilson and R. H. ffrench-Constant 2002. A single p450 allele associated with insecticide resistance in Drosophila. Science 297: 2253–2256. doi: 10.1126/science.1074170
11. Délye, Christophe 2013. Unravelling the genetic bases of non-target-site-based resistance (NTSR) to herbicides: a major challenge for weed science in the forthcoming decade. Pest Management Science 69: 176–187. doi: https://doi.org/10.1002/ps.3318
12. Dimaano, Niña Gracel and Satoshi Iwakami 2021. Cytochrome P450-mediated herbicide metabolism in plants: current understanding and prospects. Pest Management Science 77: 22–32. doi: https://doi.org/10.1002/ps.6040
13. Dimaano, Niña Gracel, Takuya Yamaguchi, Kanade Fukunishi, Tohru Tominaga and Satoshi Iwakami 2020. Functional characterization of cytochrome P450 CYP81A

subfamily to disclose the pattern of cross-resistance in Echinochloa phyllopogon. Plant Molecular Biology 102: 403–416. doi: 10.1007/s11103-019-00954-3
14. Dobin, A., C. A. Davis, F. Schlesinger, J. Drenkow, C. Zaleski, S. Jha, P. Batut, M. Chaisson and T. R. Gingeras 2013. STAR: ultrafast universal RNA-seq aligner. Bioinformatics 29: 15–21. doi: 10.1093/bioinformatics/bts635
15. Gaines, Todd A., Stephen O. Duke, Sarah Morran, Carlos A. G. Rigon, Patrick J. Tranel, Anita Küpper and Franck E. Dayan 2020. Mechanisms of evolved herbicide resistance. Journal of Biological Chemistry 295: 10307–10330. doi: https://doi.org/10.1074/jbc.REV120.013572
16. Geier, Patrick W., Phillip W. Stahlman, Anthony D. White, Stephen D. Miller, Craig M. Alford and Drew J. Lyon 2004. Imazamox for Winter Annual Grass Control in Imidazolinone-Tolerant Winter Wheat. Weed Technology 18: 924–930. doi: 10.1614/WT-03-115R1
17. Giacomini, Darci A, Todd Gaines, Roland Beffa and Patrick J Tranel 2018. Optimizing RNA-seq studies to investigate herbicide resistance. Pest Management Science 74: 2260–2264. doi: https://doi.org/10.1002/ps.4822
18. Gomes, Anthony Côrtes, Jacob Montgomery, André Lucas Simões Araujo, Sarah Morran, Luan Cutti, Eric Patterson, Sofia Marques Hill, Maor Matzrafi, Anil Shrestha, Aldo Merotto, Fatemeh Abdollahi, David R Nelson, Victor Llaca, Kevin Fengler, Camila Ferreira de Pinho and Todd A Gaines 2025. Chromosome-Level Assemblies of the Allohexaploid Genomes of Conyza sumatrensis and Conyza bonariensis. Genome Biology and Evolution 17. doi: 10.1093/gbe/evaf065
19. Guo, Feng, Satoshi Iwakami, Takuya Yamaguchi, Akira Uchino, Yukari Sunohara and Hiroshi Matsumoto 2019. Role of CYP81A cytochrome P450s in clomazone metabolism in Echinochloa phyllopogon. Plant Science 283: 321–328. doi: https://doi.org/10.1016/j.plantsci.2019.02.010
20. Han, H., Q. Yu, R. Beffa, S. González, F. Maiwald, J. Wang and S. B. Powles 2021. Cytochrome P450 CYP81A10v7 in Lolium rigidum confers metabolic resistance to herbicides across at least five modes of action. Plant J 105: 79–92. doi: 10.1111/tpj.15040
21. Heap, Ian 2014. Global perspective of herbicide-resistant weeds. Pest Management Science 70: 1306–1315. doi: https://doi.org/10.1002/ps.3696
22. Ito, H., Y. Fukuda, K. Murata and A. Kimura 1983. Transformation of intact yeast cells treated with alkali cations. J Bacteriol 153: 163–168. doi: 10.1128/jb.153.1.163-168.1983
23. Iwakami, S., M. Endo, H. Saika, J. Okuno, N. Nakamura, M. Yokoyama, H. Watanabe, S. Toki, A. Uchino and T. Inamura 2014. Cytochrome P450 CYP81A12 and CYP81A21 Are Associated with Resistance to Two Acetolactate Synthase Inhibitors in Echinochloa phyllopogon. Plant Physiol 165: 618–629. doi: 10.1104/pp.113.232843
24. Iwakami, S., Y. Kamidate, T. Yamaguchi, M. Ishizaka, M. Endo, H. Suda, K. Nagai, Y. Sunohara, S. Toki, A. Uchino, T. Tominaga and H. Matsumoto 2019. CYP81A P450s are involved in concomitant cross-resistance to acetolactate synthase and acetyl-CoA carboxylase herbicides in Echinochloa phyllopogon. New Phytol 221: 2112–2122. doi: 10.1111/nph.15552
25. Jugulam, Mithila and Chandrima Shyam 2019. Non-Target-Site Resistance to Herbicides: Recent Developments. Plants 8: 417.
26. Keurentjes, J. J., L. Bentsink, C. Alonso-Blanco, C. J. Hanhart, H. Blankestijn-De Vries, S. Effgen, D. Vreugdenhil and M. Koornneef 2007. Development of a near-isogenic line

population of Arabidopsis thaliana and comparison of mapping power with a recombinant inbred line population. Genetics 175: 891–905. doi: 10.1534/genetics.106.066423
27. Kreiner, J. M., J. R. Stinchcombe and S. I. Wright 2018. Population Genomics of Herbicide Resistance: Adaptation via Evolutionary Rescue. Annu Rev Plant Biol 69: 611–635. doi: 10.1146/annurev-arplant-042817-040038
28. Lenth, Russell V. 2016. Least-Squares Means: The R Package lsmeans. Journal of Statistical Software 69: 1 – 33. doi: 10.18637/jss.v069.i01
29. Montgomery, Jacob, Sarah Morran, Dana R. MacGregor, J. Scott McElroy, Paul Neve, Célia Neto, Martin M. Vila-Aiub, Maria Victoria Sandoval, Analia I. Menéndez, Julia M. Kreiner, Longjiang Fan, Ana L. Caicedo, Peter J. Maughan, Bianca Assis Barbosa Martins, Jagoda Mika, Alberto Collavo, Aldo Merotto, Nithya K. Subramanian, Muthukumar V. Bagavathiannan, Luan Cutti, Md Mazharul Islam, Bikram S. Gill, Robert Cicchillo, Roger Gast, Neeta Soni, Terry R. Wright, Gina Zastrow-Hayes, Gregory May, Jenna M. Malone, Deepmala Sehgal, Shiv Shankhar Kaundun, Richard P. Dale, Barend Juan Vorster, Bodo Peters, Jens Lerchl, Patrick J. Tranel, Roland Beffa, Alexandre Fournier-Level, Mithila Jugulam, Kevin Fengler, Victor Llaca, Eric L. Patterson and Todd A. Gaines 2024. Current status of community resources and priorities for weed genomics research. Genome Biology 25: 139. doi: 10.1186/s13059-024-03274-y
30. Montgomery, Jacob S., Jan E. Leach, Stephen L. Young and Todd A. Gaines 2025. Using weedy traits in crops as part of a new green revolution. New Phytologist 247: 1071–1074. doi: https://doi.org/10.1111/nph.70224
31. Newhouse, K. E., W. A. Smith, M. A. Starrett, T. J. Schaefer and B. K. Singh 1992. Tolerance to imidazolinone herbicides in wheat. Plant Physiol 100: 882–886. doi: 10.1104/pp.100.2.882
32. Pan, Lang, Qiushuang Guo, Junzhi Wang, Li Shi, Xiao Yang, Yaoyu Zhou, Qin Yu and Lianyang Bai 2022. CYP81A68 confers metabolic resistance to ALS and ACCase-inhibiting herbicides and its epigenetic regulation in Echinochloa crus-galli. Journal of Hazardous Materials 428: 128225. doi: https://doi.org/10.1016/j.jhazmat.2022.128225
33. Pester, Todd A., Scott J. Nissen and Philip Westra 2001. Absorption, translocation, and metabolism of imazamox in jointed goatgrass and feral rye. Weed Science 49: 607–612. doi: 10.1614/0043-1745(2001)049[0607:ATAMOI]2.0.CO;2
34. Pompon, D., B. Louerat, A. Bronine and P. Urban 1996. Yeast expression of animal and plant P450s in optimized redox environments. Methods Enzymol 272: 51–64. doi: 10.1016/s0076-6879(96)72008-6
35. Rabanus-Wallace, M. Timothy, Bernd Hackauf, Martin Mascher, Thomas Lux, Thomas Wicker, Heidrun Gundlach, Mariana Baez, Andreas Houben, Klaus F. X. Mayer, Liangliang Guo, Jesse Poland, Curtis J. Pozniak, Sean Walkowiak, Joanna Melonek, Coraline R. Praz, Mona Schreiber, Hikmet Budak, Matthias Heuberger, Burkhard Steuernagel, Brande Wulff, Andreas Börner, Brook Byrns, Jana Čížková, D. Brian Fowler, Allan Fritz, Axel Himmelbach, Gemy Kaithakottil, Jens Keilwagen, Beat Keller, David Konkin, Jamie Larsen, Qiang Li, Beata Myśków, Sudharsan Padmarasu, Nidhi Rawat, Uğur Sesiz, Sezgi Biyiklioglu-Kaya, Andy Sharpe, Hana Šimková, Ian Small, David Swarbreck, Helena Toegelová, Natalia Tsvetkova, Anatoly V. Voylokov, Jan Vrána, Eva Bauer, Hanna Bolibok-Bragoszewska, Jaroslav Doležel, Anthony Hall, Jizeng Jia, Viktor Korzun, André Laroche, Xue-Feng Ma, Frank Ordon, Hakan Özkan, Monika

Rakoczy-Trojanowska, Uwe Scholz, Alan H. Schulman, Dörthe Siekmann, Stefan Stojałowski, Vijay K. Tiwari, Manuel Spannagl and Nils Stein 2021. Chromosome-scale genome assembly provides insights into rye biology, evolution and agronomic potential. Nature genetics 53: 564–573. doi: 10.1038/s41588-021-00807-0
36. Rigon, C. A. G., A. Küpper, C. Sparks, J. Montgomery, F. Peter, S. Schepp, A. Perez-Jones, P. J. Tranel, R. Beffa, F. E. Dayan and T. A. Gaines 2025. Function of cytochrome P450 CYP72A1182 in metabolic herbicide resistance evolution in Amaranthus palmeri populations. J Exp Bot 76: 2891–2907. doi: 10.1093/jxb/eraf114
37. Rigon, Carlos, Todd Gaines, Anita Kuepper and Franck Dayan 2020. Metabolism-Based Herbicide Resistance, the Major Threat Among the Non-Target Site Resistance Mechanisms. Outlooks on Pest Management 31: 162–168. doi: 10.1564/v31_aug_04
38. Ritz, Christian, Florent Baty, Jens C. Streibig and Daniel Gerhard 2016. Dose-Response Analysis Using R. PLoS One 10: e0146021. doi: 10.1371/journal.pone.0146021
39. Saika, H., J. Horita, F. Taguchi-Shiobara, S. Nonaka, A. Nishizawa-Yokoi, S. Iwakami, K. Hori, T. Matsumoto, T. Tanaka, T. Itoh, M. Yano, K. Kaku, T. Shimizu and S. Toki 2014. A novel rice cytochrome P450 gene, CYP72A31, confers tolerance to acetolactate synthase-inhibiting herbicides in rice and Arabidopsis. Plant Physiol 166: 1232–1240. doi: 10.1104/pp.113.231266
40. Shaner, D. L., P. C. Anderson and M. A. Stidham 1984. Imidazolinones: potent inhibitors of acetohydroxyacid synthase. Plant Physiol 76: 545–546. doi: 10.1104/pp.76.2.545
41. Shen, J., Q. Yang, F. Xu, Y. Han, Y. Li and M. Zheng 2025. Effects of Amino Acid Mutation in Cytochrome P450 (CYP96A146) of Descurainia sophia on the Metabolism and Resistance to Tribenuron-Methyl. J Agric Food Chem 73: 370–379. doi: 10.1021/acs.jafc.4c10217
42. Soni, N., E. P. Westra, G. Allegretta, A. L. S. Araujo, C. F. de Pinho, S. Morran, J. Lerchl, F. E. Dayan, P. Westra and T. A. Gaines 2022. Survey of ACCase and ALS resistance in winter annual grasses identifies target-site and nontarget-site imazamox resistance in Secale cereale. Pest Manag Sci 78: 5080–5089. doi: 10.1002/ps.7154
43. Stougaard, Robert N., Carol A. Mallory-Smith and James A. Mickelson 2004. Downy Brome (Bromus tectorum) Response to Imazamox Rate and Application Timing in Herbicide-Resistant Winter Wheat. Weed Technology 18: 1043–1048. doi: 10.1614/WT-03-216R1
44. Tranel, Patrick J. and Terry R. Wright 2002. Resistance of weeds to ALS-inhibiting herbicides: what have we learned? Weed Science 50: 700–712. doi: 10.1614/0043-1745(2002)050[0700:RROWTA]2.0.CO;2
45. Urban, P., C. Mignotte, M. Kazmaier, F. Delorme and D. Pompon 1997. Cloning, yeast expression, and characterization of the coupling of two distantly related Arabidopsis thaliana NADPH-cytochrome P450 reductases with P450 CYP73A5. J Biol Chem 272: 19176–19186. doi: 10.1074/jbc.272.31.19176
46. Werck-Reichhart, D. 2023. Promiscuity, a Driver of Plant Cytochrome P450 Evolution? Biomolecules 13. doi: 10.3390/biom13020394
47. Werck-Reichhart, Danièle and René Feyereisen 2000. Cytochromes P450: a success story. Genome Biology 1: reviews3003.3001. doi: 10.1186/gb-2000-1-6-reviews3003
48. Wright, Alice, Raj Sasidharan, Liisa Koski, Marianela Rodriguez-Carres, Daniel Peterson, Vijay Nandula, Jeffery Ray, Jason Bond and David Shaw 2018. Transcriptomic

changes in Echinochloa colona in response to treatment with the herbicide imazamox. Planta 247. doi: 10.1007/s00425-017-2784-7
49. Xiang, Wensheng, Xiangjing Wang and Tianrui Ren 2006. Expression of a wheat cytochrome P450 monooxygenase cDNA in yeast catalyzes the metabolism of sulfonylurea herbicides. Pesticide Biochemistry and Physiology 85: 1–6. doi: https://doi.org/10.1016/j.pestbp.2005.09.001
50. Yao, Sai, Hanqi Yin, Yang Li, Qian Yang, Shuzhong Yuan and Wei Deng 2024. Cytochrome P450 CYP81A104 in Eleusine indica confers resistance to multiherbicide with different modes of action. Pest Management Science 80: 5791–5798. doi: https://doi.org/10.1002/ps.8310
51. Zhao, N., Y. Yan, W. Liu and J. Wang 2022. Cytochrome P450 CYP709C56 metabolizing mesosulfuron-methyl confers herbicide resistance in Alopecurus aequalis. Cell Mol Life Sci 79: 205. doi: 10.1007/s00018-022-04171-y
52. Zhu, A., J. G. Ibrahim and M. I. Love 2019. Heavy-tailed prior distributions for sequence count data: removing the noise and preserving large differences. Bioinformatics 35: 2084–2092. doi: 10.1093/bioinformatics/bty895

CHAPTER III - DICAMBA RESISTANCE CONFERRED BY KOCHIA (*BASSIA SCOPARIA*) AUX/IAA16 MUTATION IN TOBACCO (*NICOTIANA TABACUM*)

SUMMARY

A mutation in AUX/IAA16 in *Bassia scoparia* (kochia) was recently shown to confer resistance to the synthetic auxin herbicide dicamba by altering the degron motif required for TIR1/AFB receptor interaction, thereby disrupting auxin-mediated signaling. To evaluate the transferability of this trait, the kochia IAA16 mutant allele ($IAA16_{mut}$) was introduced into *Nicotiana tabacum* (tobacco) to determine whether dicamba resistance can be conferred in a heterologous system. This research aims to assess (i) the phylogenetic and structural similarity of AUX/IAA and TIR1/AFB gene families between kochia and tobacco to determine compatibility of auxin-signaling components, and (ii) the capacity of $IAA16_{mut}$ to provide dicamba resistance in transgenic tobacco. Sequence alignment and phylogenetic analysis confirmed strong conservation of AUX/IAA and AFB families between species, including preservation of the degron region essential for receptor recognition. Transgenic tobacco expressing $IAA16_{mut}$ exhibited pronounced dicamba resistance compared with wild type controls, demonstrating that disruption of AUX/IAA and TIR1/AFB interaction is sufficient to impart resistance outside the native kochia genetic background. Importantly, no vegetative growth penalties were observed, suggesting minimal fitness cost associated with the introduction of this mutation. This research demonstrates that dicamba resistance mediated by the $IAA16_{mut}$ allele is functionally transferable across species and highlights AUX/IAA genes as promising molecular targets for rational development of auxin-herbicide resistant crops.

INTRODUCTION

Meeting the rising global demand for agriculture production requires the development of unique production systems that can deliver higher yields while relying on the available resources. As crop production continues to intensify, weed competition remains as one of the most persistent limitations to yield potential (Horvath et al., 2023). Effective weed management is therefore essential for maintaining productivity and ensuring stable yields across variable growing conditions. Chemical weed control persists as one of the most effective tools for suppression of early-season weed competition, stabilizing crop yields, and providing growers with reliable management options. Before the introduction of herbicide-resistant (HR) crops, selective herbicides were essential for protecting crops from weed pressure and maintaining productivity. The development of HR cropping systems improved weed management as growers could rely on an alternative herbicide mode of action instead of the traditional selective herbicides for weed control (Green, 2012). HR cropping systems improved production efficiency and increased yield stability, particularly in environments where weed pressure is severe. However, widespread dependence on single mode of action herbicide only increased the evolution of herbicide resistant weed populations, reducing the effectiveness of existing herbicide chemistries and increasing the complexity of controlling persistent weeds (Délye et al., 2013; Duke, 2015; Green, 2014; Heap and Duke, 2018). As resistance continues to intensify globally, growers require crops with alternative options to additional herbicide mode of actions to maintain effective weed suppression.

With the rapid expansion of weed genomics (Montgomery et al., 2024; Montgomery et al., 2025a), our understanding of herbicide resistance mechanisms has advanced considerably. These insights on the molecular basis of herbicide resistance have provided new opportunities in the identification of new targets for engineering HR crops. One notable example comes from recent

work in *Bassia scoparia* (kochia), where a naturally occurring mutation in Auxin/Indole-3-acetic acid (AUX/IAA16) was shown to confer resistance to the group 4 auxin herbicide dicamba (Montgomery et al., 2025b). Long-read sequencing discovered that this resistant kochia population carried a LTR retrotransposon insertion within the second exon of **AUX/IAA16**, disrupting normal splicing and altering the degron motif in Domain II, an essential site for TIR1/AFB-mediated auxin interaction. Functional validation experiments demonstrated that this mutation reduces the interaction between AUX/IAA16 and Transport Inhibitor Response 1 / Auxin Signaling F-box (TIR1/AFB6) (LeClere et al., 2018; Montgomery et al., 2025b). Additionally, transgenic *Arabidopsis thaliana* (Arabidopsis) lines carrying this mutant allele showed reduced sensitivity to dicamba and biochemical assays confirmed lower binding affinity and faster dissociation from TIR1 in the presence of auxins (Montgomery et al., 2025b). Such results demonstrated that this alteration in the degron is sufficient to disrupt the normal auxin signaling and imparts dicamba resistance. Auxin herbicides act by leveraging the endogenous auxin-signaling pathway, in which auxin binds to TIR1/AFB receptors and promotes their interaction with AUX/IAA repressors, leading to AUX/IAA ubiquitination, degradation, and activation of auxin-responsive genes (Busi et al., 2018; Grossmann, 2010; Todd et al., 2020). As this process depends on precise interactions between TIR1/AFB proteins and the degron in domain II of AUX/IAA, minor alterations in this region can result in auxin herbicide resistance. The AUX/IAA16 mutation identified in kochia represents a clear example of this mechanism, in which the retrotransposon insertion alters the degron residue, reducing the interaction with TIR1/AFB proteins thereby reducing activation of auxin responsive genes, resulting in a resistance phenotype

Given the evidence of dicamba resistance that arises through alterations in the AUX/IAA16 in kochia by disrupting the auxin-signaling pathway, an important next step would be to determine

if this mechanism of resistance can function in the same way in other species. If the AUX/IAA and TIR1/AFB interaction is sufficiently conserved, the IAA16 mutant allele from kochia ($IAA16_{mut}$) may act similarly outside of the native genetic background. Tobacco serves as an ideal candidate for heterologous expression due to its well characterized genome, its developed transformation system, and the presence of multiple AUX/IAA and TIR1/AFB homologs (Jube and Borthakur, 2007; Tong et al., 2024; Xu et al., 2017). Therefore, the objectives of this study were to (i) evaluate the structural similarity between kochia and tobacco AUX/IAA and TIR1/AFB gene families to determine if tobacco encodes compatible systems with the $IAA16_{mut}$ from kochia, and (ii) to assess whether the introduced $IAA16_{mut}$ confers resistance to dicamba in tobacco, consistent with its function in kochia. By integrating sequence alignments, phylogenetic analyses, and herbicide resistance phenotypic evaluations of transgenic tobacco, this research aimed to determine whether the molecular mechanism of dicamba resistance is conserved across species.

MATERIALS AND METHODS

Vector assembly and production of transgenic tobacco lines

The coding sequence from mutant AUX/IAA16 alleles in kochia were amplified from cDNA using PrimeSTAR MAX polymerase (Takara Bio USA) together with primers designed to introduce overhangs compatible with the pFGC5941 expression vector (Table S1). The pFGC5941 vector was linearized with AscI and BamHI (New England Biolabs), and purified PCR products were inserted into the digested vector using the In-Fusion cloning system (Takara Bio USA). This construct places the transgene under control of the CaMV 35S promoter with an OCS terminator. All assemblies were validated by Sanger sequencing (Plasmidsaurus; Louisville, KY, USA). Generation of transformed tobacco events were competed at the UC Davis Plant Transformation

Facilities (https://ptf.ucdavis.edu/) using agrobacterium-mediated transformations (Topping, 1998). Integration of the AUX/IAA16$_{mut}$ transgene into tobacco genomes was verified by PCR amplification of a region within the pFGC5941 vector encompassing the inserted sequence. Reactions were performed using the primers forward primers: CCAACCACGTCTTCAAAGCA and reverse: GGCGTCTCGCATATCTCATT (5'-3'). Thermocycling conditions consisted of an initial denaturation at 95 °C for 5 min, followed by 35 cycles of 95 °C for 15 s, 60 °C for 15 s, and 72 °C for 2 min, with a final extension at 72 °C for 5 min.

Tobacco growth conditions:

Nicotiana tabacum (Tobacco) was pregerminated for two weeks under 22/18°C and a light intensity of 120 μE m^{-2} s^{-1} for 10/14h light/dark cycle before being transplanted to 3.8-cm by 3.8-cm by 5.8-cm pots containing LM-HP high porosity potting mix (Lambert, Rivière-Ouelle, QC, Canada). Pots were moved to the greenhouse and grown under a temperature range of 22–24 °C for approximately three weeks. Supplemental illumination from liquid halogen grow lights was used to sustain a 14 h light / 10 h dark photoperiod and relative humidity of ~75%.

Tobacco dicamba resistance evaluation:

At four leaf stage, four tobacco plants were treated with one of the following rates of dicamba (0.0, 4.3, 8.7, 17.5, 35.0, 70.0, 140.0, 280.0, and 560.0 g ha $^{-1}$ of dicamba (Engenia®, N,N-Bis-(3-aminopropyl) methylamine salt, BASF, Research Triangle Park, NC) with 0.25% (v/v) non-ionic surfactant). Dose response experiments were replicated twice. Applications were made using a calibrated single-nozzle track sprayer (DeVries Manufacturing, Hollandale, MN) delivering 187 L ha^{-1} spray volume. Visual injury ratings and survival were recorded 21 days after treatment (21 DAT). The drc package v3.0-1 (Ritz et al., 2016) was used in R v4.5.0 (RCore Team, 2020) to assess injury rating. Independent curves were fit for each event using a four-parameter

log–logistic model with event specified as the curve identifier. Effective dose estimates (ED_{50}) were obtained, and pairwise differences among events were evaluated using EDcomp to assess statistically supported differences in dicamba resistance.

Quantification of Transgene Expression by qPCR

Expression of the *IAA16* transgene in transformed tobacco lines was quantified using SYBR Green based quantitative PCR. Gene specific primers targeting the IAA16 coding region (: GCAACCAAAACTACAGCGGA and R: GCGACGATGTTCTTCCTGAA) were used to amplify a 185 bp fragment of the transgene. Reactions were carried out alongside two endogenous reference genes: ribosomal protein L25 (F: CCCCTCACCACAGAGTCTGC; R: AAGGGTGTTGTTGTCCTCAATCTT) and elongation factor 1-α (EF-1α) (F: TGAGATGCACCACGAAGCTC; R: CCAACATTGTCACCAGGAAGTG) (Schmidt and Delaney, 2010). All qPCR assays were performed using the same thermocycler program: an initial denaturation at 95 °C for 3 min, followed by 40 cycles of 95 °C for 15 s and 60 °C for 30 s, with SYBR fluorescence measured during the 60 °C step of each cycle. Relative transcript abundance was calculated as 2^(–ΔCt), where ΔCt represents the difference between the target gene Ct value and the mean of the two housekeeping genes. Event level means and standard errors were obtained by averaging relative expression values across biological replicates. Differences in transgene expression among events were evaluated using a one-way ANOVA followed by Tukey's HSD test to determine statistically distinct groups. All analyses were conducted in R v4.5.0.

Phylogenetic analysis of AUX/IAA and AFB genes between kochia and tobacco

AUX/IAA and AFB gene models from *Bassia scoparia* were identified using the GFF3 genome annotation retrieved from WeedPedia (Hall et al., 2025). Genes annotated as IAA or AFB were extracted, and corresponding protein sequences were retrieved from the reference proteome.

An equivalent workflow was applied to *Nicotiana attenuata*, using the NIATTr2 GFF3 annotation to collect all gene models explicitly annotated as IAA or AFB and obtain their associated amino acid sequences (Xu et al., 2017). Protein sequences from both species were aligned using MUSCLE in MEGA12 with default parameters. Pairwise BLASTP (NCBI BLAST+ v2.14) was used to quantify sequence identity between kochia and tobacco IAA16 proteins and to support orthology assignments. Phylogenetic reconstruction of the AUX/IAA and AFB families was conducted using the Neighbor-Joining method with evolutionary distances estimated under the Poisson correction model. Ambiguous positions were removed by pairwise deletion, and node support was assessed using 1,000 bootstrap replicates, with branches below 50% support collapsed. The resulting phylogenies were used to resolve lineage relationships and assess the placement of kochia and tobacco IAA16 and AFB6 orthologs.

RESULTS

Characterization of dicamba resistance in transgenic tobacco

All WT tobacco samples exhibited dicamba sensitivity, reflected by an ED_{50} of only 6.6 g ha^{-1}, confirming that the non-transgenic background lacks resistance to dicamba. In contrast, all transgenic events showed markedly higher ED_{50} values, indicating clear dicamba resistance. Events 81-02 and 81-09 displayed moderate increases in resistance (ED_{50} = 19.4 and 22.4 g ha^{-1}), while events 94-10, 94-07, and 94-05 exhibited the highest level of resistance, with ED_{50} values between 45.9 and 58.6 g ha^{-1} (Figure 1 & 2). Pairwise comparisons confirmed that every transgenic line required significantly higher dicamba doses to reach 50% injury relative to the WT tobacco plants. These results demonstrate that the IAA16 transgene consistently confers dicamba resistance, whereas the WT remains fully susceptible.

Across tobacco transformation events, all lines exhibited detectable expression of the *IAA16* transgene, confirming successful transcriptional activity in each event. Event 81-02 showed a relative expression of 2.55, and 81-09 showed 4.69. The remaining events showed intermediate levels, including 94-05 at 4.37, 94-07 at 3.03, and 94-10 at 3.46 (Figure 2). Although the magnitude of expression varies among each event, with 81-02 showing the lowest level of expression, no statistical differences were observed among events ($p > 0.05$).

Vegetative growth measurements revealed no differences in early plant development between transgenic tobacco plants and wild-type controls. Mean leaf width, recorded weekly over a six-week period following uniform transplanting, increased consistently across all events, regardless of the transgene expression (Figure 4). The growth curves of the 81-02, 81-09, 94-05, 94-07, and 94-10 transformation events overlapped closely with those of the WT controls throughout the experiment. Collectively, these results demonstrate that introduction of the *IAA16* transgene does not impose detectable growth or fitness penalties when comparing vegetative growth parameters.

Phylogenetic analysis of AUX/IAA and TIR1/AFB gene families supports functional compatibility between kochia and tobacco

Multiple sequence alignment revealed that tobacco IAA16 is highly conserved relative to kochia IAA16 (Figure 6). Across the full-length protein coding sequence, tobacco IAA16 aligns closely with both the wild-type and mutant kochia IAA16 isoforms, with divergence restricted to the N-terminal region. This high similarity is supported by pairwise BLAST analysis, in which tobacco IAA16 aligned to kochia IAA16 with 61.8% identity across 283 aligned residues. The remainder of the alignment, including the degron and AUX/IAA domains, critical for TIR1/AFB co-receptor recognition, showed strong conservation. Together, these alignment results provide

molecular support that tobacco contains the necessary components for interaction with the introduced mutant IAA16 protein from kochia. Phylogenetic analysis of the broader AUX/IAA family further reinforced this relationship, as kochia IAA16 clustered within a well-supported clade containing the tobacco IAA16 ortholog (Figure 5). The similar grouping of kochia and tobacco IAA16 sequence indicates that there is minimal evolutionary divergence. This placement aligns with the high conservation observed in the pairwise alignment and confirms that both species share a homologous IAA16 lineage and therefore may have similar auxin responsive regulatory features. To further assess whether the corresponding AFB co-receptor shows a similar conservation, a separate phylogenetic analysis was performed on the TIR1/AFB family (Figure _). The resulting tree resolved three major receptor clades, TIR1, AFB2, and AFB5/6, with strong bootstrap support. Notably, tobacco AFB6 clustered with kochia AFB6 within the AFB5/6 clade, demonstrating that the receptor partner implicated in kochia's dicamba resistance mechanism is evolutionarily conserved in tobacco (Montgomery et al., 2025b). The presence of a closely related tobacco AFB6 ortholog suggests that the introduced *BsIAA16* transgene has access to a native co-receptor found in tobacco and may have compatible recognition sites. This conservation provides a strong mechanistic basis for the dicamba resistance phenotype observed in the transgenic tobacco lines.

DISCUSSION

This study demonstrates that expression of AUX/IAA16 mutant allele from kochia is sufficient to confer dicamba resistance in a heterologous crop system. Wild-type tobacco, which has no inherent tolerance to dicamba, expressed sensitivity to dicamba, with an ED_{50} of only 6.6 g

ha^{-1}. In contrast, each tobacco event that expressed the kochia IAA16 transgene exhibited significantly higher ED_{50} values, ranging from 19.4 to 58.6 g ha^{-1} (Figure 1). This increased resistant factor is also matches the observed resistance in this population of kochia (M32) to dicamba (Montgomery et al., 2025b). The consistent shift in resistance between the wild type and independent transgenic tobacco events provides strong evidence that the kochia IAA16 allele reduced dicamba activity and lowers auxin-signaling sensitivity, even outside of the native genetic background.

Differences in dicamba resistance among transgenic events were not statistically explained by variation in transgene expression. Although relative expression ranged from 2.55 to 4.69, none of the events differed significantly in transcript abundance. However, the numerical pattern suggests a possible biological relationship between expression level and resistance magnitude. Event 81-02, which exhibited the lowest expression at 2.55, also showed the weakest resistance (ED_{50} = 19.4 g ha^{-1}). In contrast, event 94-05 displayed both one of the highest expression levels (4.37) and the greatest resistance (ED_{50} = 58.6 g ha^{-1}). While not statistically supported in this dataset, this trend may suggest that transgene dosage can contribute to resistance and requires further investigation, particularly given prior reports in which variation in transgene expression has been directly linked to differences in herbicide resistance phenotypes (Ko et al., 2018). Although the level of dicamba resistance observed is sufficient to fully protect tobacco, future work could explore whether increasing transgene expression could further enhance resistance.

The absence of detectable growth penalties in transgenic tobacco aligns with fitness assessments conducted in kochia, where AUX/$IAA16_{mut}$ conferred herbicide resistance with limited costs under untreated conditions (Montgomery et al., 2025b). In segregating F_3 kochia families, the mutant allele did not reduce above-ground biomass relative to wild-type plants,

despite mild effects on germination and plant height. A similar pattern was observed in tobacco, where none of the transgenic events showed reductions in vegetative vigor or early growth rate despite expressing the mutant allele (Figure 4). Together, these findings indicate that the mutant AUX/IAA16 protein cause minimal developmental penalties in the absence of herbicide, supporting the conclusion that the AUX/IAA repressors can function as effective resistance factors without compromising plant fitness. Future work should assess fitness consequences under biotic and abiotic stress to determine whether environmental challenges reveal additional costs associated with the mutant allele and dicamba resistance.

Understanding whether tobacco can support the same auxin-signaling interactions that confer dicamba resistance in kochia first requires evaluating the structural similarity between AUX/IAA proteins. Sequence alignment results (Figure 7) directly address this question by assessing whether tobacco encodes the molecular machinery needed to interact with the introduced mutant *Bs*IAA16 allele. Tobacco IAA16 shares 61.8% identity with kochia IAA16 across 283 aligned amino acids, with the highest conservation occurring across Domains II–IV. These domains have been reported as essential for TIR1/AFB recognition and ARF interaction (Luo et al., 2018; Ramans-Harborough et al., 2023; Uzunova et al., 2016). As Domains II–IV are among the most evolutionarily constrained regions of the AUX/IAA family (Remington et al., 2004), their strong conservation between kochia and tobacco indicates that the sequence motifs required for co-receptor assembly and downstream auxin-response regulation remain intact. The phylogenetic analyses further reinforce this interaction. In the AUX/IAA phylogeny (Figure 5), kochia IAA16 clusters tightly with the tobacco IAA16 ortholog within a well-supported clade, indicating strong evolutionary conservation and suggesting that both proteins retain similar regulatory functions. This clustering supports the conclusion that the introduced kochia mutant allele can interact

effectively with the native auxin-signaling machinery in tobacco. Similarly, the TIR1/AFB phylogeny (Figure 6) shows tobacco AFB6 as the closest ortholog to the kochia AFB6 receptor. The presence of a clear AFB6 ortholog in tobacco is especially important, as the kochia AUX/IAA16$_{mut}$ variant is known to selectively interact with TIR1 and AFB6 receptors in its native system (LeClere et al., 2018; Montgomery et al., 2025b), implying that the same co-receptor interactions are likely similar in the tobacco background. This provides strong molecular evidence that the BsIAA16$_{mut}$ transgene disrupts auxin signaling in tobacco through the *same biochemical mechanism* characterized in resistant kochia.

Taken together, these results demonstrate that the molecular mechanism driving dicamba resistance in kochia is transferable to other species. The interaction between AUX/IAA and TIR1/AFB are modular, and alterations in the degron composition can shift the receptor affinity and result in herbicide resistance beyond the species in which the mutation originated. Understanding this interaction has direct relevance for crop improvement, as knowledge of herbicide resistance mechanism can be used to inform target modification of AUX/IAA genes in tobacco and other broadleaf crops. A better understanding of these mechanisms provides a foundation for designing plants with predictable and controlled forms of auxin insensitivity that could support the development of new herbicide-tolerant cropping systems.

FIGURES

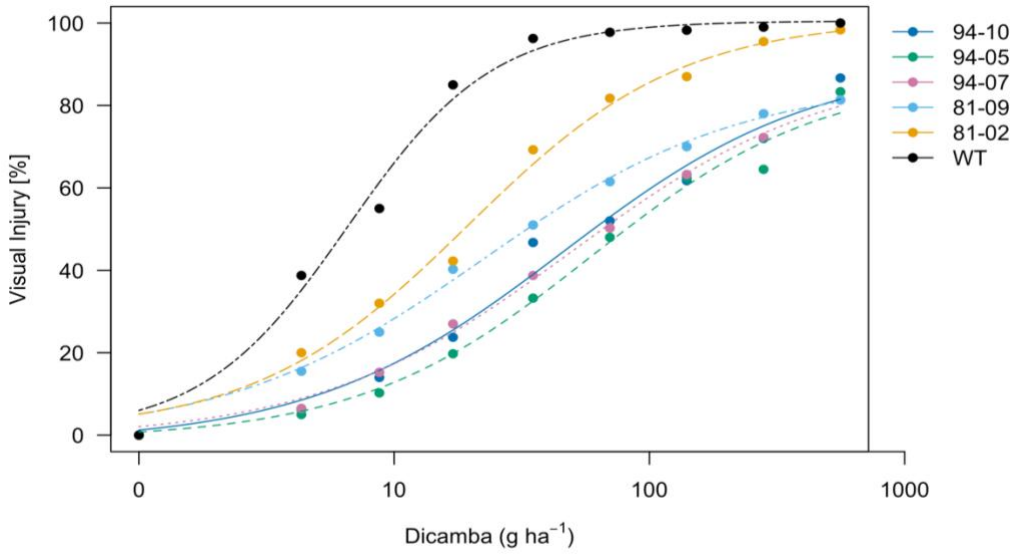

Figure 1. Dicamba dose response curves for visual injury in transgenic tobacco lines. Visual injury ratings for each tobacco event and the WT control sampled 21 DAT. Plants were sprayed at four leaf stage with one of the following rates of dicamba: 0.0, 4.3, 8.7, 17.5, 35.0, 70.0, 140.0, 280.0, and 560.0 g ha $^{-1}$ of dicamba with 0.25% (v/v) non-ionic surfactant. Points represent individual biological replicates, and lines show model predictions.

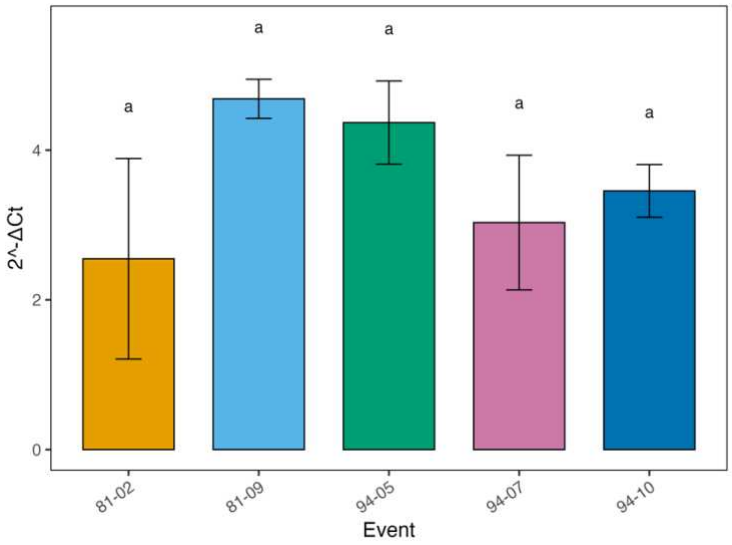

Figure 2. Relative expression of IAA16 transgene across tobacco events.
Bars represent mean expression (± SE) across biological replicates for each transformation event and letters indicate statistically significant differences ($p < 0.05$).

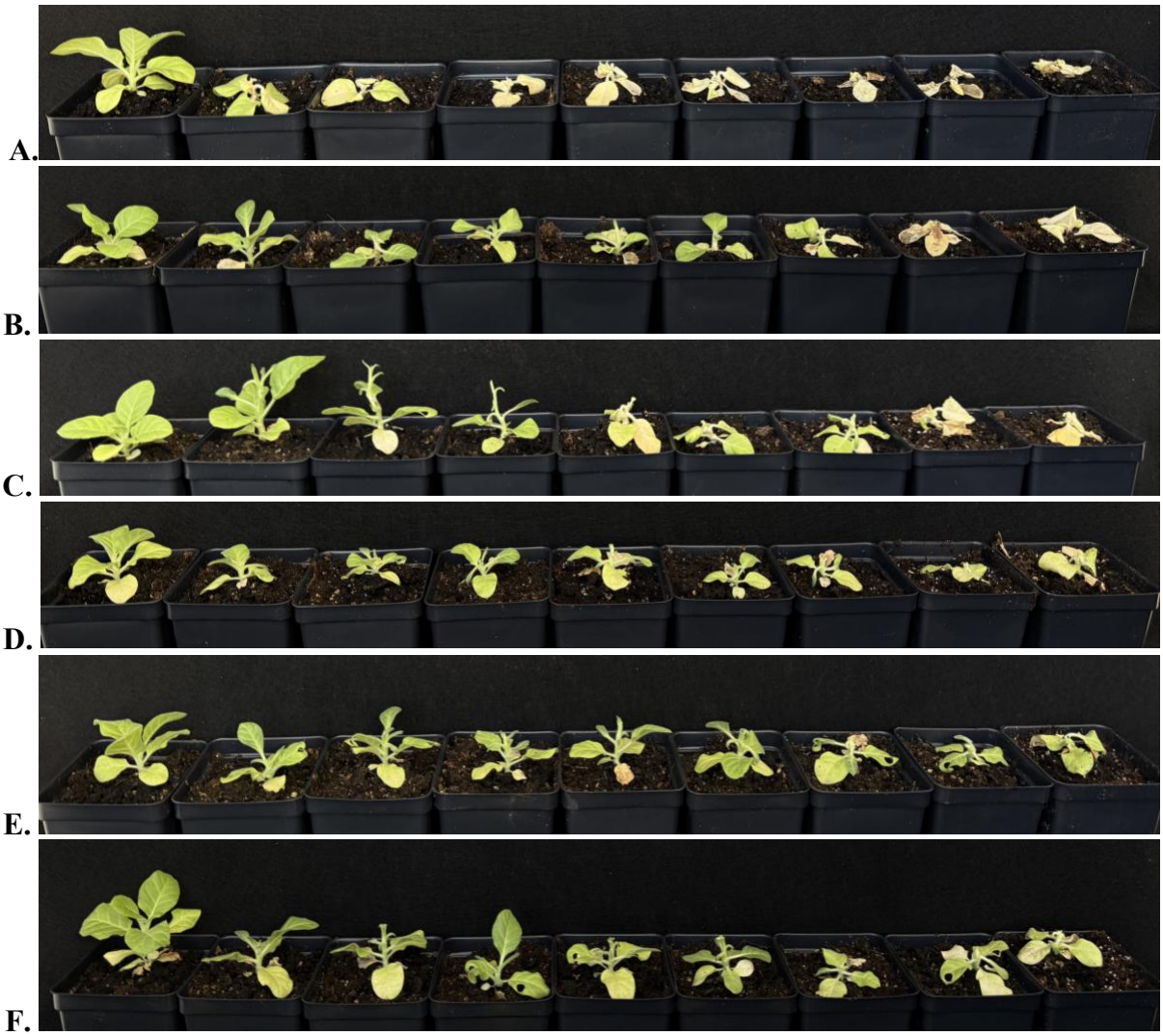

Figure 3. Comparative visual injury responses of wild-type and IAA16 transgenic tobacco to dicamba.
Visual injury symptoms observed in wild-type tobacco (A) and IAA16 transgenic events 81-02 (B), 81-09 (C), 94-10 (D), 94-07 (E), and 94-05 (F) following dicamba application. Plants in each panel were treated left to right with 0, 4.3, 8.7, 17.5, 35.0, 70.0, 140.0, 280.0, and 560.0 g ha^{-1} dicamba, applied with 0.25% (v/v) non-ionic surfactant. Visual observations were recorded three weeks after dicamba applications.

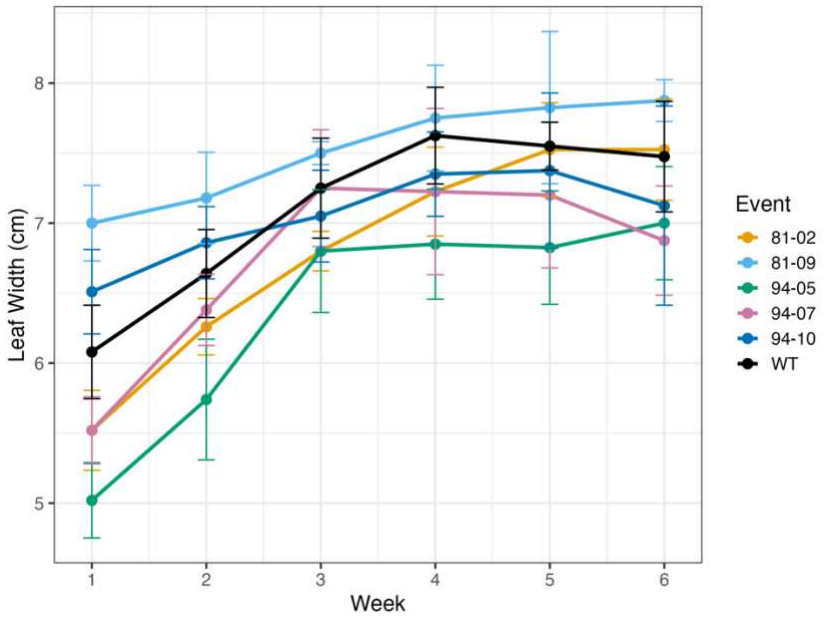

Figure 4. Vegetative growth comparison between transgenic and wild-type tobacco. Mean leaf width (cm) of tobacco plants representing each transformation event, measured weekly beginning one week after transplanting. Width measurements were recorded from five biological replicates per event and averaged to obtain event-level means (± SE).

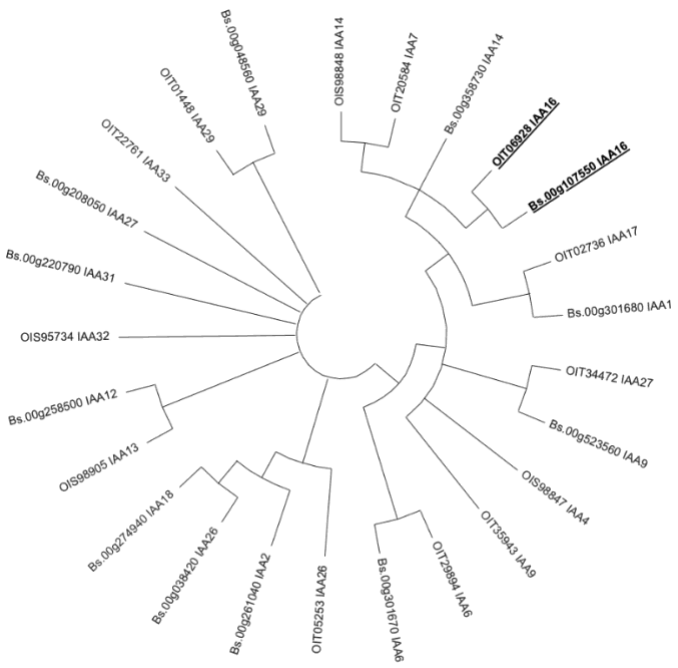

Figure 5. Phylogenetic relationships among AUX/IAA family members from *Bassia scoparia* and *Nicotiana attenuate.*
This circular Neighbor-Joining phylogony illustrates the evolutionary relationships among 25 AUX/IAA protein sequences identified in *Bassia scoparia* and *Nicotiana attenuata*. Protein sequences were aligned using MUSCLE in MEGA12, and evolutionary distances were computed using the Poisson correction model. The topology shown represents the consensus of 1,000 bootstrap replicates; branches with <50% support was collapsed.

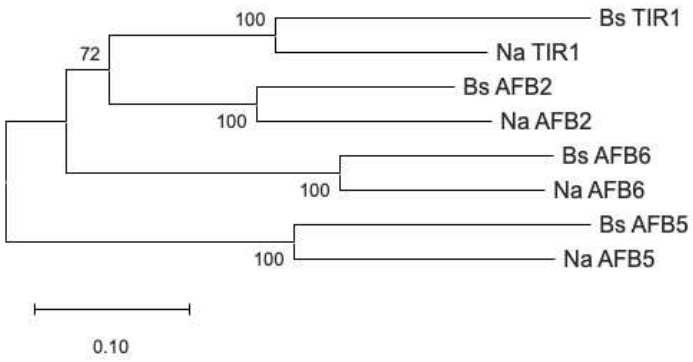

Figure 6. Phylogenetic relationships of TIR1/AFB auxin receptor homologs from *Bassia scoparia* and *Nicotiana attenuate.*
This Neighbor-Joining phylogeny depicts the evolutionary relationships among TIR1/AFB auxin receptor homologs identified in *Bassia scoparia* (Bs) and *Nicotiana attenuata* (Na). Protein sequences were aligned using MUSCLE, and evolutionary distances were estimated using the Poisson correction model in MEGA12. The consensus tree was inferred from 1,000 bootstrap replicates, with bootstrap support values shown above major branches. Scale bar indicates 0.10 amino acid substitutions per site.

Figure 7. Multiple protein sequence alignment of tobacco IAA16 and wild-type and mutant IAA16 alleles from kochia

A CLUSTAL O (v1.2.4) amino acid alignment comparing *Nicotiana attenuata* IAA16 (Na_IAA16) with the wild-type (Bs_IAA16_WT) and mutant (Bs_IAA16_Mut) IAA16 alleles from *Bassia scoparia*. Conserved residues are indicated by asterisks, with high-similarity positions marked by colons and periods. The degron domain is bolded.

REFERENCES

1. Busi, Roberto, Danica E Goggin, Ian M Heap, Michael J Horak, Mithila Jugulam, Robert A Masters, Richard M Napier, Dilpreet S Riar, Norbert M Satchivi, Joel Torra, Phillip Westra and Terry R Wright 2018. Weed resistance to synthetic auxin herbicides. Pest Management Science 74: 2265–2276. doi: https://doi.org/10.1002/ps.4823
2. Délye, Christophe, Marie Jasieniuk and Valérie Le Corre 2013. Deciphering the evolution of herbicide resistance in weeds. Trends in Genetics 29: 649–658. doi: 10.1016/j.tig.2013.06.001
3. Duke, S. O. 2015. Perspectives on transgenic, herbicide-resistant crops in the United States almost 20 years after introduction. Pest Manag Sci 71: 652–657. doi: 10.1002/ps.3863
4. Green, J. M. 2012. The benefits of herbicide-resistant crops. Pest Manag Sci 68: 1323–1331. doi: 10.1002/ps.3374
5. Green, Jerry M 2014. Current state of herbicides in herbicide-resistant crops. Pest Management Science 70: 1351–1357. doi: https://doi.org/10.1002/ps.3727
6. Grossmann, Klaus 2010. Auxin herbicides: current status of mechanism and mode of action. Pest Management Science 66: 113–120. doi: https://doi.org/10.1002/ps.1860
7. Hall, Nathan, Jacob Montgomery, Jinyi Chen, Christopher Saski, Maor Matzrafi, Phil Westra, Todd Gaines and Eric Patterson 2025. FHY3/FAR1 transposable elements generate adaptive genetic variation in the Bassia scoparia genome. Pest Management Science 81: 4393–4402. doi: https://doi.org/10.1002/ps.8798
8. Heap, I. and S. O. Duke 2018. Overview of glyphosate-resistant weeds worldwide. Pest Manag Sci 74: 1040–1049. doi: 10.1002/ps.4760
9. Horvath, David, Sharon Clay, Clarence Swanton, James Anderson and Wun Chao 2023. Weed-induced crop yield loss: a new paradigm and new challenges. Trends in plant science 28. doi: 10.1016/j.tplants.2022.12.014
10. Jube, S. and D. Borthakur 2007. Expression of bacterial genes in transgenic tobacco: methods, applications and future prospects. Electron J Biotechnol 10: 452–467. doi: 10.2225/vol10-issue3-fulltext-4
11. Ko, D. K., S. S. Nadakuduti, D. S. Douches and C. R. Buell 2018. Transcriptome profiling of transgenic potato plants provides insights into variability caused by plant transformation. PLoS One 13: e0206055. doi: 10.1371/journal.pone.0206055
12. LeClere, Sherry, Chenxi Wu, Philip Westra and R. Douglas Sammons 2018. Cross-resistance to dicamba, 2,4-D, and fluroxypyr in Kochia scoparia is endowed by a mutation in an AUX/IAA gene. Proceedings of the National Academy of Sciences 115: E2911–E2920. doi: doi:10.1073/pnas.1712372115
13. Luo, J., J. J. Zhou and J. Z. Zhang 2018. Aux/IAA Gene Family in Plants: Molecular Structure, Regulation, and Function. Int J Mol Sci 19. doi: 10.3390/ijms19010259
14. Montgomery, Jacob, Sarah Morran, Dana R. MacGregor, J. Scott McElroy, Paul Neve, Célia Neto, Martin M. Vila-Aiub, Maria Victoria Sandoval, Analia I. Menéndez, Julia M. Kreiner, Longjiang Fan, Ana L. Caicedo, Peter J. Maughan, Bianca Assis Barbosa Martins, Jagoda Mika, Alberto Collavo, Aldo Merotto, Nithya K. Subramanian, Muthukumar V. Bagavathiannan, Luan Cutti, Md Mazharul Islam, Bikram S. Gill, Robert Cicchillo, Roger Gast, Neeta Soni, Terry R. Wright, Gina Zastrow-Hayes, Gregory May, Jenna M. Malone, Deepmala Sehgal, Shiv Shankhar Kaundun, Richard P. Dale, Barend

Juan Vorster, Bodo Peters, Jens Lerchl, Patrick J. Tranel, Roland Beffa, Alexandre Fournier-Level, Mithila Jugulam, Kevin Fengler, Victor Llaca, Eric L. Patterson and Todd A. Gaines 2024. Current status of community resources and priorities for weed genomics research. Genome Biology 25: 139. doi: 10.1186/s13059-024-03274-y

15. Montgomery, Jacob S., Jan E. Leach, Stephen L. Young and Todd A. Gaines 2025a. Using weedy traits in crops as part of a new green revolution. New Phytologist 247: 1071–1074. doi: https://doi.org/10.1111/nph.70224
16. Montgomery, Jacob S., Neeta Soni, Sofia Marques Hill, Sarah Morran, Eric L. Patterson, Seth A. Edwards, Sandaruwan Ratnayake, Yu-Hung Hung, Pratheek H. Pandesha, R. Keith Slotkin, Richard Napier, Franck Dayan and Todd Gaines 2025b. A transposable element insertion in AUX/IAA16 disrupts splicing and causes auxin resistance in Bassia scoparia. The Plant Journal 123: e70339. doi: https://doi.org/10.1111/tpj.70339
17. Ramans-Harborough, S., A. P. Kalverda, I. W. Manfield, G. S. Thompson, M. Kieffer, V. Uzunova, M. Quareshy, J. M. Prusinska, S. Roychoudhry, K. I. Hayashi, R. Napier, C. D. Genio and S. Kepinski 2023. Intrinsic disorder and conformational coexistence in auxin coreceptors. Proc Natl Acad Sci U S A 120: e2221286120. doi: 10.1073/pnas.2221286120
18. Remington, David L., Todd J. Vision, Thomas J. Guilfoyle and Jason W. Reed 2004. Contrasting Modes of Diversification in the Aux/IAA and ARF Gene Families Plant Physiology 135: 1738–1752. doi: 10.1104/pp.104.039669
19. Ritz, Christian, Florent Baty, Jens C. Streibig and Daniel Gerhard 2016. Dose-Response Analysis Using R. PLoS One 10: e0146021. doi: 10.1371/journal.pone.0146021
20. Schmidt, G. W. and S. K. Delaney 2010. Stable internal reference genes for normalization of real-time RT-PCR in tobacco (Nicotiana tabacum) during development and abiotic stress. Mol Genet Genomics 283: 233–241. doi: 10.1007/s00438-010-0511-1
21. Todd, O. E., M. R. A. Figueiredo, S. Morran, N. Soni, C. Preston, M. F. Kubeš, R. Napier and T. A. Gaines 2020. Synthetic auxin herbicides: finding the lock and key to weed resistance. Plant Sci 300: 110631. doi: 10.1016/j.plantsci.2020.110631
22. Tong, Z., Y. Huang, Q. H. Zhu, L. Fan, B. Xiao and E. Shen 2024. Retrospect and prospect of Nicotiana tabacum genome sequencing. Front Plant Sci 15: 1474658. doi: 10.3389/fpls.2024.1474658
23. Topping, Jennifer F. 1998. Tobacco Transformation. In Plant Virology Protocols: From Virus Isolation to Transgenic Resistance, eds. Gary D. Foster and Sally C. Taylor, 365–372. Totowa, NJ: Humana Press.
24. Uzunova, V. V., M. Quareshy, C. I. Del Genio and R. M. Napier 2016. Tomographic docking suggests the mechanism of auxin receptor TIR1 selectivity. Open Biol 6. doi: 10.1098/rsob.160139
25. Xu, Shuqing, Thomas Brockmöller, Aura Navarro-Quezada, Heiner Kuhl, Klaus Gase, Zhihao Ling, Wenwu Zhou, Christoph Kreitzer, Mario Stanke, Haibao Tang, Eric Lyons, Priyanka Pandey, Shree P. Pandey, Bernd Timmermann, Emmanuel Gaquerel and Ian T. Baldwin 2017. Wild tobacco genomes reveal the evolution of nicotine biosynthesis. Proceedings of the National Academy of Sciences 114: 6133–6138. doi: doi:10.1073/pnas.1700073114

APPENDIX A

Supplemental Material for Chapter 1 – CLOQUINTOCET-MEXYL ENHANCES GLUTATHIONE-S-TRANSFERASE MEDIATED HERBICIDE METABOLISM IN WINTER WHEAT

Supplemental Table 1. TOPO cloning primers used for both GST candidates *TaGSTF1* and *TaGSTU1.*

PCR reaction used to amplify the *TaGSTF1* and *TaGSTU1* from the synthesized vectors including the associated overhangs required for TOPO cloning. PCR amplification for TOPO cloning was performed with an initial denaturation at 98 °C for 30 s, followed by 30 cycles of 98 °C for 10 s, 65 °C for 10 s, and 72 °C for 30 s, with a final extension at 72 °C for 10 min before holding at 4 °C.

Primer	Sequence (5'–3')
TaGSTF1 Forward	CACCATGGCGCCGGTGAA
TaGSTF1 Reverse	GCAGATGGTGCCGAAAAAACCG
TaGSTU1 Forward	CACCATGGCGGGCGGCGAT
TaGSTU1 Reverse	GTTGCTCGCCGCCGC

Supplemental Table 2. Forward and reverse primers for *TaGSTU1* promoter.
PCR reaction used to amplify the promoter sequence of *TaGSTU1*. Amplification was performed using the following cycling conditions: an initial denaturation at 94 °C for 30 s; 35 cycles of 94 °C for 10 s, 64 °C for 1 min, and 72 °C for 1 min; followed by a final extension at 72 °C for 2 min and a hold at 4 °C.

Primer	Sequence (5'–3')
Forward	GTTAGAATCTGATGCGGTCTAG
Reverse	TGGTCACAGATCCTTTGTTCGATGCCT

Supplemental Table 3. Summary of read and mapping assignments for each RNA sequencing samples across wheat genome.

Read-assignment metrics generated by featureCounts for RNA-seq libraries from Byrd, AP18 (AP18AX), and Cres (Crescent AX) wheat lines under treated (T) and untreated (U) conditions. Total reads reflect raw FASTQ sequencing depth, while mapped reads represent STAR-retained alignments. Within each BAM file, reads were classified as Assigned (overlapping annotated genes), No Features (intergenic or unannotated), or Ambiguity (overlapping multiple genes). All other unassigned categories were zero, indicating that STAR output contained only confidently mapped reads.

Sample	Total Reads (FASTQ)	Mapped Reads (STAR)	Assigned	No Features	Ambiguous
Cres_T1	29,657,298	27,169,492	23,325,349	3,486,218	357,925
Cres_T2	24,726,542	22,616,664	19,654,842	2,706,450	255,372
Cres_T3	29,220,194	25,917,129	22,683,193	2,987,061	246,875
Cres_U1	31,190,631	28,357,488	25,133,664	2,777,130	446,694
Cres_U2	30,628,912	27,830,813	24,210,032	3,229,386	391,395
Cres_U3	34,864,207	31,660,634	27,868,031	3,294,280	498,323
Byrd_T1	32,350,957	29,443,596	25,675,552	3,340,923	427,121
Byrd_T2	28,400,379	25,081,964	21,868,202	2,906,742	307,020
Byrd_T3	30,692,598	30,692,598	27,172,307	3,043,255	477,036
Byrd_U1	34,033,334	31,911,205	28,493,021	3,118,776	299,408
Byrd_U2	23,354,224	21,130,887	18,229,871	2,643,210	257,806
Byrd_U3	29,644,069	27,014,743	23,693,162	2,914,702	406,879
AP18_T1	33,475,428	22,680,657	19,964,819	2,494,596	221,242
AP18_T2	33,475,428	31,409,279	27,184,195	3,878,040	347,044
AP18_T3	33,177,458	30,661,790	26,521,197	3,843,660	296,933
AP18_U1	33,212,271	30,624,989	26,851,031	3,467,859	306,099
AP18_U2	26,547,142	24,537,551	21,281,670	2,894,774	361,107
AP18_U3	28,005,828	25,918,211	22,386,696	3,163,175	368,340

Supplemental Table 4. Constitutive differences in Glutathione S-transferase (GST) expression between untreated Crescent AX and AP18 AX.
Average normalized gene counts, log_2 fold-change (L2FC), and adjusted p-values (Padj) for GST genes between untreated Crescent AX and AP18 AX samples.

WHEAT LINE	GENE NAME	L_2FC	PADJ	NORMALIZED COUNTS CRES UNT	AP18 UNT
GST	TraesCS7B03G1197500	12.92	$2.57x10^{-4}$	540	0
	TraesCS1B03G0260500	11.37	$1.21x10^{-12}$	322	0
	TraesCS1B03G0260800	7.90	$7.34x10^{-4}$	47	0
	TraesCS1D03G0222800	7.44	$5.20x10^{-4}$	33	0
	TraesCS2B03G1334300	1.77	0.09	2154	340
	TraesCS1A03G0501600	-3.54	$1.63x10^{-15}$	32	448
CYP	TraesCS2D03G0217400	7.59	0.02	53	0
	TraesCS2D03G0081200	5.17	$4.88x10^{-11}$	2343	65
	TraesCS1A03G0529000	3.80	0.02	41	1
	TraesCS5A03G0601100	2.57	0.09	36	2
	TraesCS6D03G0881700	2.15	$9.26x10^{-6}$	339	77
	TraesCS1D03G0001300	1.53	0.09	73	10
	TraesCS7D03G0368900	1.06	0.03	406	146
UGT	TraesCS1A03G0217900	12.22	$1.09x10^{-16}$	553	0
	TraesCS2B03G0086500	10.29	$4.05x10^{-11}$	170	0
	TraesCS1A03G0293500	7.85	$3.55x10^{-7}$	41	0
	TraesCS2B03G0147200	2.50	$1.89x10^{-4}$	547	60
	TraesCS6D03G0214700	1.84	$8.67x10^{-4}$	208	28
	TraesCS1D03G0822400	-1.69	$5.46x10^{-3}$	85	337
	TraesCS5D03G0353000	-3.06	$3.83x10^{-06}$	18	200
ABC	TraesCS5A03G0502600	1.93	0.02	96	33
	TraesCS5B03G1170400	-2.45	$4.58x10^{-6}$	335	2104
	TraesCS2A03G0057000	-3.50	$8.82x10^{-16}$	33	394

Supplemental Table 5. Normalized counts and differential expression for glutamate-cysteine ligase across each wheat line treated with cloquintocet.
Average normalized gene count, log_2foldchange (L2FC) and adjusted p-value (Padj) for glutamate-cysteine ligase for Byrd, AP18 (AP18 AX), and Cres (Crescent AX).

WHEAT LINE	GENE NAME	L_2FC	PADJ	NORMALIZEDCOUNTS TREATED	UNTREATED
BYRD	TraesCS1A03G0175800	NA	NA	109	130
	TraesCS1B03G0240900	NA	NA	1389	940
	TraesCS1D03G0170700	NA	NA	882	553
AP18	TraesCS1A03G0175800	0.92	0.06	790	419
	TraesCS1B03G0240900	NA	NA	868	469
	TraesCS1D03G0170700	NA	NA	750	422
CRES	TraesCS1A03G0175800	1.01	0.01	1596	802
	TraesCS1B03G0240900	0.75	6.72×10^{-3}	1210	719
	TraesCS1D03G0170700	1.04	1.97×10^{-4}	1362	663

Supplemental Table 6. Normalized counts and differential expression for glutathione synthase across each wheat line treated with cloquintocet.
Average normalized gene count, log_2foldchange (L2FC) and adjusted p-value (Padj) for glutathione synthease for Byrd, AP18 (AP18 AX), and Cres (Crescent AX).

WHEAT LINE	GENE NAME	L_2FC	PADJ	NORMALIZEDCOUNTS TREATED	UNTREATED
BYRD	TraesCS4D03G0314100	NA	NA	4	1
	TraesCS5A03G0249300	1.89	0.06	370	189
	TraesCS5B03G0265000	1.96	0.05	1587	408
	TraesCS5D03G0261100	1.74	0.07	803	240
	TraesCS6A03G0334300	NA	NA	286	180
	TraesCS6B03G0431500	NA	NA	121	62
	TraesCS6D03G0288400	NA	NA	150	88
	TraesCS7A03G1072200	NA	NA	83	74
	TraesCS7B03G0915200	NA	NA	132	122
	TraesCS7D03G1022000	NA	NA	22	12
	TraesCS7D03G1022100	NA	NA	0	0
AP18	TraesCS4D03G0314100	NA	NA	24	4
	TraesCS5A03G0249300	NA	NA	292	127
	TraesCS5B03G0265000	1.39	0.01	672	271
	TraesCS5D03G0261100	1.28	0.06	389	159
	TraesCS6A03G0334300	NA	NA	161	105
	TraesCS6B03G0431500	NA	NA	219	20
	TraesCS6D03G0288400	NA	NA	103	59
	TraesCS7A03G1072200	NA	NA	26	71
	TraesCS7B03G0915200	NA	NA	82	94
	TraesCS7D03G1022000	NA	NA	12	15
	TraesCS7D03G1022100	NA	NA	1	0
CRES	TraesCS4D03G0314100	NA	NA	10	13
	TraesCS5A03G0249300	1.46	0.01	481	175
	TraesCS5B03G0265000	1.88	7.68×10^{-4}	1407	382
	TraesCS5D03G0261100	1.49	6.94×10^{-4}	742	265
	TraesCS6A03G0334300	NA	NA	194	129
	TraesCS6B03G0431500	1.41	0.01	123	46
	TraesCS6D03G0288400	NA	NA	103	88

	TraesCS7A03G1072200	1.13	0.01	203	93
	TraesCS7B03G0915200	NA	NA	174	122
	TraesCS7D03G1022000	NA	47	47	11
	TraesCS7D03G1022100	NA	1	1	2

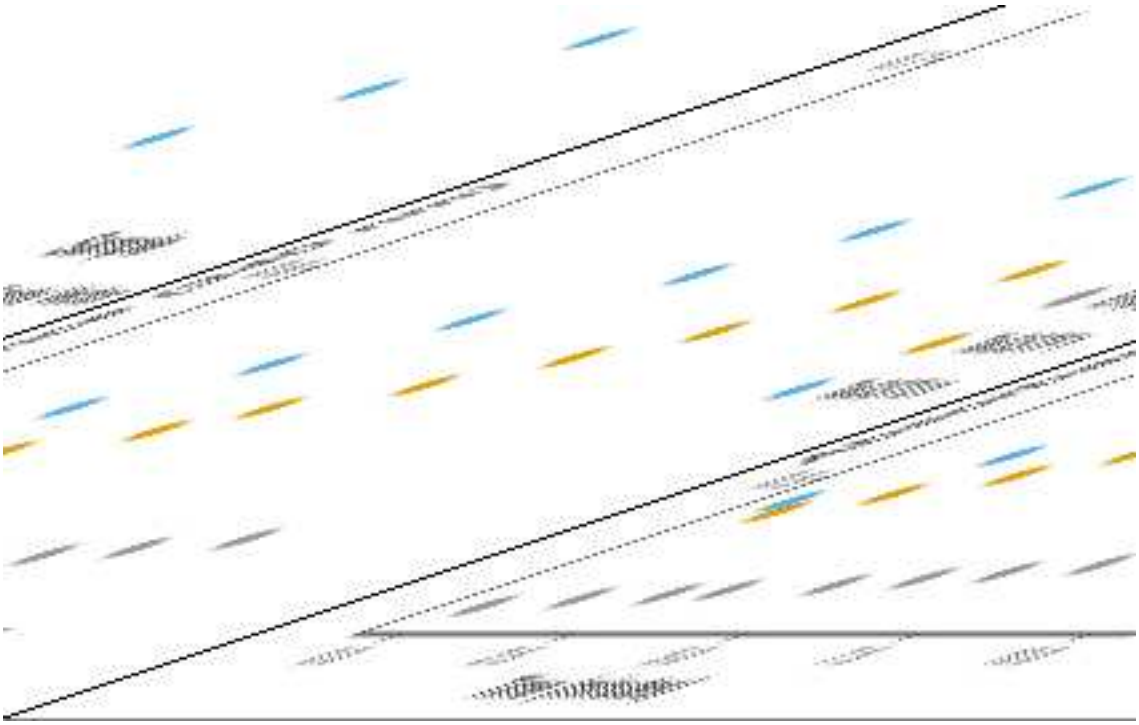

Supplemental Figure 1. Measurement of GST enzyme activity using the CDNB assay. Enzymatic activity for two candidate GST genes, TaGSTF1 and TaGSTU1, compared to the empty vector control. GST activity was quantified by monitoring the conjugation of reduced glutathione (GSH) to the model substrate 1-chloro-2,4-dinitrobenzene (CDNB). Formation of the GS-DNB conjugate was measured spectrophotometrically at 340 nm over a 10-min reaction period, and activity was calculated based on the linear increase in absorbance.

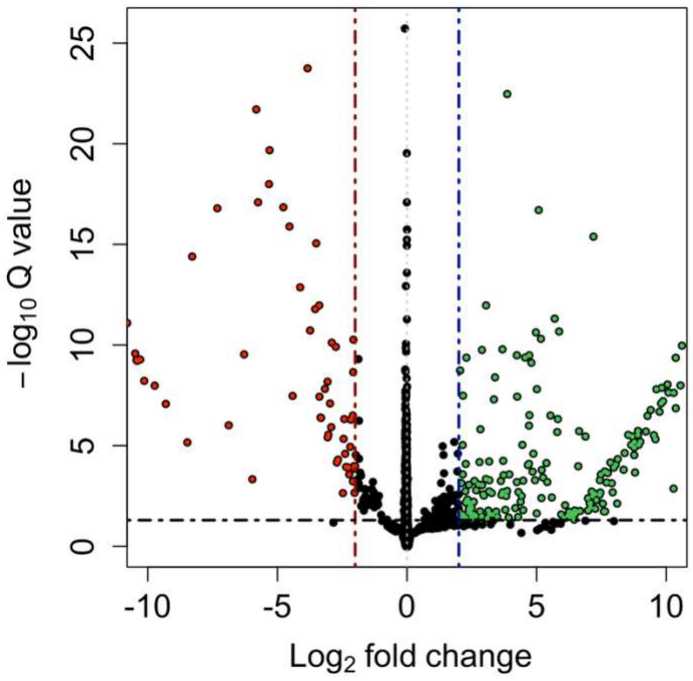

Supplemental Figure 2. Constitutive expression comparison between Crescent AX Untreated and AP18 AX Untreated.

Volcano plot that represents $\log_2$ fold change (x-axis) and $-\log_{10}$ (Q value) (y-axis) between Crescent AX untreated and AP18 AX untreated. Genes meeting significance thresholds ($Q < 0.1$ and $\log_2 FC > 1$) are highlighted in green (higher constitutive expression in Cres) and red (higher constitutive expression in AP18), while non-significant genes are shown in black. Vertical dashed lines indicate the ± 1 $\log_2$ fold-change cutoff, and the horizontal dashed line marks the $Q = 0.1$ threshold.

```
TaGSTF1      MAPVKLYGATLSWNVTRCVAALEEAGVGYEIVPINFGTGEHKSPDHLARNPFGGVPALGD         60
PfGSTF2      MAPVKVFGPAMSTNVARVLVFLEEVGAEYEVVNMDYKLQEQKSPEHLARNPFGQIPAFQD         60
AmGSTF1      MAPVKVFGPAMSTNVARVTLCLEEVGAEYEVVNIDFNTMEHKSPEHLARNPFGQIPAFQD         60
*****:** ::* **:*    ***.*. **:* :::   *:***:******** :**: *

TaGSTF1      GDLYVFESRAICKYACRKNK---PELLKEGDIKESAMVDVWLEVEAHGYTAALSPILFEC         117
PfGSTF2      GDLLLFESRAISKYVLRKYKSNGVDLLREGNLKEAALVDVWTEVDAHTYNPALSPVIYEC         120
AmGSTF1      GDLLLWESRAISKYVLRKYKTDEVDLLRESNLEEAAMVDVWTEVDAHTYNPALSPIVYQC         120
*** ::******.**. ** *    :**:*.:::*:*:**** **:** *. ****::::*

TaGSTF1      LIHPMLGGA-TDGKVIDDNLVKIKNVLAVYEAHLSK-SKYLAGDFLSLADLNHVSVTLCL         175
PfGSTF2      LFNPLMRGIPTNDNVVAESLEKLKKVLEVYEARLSKH-EYLAGDFVSFADLNHFPYTFYF         179
AmGSTF1      LFNPMMRGLPTDEKVVAESLEKLKKVLEVYEARLSKH-SYLAGDFVSFADLNHFPYTFYF         179
*::*:: *  *: :*: :.* *:*:** ****:***  .******:*:*****.  *: :

TaGSTF1      AATPYASLFDAYPHVKAWWTDLLARPSVGKVAALMKP---      212
PfGSTF2      MTTPHASLFDSYPHVKAWWERIMARPAVKKVAASMVPPKA      219
AmGSTF1      MATPHAALFDSYPHVKAWWDRLMARPAVKKIAATMVPPKA      219
:**:*:***:********  ::***:* *:** * *
```

Supplemental Figure 3. Comparative amino acid alignment of phi-class GSTs
Multiple sequence alignment of wheat TaGSTF1 with two phi-class glutathione S-transferases (GSTFs) from Asian Minor Bluegrass (PfGSTF2) and Blackgrass (AmGSTF1). Conserved and semi-conserved residues are indicated by standard Clustal notation (*, :, .), highlighting the high structural conservation typical of GSTF enzymes.

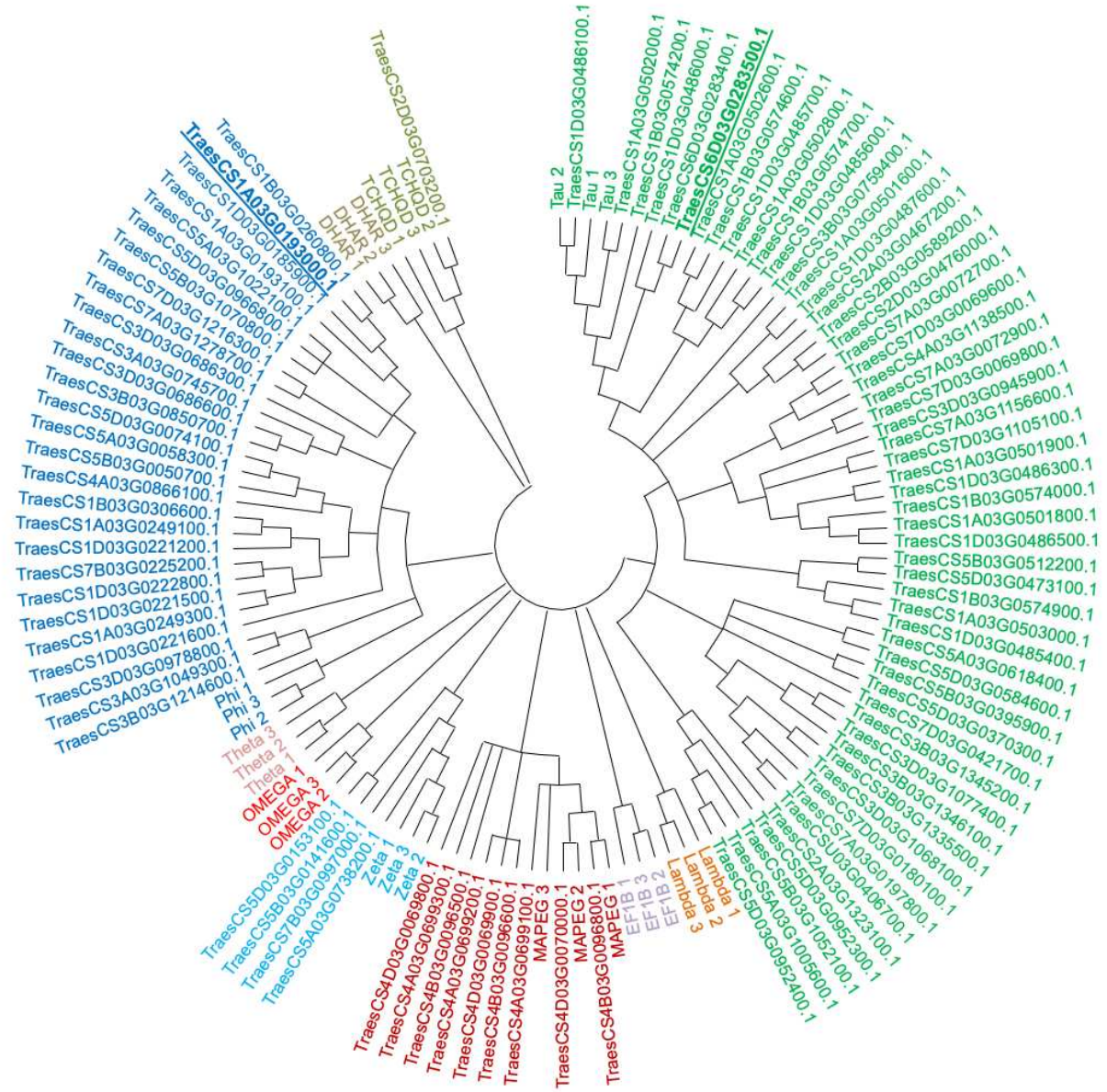
TraesCS2D03G0703200.1
TCHQD 2
TCHQD 3
TCHQD 1
DHAR 3
DHAR 2
DHAR 1
TraesCS1B03G0260800.1
TraesCS1A03G0193000.1
TraesCS1D03G0185900.1
TraesCS1A03G0193100.1
TraesCS5A03G0102100.1
TraesCS5D03G0966800.1
TraesCS5B03G1070800.1
TraesCS7D03G1216300.1
TraesCS7A03G1278700.1
TraesCS3D03G0686300.1
TraesCS3A03G0745700.1
TraesCS3D03G0686600.1
TraesCS3B03G0850700.1
TraesCS5D03G0074100.1
TraesCS5A03G0058300.1
TraesCS5B03G0050700.1
TraesCS4A03G0866100.1
TraesCS1B03G0306600.1
TraesCS1A03G0249100.1
TraesCS1D03G0221200.1
TraesCS7B03G0225200.1
TraesCS1D03G0222800.1
TraesCS1D03G0221500.1
TraesCS1A03G0249300.1
TraesCS1D03G0221600.1
TraesCS1D03G0978800.1
TraesCS3D03G1049300.1
TraesCS3A03G1214600.1
TraesCS3B03G1214600.1
Phi 1
Phi 3
Phi 2
Theta 3
Theta 2
Theta 1
OMEGA 1
OMEGA 3
OMEGA 2
OMEGA 4
TraesCS5D03G0153100.1
TraesCS5B03G0141600.1
TraesCS7B03G0997000.1
TraesCS5A03G0738200.1
Zeta 1
Zeta 3
Zeta 2
TraesCS4D03G0069800.1
TraesCS4A03G0699300.1
TraesCS4B03G0096500.1
TraesCS4D03G0699200.1
TraesCS4D03G0069900.1
TraesCS4B03G0096600.1
TraesCS4A03G0699100.1
MAPEG 3
TraesCS4D03G0070000.1
MAPEG 2
TraesCS4B03G0096800.1
MAPEG 1
EF1B 1
EF1B 3
EF1B 2
Lambda 3
Lambda 2
Lambda 1
TraesCS2A03G1323100.1
TraesCS5D03G0952400.1
TraesCS5B03G1005600.1
TraesCS5A03G1052100.1
TraesCS7A03G0406700.1
TraesCS7D03G0180100.1
TraesCS3D03G1068100.1
TraesCS3B03G1335500.1
TraesCS3B03G1346100.1
TraesCS3D03G1077400.1
TraesCS3B03G1345200.1
TraesCS3D03G0421700.1
TraesCS7D03G0370300.1
TraesCS5D03G0395900.1
TraesCS5B03G0584600.1
TraesCS5A03G0618400.1
TraesCS1D03G0485400.1
TraesCS1A03G0503000.1
TraesCS1B03G0574900.1
TraesCS5D03G0473100.1
TraesCS5B03G0512200.1
TraesCS1D03G0486500.1
TraesCS1A03G0501800.1
TraesCS1B03G0574000.1
TraesCS1D03G0486300.1
TraesCS1A03G0501900.1
TraesCS7D03G1105100.1
TraesCS7A03G1156600.1
TraesCS3D03G0945900.1
TraesCS7D03G0069800.1
TraesCS4A03G0072900.1
TraesCS7D03G1138500.1
TraesCS7A03G0069600.1
TraesCS7A03G0072700.1
TraesCS2B03G0476000.1
TraesCS2A03G0589200.1
TraesCS1D03G0487600.1
TraesCS1A03G0467200.1
TraesCS3B03G0501600.1
TraesCS1D03G0759400.1
TraesCS1A03G0485600.1
TraesCS1B03G0574700.1
TraesCS1D03G0485700.1
TraesCS1A03G0502800.1
TraesCS1B03G0574600.1
TraesCS6D03G0283500.1
TraesCS6D03G0283400.1
TraesCS1D03G0486000.1
TraesCS1B03G0574200.1
TraesCS1A03G0502000.1
TraesCS1D03G0486100.1
Tau 2
Tau 1
Tau 3

A.

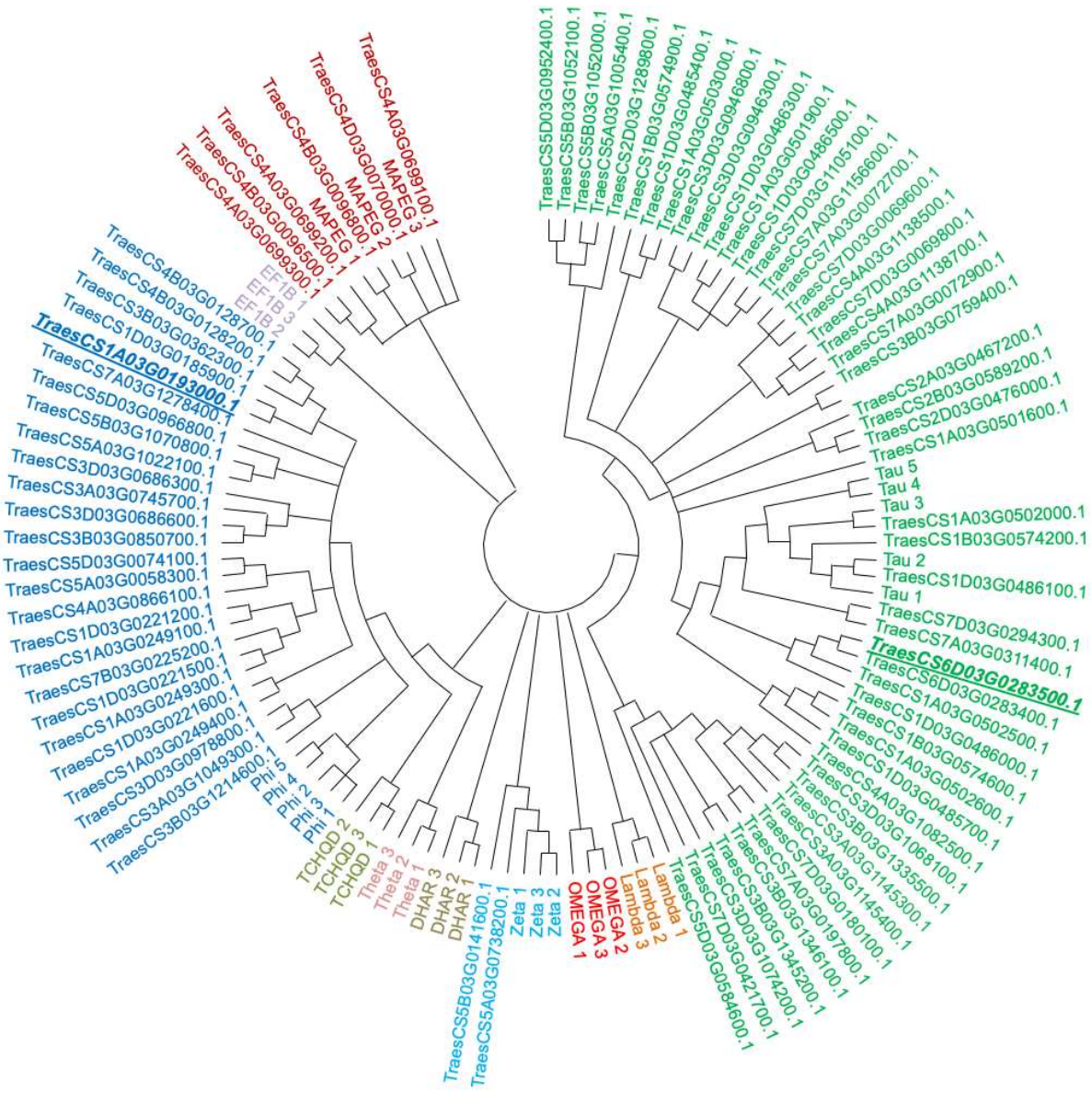
TraesCS5D03G0952400.1
TraesCS5B03G1052100.1
TraesCS5B03G1052000.1
TraesCS5A03G1005400.1
TraesCS2D03G1289800.1
TraesCS1B03G0574900.1
TraesCS1D03G0485400.1
TraesCS1A03G0503000.1
TraesCS3D03G0946800.1
TraesCS3D03G0946300.1
TraesCS1D03G0486300.1
TraesCS1A03G0501900.1
TraesCS1D03G0486500.1
TraesCS7D03G1105100.1
TraesCS7A03G1156600.1
TraesCS7D03G0072700.1
TraesCS7A03G0069600.1
TraesCS7D03G1138500.1
TraesCS4A03G0069800.1
TraesCS4A03G1138700.1
TraesCS7D03G0072900.1
TraesCS7A03G0759400.1
TraesCS3B03G0759400.1
TraesCS2A03G0467200.1
TraesCS2B03G0589200.1
TraesCS2D03G0476000.1
TraesCS1A03G0501600.1
Tau 5
Tau 4
Tau 3
TraesCS1A03G0502000.1
TraesCS1B03G0574200.1
Tau 2
TraesCS1D03G0486100.1
Tau 1
TraesCS7D03G0294300.1
TraesCS7A03G0311400.1
TraesCS6D03G0283500.1
TraesCS6D03G0283400.1
TraesCS1A03G0502500.1
TraesCS1B03G0486000.1
TraesCS1D03G0574600.1
TraesCS1D03G0502600.1
TraesCS4A03G0485700.1
TraesCS3D03G1082500.1
TraesCS3B03G1068100.1
TraesCS3A03G1335500.1
TraesCS7D03G1145400.1
TraesCS7A03G0180100.1
TraesCS3B03G1346100.1
TraesCS3D03G1074200.1
TraesCS5D03G0584600.1
TraesCS7D03G0421700.1
Lambda 1
Lambda 2
Lambda 3
OMEGA 1
OMEGA 2
OMEGA 3
Zeta 2
Zeta 3
Zeta 1
TraesCS5A03G0738200.1
TraesCS5B03G0141600.1
DHAR 1
DHAR 2
DHAR 3
Theta 1
Theta 2
Theta 3
TCHQD 1
TCHQD 3
TCHQD 2
Phi
Phi 3
Phi 2
Phi 4
Phi 5
TraesCS3B03G1214600.1
TraesCS3A03G1049300.1
TraesCS3D03G0978800.1
TraesCS1A03G0249400.1
TraesCS1D03G0221600.1
TraesCS1A03G0249300.1
TraesCS1D03G0221500.1
TraesCS7B03G0225200.1
TraesCS1A03G0249100.1
TraesCS1D03G0221200.1
TraesCS4A03G0866100.1
TraesCS5A03G0058300.1
TraesCS5D03G0074100.1
TraesCS3B03G0850700.1
TraesCS3D03G0686600.1
TraesCS3A03G0745700.1
TraesCS3D03G0686300.1
TraesCS5A03G1022100.1
TraesCS5B03G1070800.1
TraesCS5D03G0966800.1
TraesCS7A03G1278400.1
TraesCS1A03G0193000.1
TraesCS1D03G0185900.1
TraesCS3B03G0362300.1
TraesCS4B03G0128200.1
TraesCS4B03G0128700.1
EF-1B 1
EF-1B 3
EF-1B 2
TraesCS4A03G0699300.1
TraesCS4B03G0096500.1
MAPEG 1
TraesCS4B03G0096800.1
TraesCS4D03G0070000.1
MAPEG 2
TraesCS4A03G0699100.1
MAPEG 3

B.

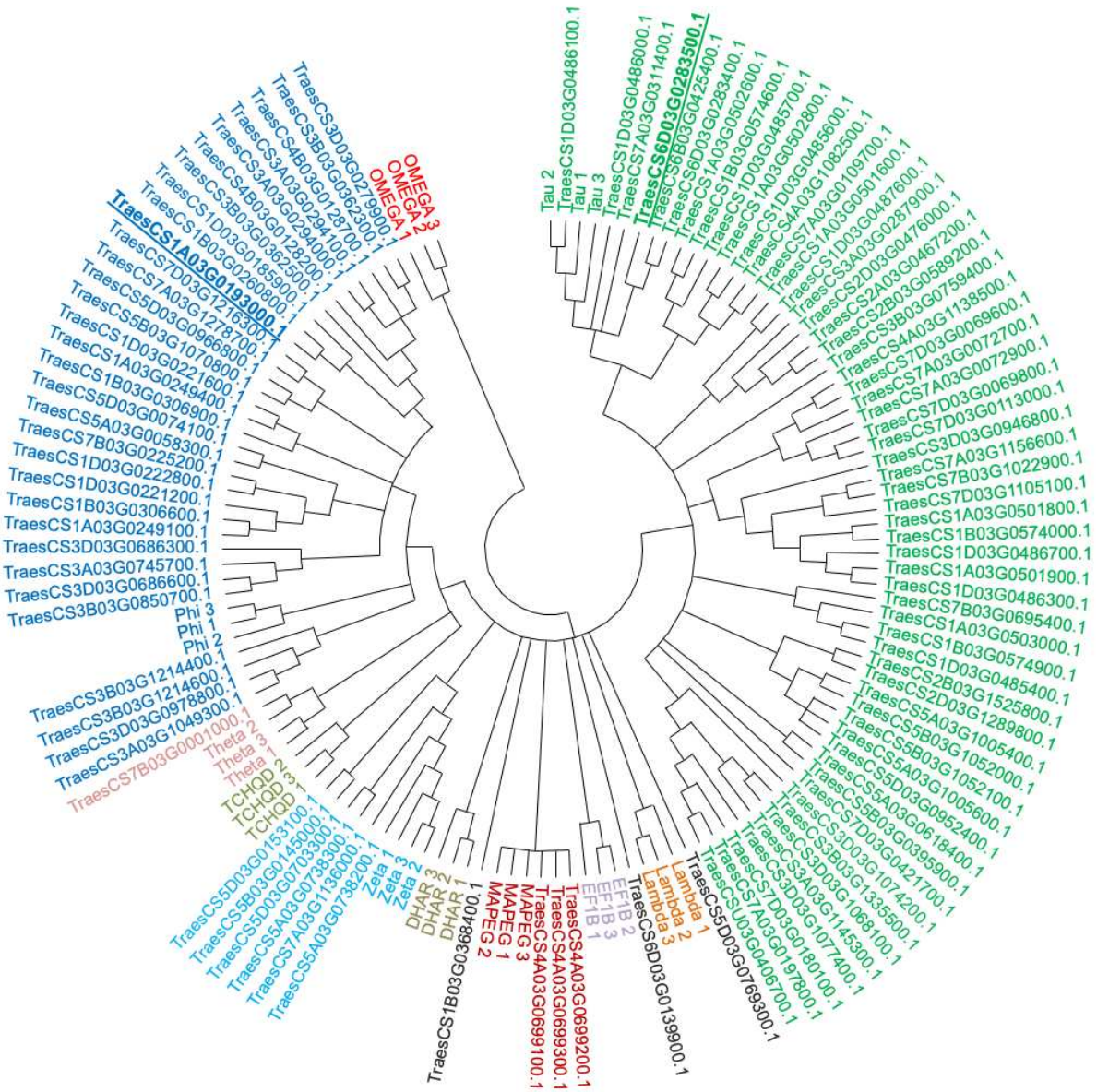

C.

Supplemental Figure 4. Neighbor joining phylogenetic tree of GST proteins from each wheat line.

Multiple sequence alignment of GST protein that were differentially expressed in each wheat line was performed using MUSCLE with default parameters. A phylogenetic tree was constructed in MEGA X using the neighbor-joining method with the Poisson substitution model and 1,000 bootstrap replicates. Branches with bootstrap support values ≥50% are shown. The tree is displayed in circular format, and GST classes are color-coded to highlight major clades. Previously reported GSTs classes were included to help build this tree (Hao et al., 2021). (A) Byrd showed 54 Tau, 28 Phi, 9 MAPEG, 4 Zeta, and 1 TCHQD class GSTs. (B) AP18

(AP18AX) showed 51 Tau, 26 Phi, 6 MAPEG, and 2 Zeta class GSTs. Finally, (C) Cres (Crescent AX) showed 57 Tau, 32 Phi, 6 Zeta, 3 MAPEG, and 1 Theta class GSTs. Three GSTs annotated through the Phytozome database did not group with any family.

Supplemental Material for Chapter 2 – IDENTIFICATION AND FUNCTIONAL VALIDATION OF CYTOCHROME P450S CONFERRING IMAZAMOX RESISTANCE IN FERAL RYE

Primer	Sequence (5' → 3')
PPO_F	ATGACTTGGTGTTCGGGGAC
PPO_R	GAACTTAGGTCCTGTGGGGC

Supplemental Table 1. PPO Sequencing
Polymerase chain reaction primers used to amplify a section of PPO genes of R, S and F1 hybrid feral rye plants. Thermocycler conditions were 95 C for 5 minutes; 35 cycles of 95 C for 15 seconds, 65 C for 15 seconds, 72 C for 2 minutes; 72 C for 5 minutes.
Gene: SECCE5Rv1G0302760 (Protoporphyrinogen oxidase)
Primary_assembly 5R: 41,786,107-41,789,550

Primer	Sequence (5’ → 3’)
pFGC_F	CCAACCACGTCTTCAAAGCA
pFGC_R	GGCGTCTCGCATATCTCATT

Table S2. pFGC primer and PCR settings

Polymerase chain reaction primers used to amplify a section of pFGC5941. Thermocycler conditions were 95 C for 5 minutes; 35 cycles of 95 C for 15 seconds, 60 C for 15 seconds, 72 C for 2 minutes; 72 C for 5 minutes.

```
CLUSTAL O(1.2.4) multiple sequence alignment

CYP81A10      MDKAYVAVLSFAFLFVLHYLVARRNSNGNGSKGKKCAQHKLPPSPPSVPFLGHLHL---- 56
CYP81A52      MDKAYIAILSFTFLFLLHYILGKVSN-GRRSK----GALELPPSPRAIPFLGHLHLLEKP 55
CYP81A24      MDKAYIAVISIAFLFLLHYLLGRGGG-GRSGK----GARQLPPSPPAVPFLGHLHLVKTP 55
              *****:*::*::***:***::.: .. *. .*    .  :***** ::********

CYP81A104     ------------------------------------------------------VSFD 60
CYP81A52      FHAALCGLAKRLGPVFSLRLGSRRAVVVSSPECARECFTEHDVIFANRPQFPSQLLVSYD 115
CYP81A24      FHAALARLAARHGPVFSLRMGSRRAVVVSSPECARECFTEHDVSFANRPLFPSMRLVSFD 115
                                                                    **:*

CYP81A104     GAALSTSSYGPYWRNLRRVATVHLLSAHRVGCMAGTTIAAEVRAMVRRMSRTAQAAPGGA 120
CYP81A52      GIALSTSSYGPHWRNLRRVAAVQLLSAHRVACMSGV-IGDEVRAMARRLFRAAAASPGGA 174
CYP81A24      GAMLSVSSYGPHWRNLRRVAAVQLLSAHRVACMTPA-IAAEVRAMVRRMDHAAAAAPSGA 174
              *  **.*****:********:*:*******.**: . *. *****.**: ::* *:*.**

CYP81A104     ARIELKRRLFELSLSVLMETIAQTKTSRTEADDDTDMSPEAKEFKGIVDKVVPYLGTANL 180
CYP81A52      ARVELKRRLFELSLSVLMETIAQTKGTRSEADADTDMSVEAQEFKKVVDEIIPHIGAANL 234
CYP81A24      ARVQLKRRLFELSLSVLMETIARTKTSRTEANADTDMSPEAHEFKQIVDQIVPYLGTANR 234
              **::********************:** :*:**: ***** **:*** :**:::*::*:**

CYP81A104     WDYLPVLRWLDVFGVRSKILSAVSRRDAFLRRLIDAERRRLDDGNDGGEKKSIIAVLLTL 240
CYP81A52      WDYLPVLRWFDVFGVRNKILAAVSRRDAFMLRLIDNERRRLDDGGAEGDKKSMIAVLLTL 294
CYP81A24      WDYLPVLRWLDVFGVRNKIMDAVSRRDAFLNRLIDAERQRLDDG-SESEKKSMIAVLLAL 293
              *********:******.**: ********: **** **:*****   .:***:*****:*

CYP81A104     QKSEPEIYTDTTIMALCGNLFGAGTETTSTTTEWAMSLLLNHPEKLRKAQAEIDKLVGTS 300
CYP81A52      QKTEPEVYTDTMITALCANLFGAGTETTSTTTEWAMSLLLNHPAALRKAQAEIDAAVGTS 354
CYP81A24      QKSEPEVYTDATIMALCTNLFGAGTETTSTTTEWAMSLLLNHPEKLKKAQAEIDAAVGTS 353
               **:***:***: * *** ************************  *:*******  ****

CYP81A104     RLLTADDVPHLTYLRCIIDETMRLYPAAPLLLPHESATDCKVGGYDVPAGTILLVNVYAI 360
CYP81A52      RLVTADDVPRLAYLQCIVSETLRLYPAAPLLLPHQSSADCKVGGYNVPSGTMLMVNAYSI 414
CYP81A24      RLVAADDVPRLAYLQSIIHETLRLYPAAPLLLPHEAAADTKVGGYDVPRGTMLLVNVYAI 413
              **::*****:*:**:.*: **:************::::* *****:** **:*:**.*:*

CYP81A104     HRDPVVWEKPLEFRPERFQDGKTEGKLMMPFGMGRRKCPGETLALRTIGMVLGTLIQCFD 420
CYP81A52      HRDPAVWERPLEFVPERFEDGKAEGRFMIPFGMGRRRCPGETLALRTIGMVLATLVQCFD 474
CYP81A24      HRDPAVWEDPAAFRPERFEDGKSEGRLLMPFGMGRRKCPGETLALRTVGLVLGTLVQCFD 473
              ****.*** *  * ****:***:**::::*******:**********:*:**.**:****

CYP81A104     WDRVDGVEVDMTEGGGLTIPRIVPLEAMCRPRAAMREVLQE-      461
CYP81A52      WERVDGVEVDMTESGGLTIPKAVPLEAVCRPRPAMRDVLQSL      516
CYP81A24      WDRVDGVEVDMTEGGGLTMPRAVPLEAMCRPRAAMRRVLQE-      514
              *:***********.****:*: *****:**** *** ***.
```

Supplemental Figure 1. Multiple sequence alignment of CYP81A52 from feral rye with CYP81A24 and CYP81A104, two enzymes previously shown to metabolize imazamox. A CLUSTAL O (1.2.4) multiple sequence alignment comparing the amino acid sequences of CYP81A52 (feral rye), CYP81A24 (*Echinochloa phyllopogon*), and CYP81A104 (*Eleusine indica*). Conserved residues are shaded, and symbols below the alignment indicate the degree of conservation ("*" fully conserved; ":" strongly similar; "." weakly similar). This alignment was generated using UniProt protein sequences and CLUSTAL O.

```
CYP72A31          ---MVFRGWLMWAPASAPVLVVFGLLFGLALVWQAGRLLHRLWWRPRRLEKALRARGLRG   57
CYP72A1365_S      MATSVMGSF------LPPREVLFA-AAVAAMAWCAVRALEWAWWRPRRLGRALRSQGLRG   53
CYP72A1365_R      MATSVMGSF------LPPREALYA-AAVAAMAWCAVRALEWAWWRPRRLGRALRSQGLRG   53
                      *: .:        *  .:::.     *:.* * * *.  ******* :***::****

CYP72A31          SSYRFLTGDLAEESRRRKEAW--ARPLPLRCHDIAPRIKPFLHDTLGEHGKQRQPCITWF  115
CYP72A1365_S      TAYRPVAGDAPLMQRLNREARSRAMPLGAGCHDVVPRAMPLFHRTMQEHGKM---SITWF  110
CYP72A1365_R      TAYRPVAGDAPLMQRLNREARSRAMPLGAGCHDVVPRAMPLFHQAMQEHGKM---SITWF  110
                  ::** ::**    .* .:**   * **   ***:.**  *::* :: ****    .****

CYP72A31          GPTPEVNITDPELAKVVLSNKFGHLERVRFKEVSKLLSQGLTYHEGEKWVKHRRIINPAF  175
CYP72A1365_S      GPIPRVTITKPELVREVLSNKFGHFEKLKFGRLQRMLHNGVGSHEGEKWARHRRIINPAF  170
CYP72A1365_R      GPVPRVTITKPGLVREVLSNKFGHFEKLKFGRLQRMLHNGVGSHEGEKWARHRRIINPAF  170
                  ** *.*.**.* *.: ********:*:::* .:.::* :*:  ******.:*********

CYP72A31          QLEKLKLMLPAFSACCEELISRWIGSIG--CDGSYEVDCWPELKSLTGDVISRTAFGSSY  233
CYP72A1365_S      HLEKLKRMLPAFAACCTELVERWEGLALGAGDASCEVDVWPGMQNLTGDVISRAAFGSSY  230
CYP72A1365_R      HLEKLKRMLPAFAACCTELVERWEGLALAAGNASCKVDVWPDMQNLTGDVISRAAFGSSY  230
                  :***** *****:*** **:.** *      :.* :** ** ::.********:******

CYP72A31          LEGRRVFELQAEQFERAMKCMQKISIPGYMSLPIENNRKMHQINKEIESILRGIIGKKMQ  293
CYP72A1365_S      LEGRRIFQLQGEQLELVLFAMSKTHIPGYLLLPTKANRRMKQIAAEIERVLKGIVAKREN  290
CYP72A1365_R      LEGRRIFQLQGEQLELVLFAMTKTHIPGYLLLPTKANRRMKQIATEIERVLKGIVSRREN  290
                  *****:*:**.**:* .: .* *  ****: ** : **:*:**  *** :*:**:.:: :

CYP72A31          AMKEGESTKDDLLGILLESNTKHMEENGQSSQGLTMKDIVEECKLFYFAGAETTSVLLTW  353
CYP72A1365_S      AMRAGEATSDDLLGLLLESNMAHCRDSKGARIGITTDDVIGECKLFYFAGAETTSVLLTW  350
CYP72A1365_R      AMRAGEATSDDLLGLLLESNMAHCEDSKGARIGITTDDVIGECKLFYFAGAETTSVLLTW  350
                  **: **:*.*****:*****  * .:.  :  *:* .*:: ******************

CYP72A31          AMLLLSMHPEWQDRAREEILGLFRK-NKPDYEGLSRLKIVTMILYEVLRLYPPFIEIGRK  412
CYP72A1365_S      TMILLCMHPEWQDRAREEVLHVFGAAGTPDYDGLSRLRVVTMVLYEVLRLYTPVTAIHRE  410
CYP72A1365_R      TMILLCMHPEWQDRAREEVLHVFGDAGTPDYDGLSRLRVVTMVLYEVLRLYTPVTAIHRE  410
                  :*:**.************:* :*   ..***:*****::***:******** *.  * *:

CYP72A31          TYKEMEIGGVTYPAGVSIKIPVLFIHHDPDTWGSDVHEFKPERFSEGISKASKDPGAFLP  472
CYP72A1365_S      TYKPMELGGIRYPAGVVLMLPLLCIHHDKEVWGADADEFRPERFSEGISKASVDAPAFFP  470
CYP72A1365_R      TYKPMELGGIRYPAGVVLMLPLLCVHHDKEVWGADADEFRPERFSEGISKASADAPAFFP  470
                  *** **:**: ***** : :*:* :*** :.**:*..**:************ *  **:*

CYP72A31          FGWGPRICIGQNFALLEAKMALCLILQRLEFELAPSYTHAPHTMVTLHPMHGAQIKVRAI  532
CYP72A1365_S      FGWGPRVCIGQNFALLEAKMGLAIILRRFSFQLSPSYTHAPFPVGLLQPQHGAQLMLKTL  530
CYP72A1365_R      FGWGPRVCIGQNFALLEAKMGLAIILRRFSFQLSPSYTHAPFPVGLLQPQHGAQLRLKTL  530
                  ******:**************.*.:**:*:.*:*:*******. :  *:* ****: ::::

CYP72A31          --  532
CYP72A1365_S      IQ  532
CYP72A1365_R      IQ  532
```

Supplemental Figure 2. Amino acid sequence alignment of CYP72A1365 alleles from resistant (R) and susceptible (S) feral rye plants.
A CLUSTAL O (1.2.4) multiple sequence alignment comparing the amino acid sequences of resistant (R), sensitive (S) **CYP72A1365** from feral rye and CYP72A31 from rice (Saika et el., 2014). Conserved residues are shaded, and symbols below the alignment indicate the degree of conservation ("*" fully conserved; ":" strongly similar; "." weakly similar). This alignment was generated using UniProt protein sequences and CLUSTAL O.

Supplemental Figure 3. Imazamox dose response in CYP81A52 and CYP72A1365 transgenic events compared to the wild type (WT) control.
Dose response assessment of imazamox (IM) injury across a range of application rates (0, 0.3, 0.7, 1.5, 3.0, 6.0, and 12 g ha^{-1}) applied with 1% (v/v) MSO and 5% (v/v) UAN. Rates were applied in order from left 0 to right 12 g ha^{-1}. Visual injury ratings were recorded 14 days after treatment. (A) Three transgenic CYP81A52 overexpression events and (B) two resistant (R) and two sensitive (S) of *CYP72A1365* are compared with the wild-type (WT) control.

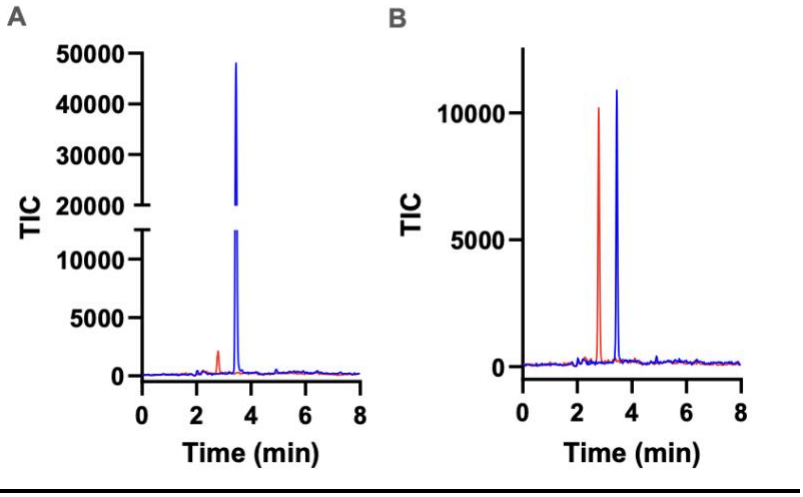

Supplemental Figure 4. Total ion chromatograms (TIC) of imazamox and its O-demethylated metabolite in wild-type and CYP-overexpressing Arabidopsis.

(A) TIC trace from wild-type (WT) *Arabidopsis thaliana*, showing a prominent peak corresponding to the parent imazamox compound (~50,000 TIC units) and minimal accumulation of the O-demethylated metabolite. (B) TIC trace from transgenic plants overexpressing the candidate CYP gene, displaying a reduced parent IM peak and a corresponding increase in the O-demethylated metabolite. Retention time (min) is shown on the x-axis.

```
CLUSTAL O(1.2.4) multiple sequence alignment


ALS_R1      MAAATSPAVAFSGAAAARPKPARQPLPRHQPASRRALPARIVRCCAASPAAAATSAAPPA          60
ALS_R2      MAAATSPAVAFSGAAAARPKPARQPLPRHQPASRRALPARIVRCCAASPAAAATSAAPPA          60
ALS_R3      MAAATSPAVAFSGAAAARPKPARQPLPRHQPASRRALPARIVRCCAASPAAAATSAAPPA          60
ALS_S1      MAAATSPAVAFSGAAAARPKPARQPLPRHQPASRRALPARIVRCCAASPAAAATSAAPPA          60
ALS_S2      MAAATSPAVAFSGAAAARPKPARQPLPRHQPASRRALPARIVRCCAASPAAAATSAAPPA          60
ALS_S3      MAAATSPAVAFSGAAAARPKPARQPLPRHQPASRRALPARIVRCCAASPAAAATSAAPPA          60
            ************************************************************

ALS_R1      TALRPWGPSEPRKGADILVEALERCGIVDVFAYPGGASMEIHQALTRSPVITNHLFRHEQ          120
ALS_R2      TALRPWGPSEPRKGADILVEALERCGIVDVFAYPGGASMEIHQALTRSPVITNHLFRHEQ          120
ALS_R3      TALRPWGPSEPRKGADILVEALERCGIVDVFAYPGGASMEIHQALTRSPVITNHLFRHEQ          120
ALS_S1      TALRPWGPSEPRKGADILVEALERCGIVDVFAYPGGASMEIHQALTRSPVITNHLFRHEQ          120
ALS_S2      TALRPWGPSEPRKGADILVEALERCGIVDVFAYPGGASMEIHQALTRSPVITNHLFRHEQ          120
ALS_S3      TALRPWGPSEPRKGADILVEALERCGIVDVFAYPGGASMEIHQALTRSPVITNHLFRHEQ          120
            ************************************************************

ALS_R1      GEAFAASGYARASGRVGVCVATSGPGATNLVSALADALLDSIPMVAITGQVPRRMIGTDA          180
ALS_R2      GEAFAASGYARASGRVGVCVATSGPGATNLVSALADALLDSIPMVAITGQVPRRMIGTDA          180
ALS_R3      GEAFAASGYARASGRVGVCVATSGPGATNLVSALADALLDSIPMVAITGQVPRRMIGTDA          180
ALS_S1      GEAFAASGYARASGRVGVCVATSGPGATNLVSALADALLDSIPMVAITGQVPRRMIGTDA          180
ALS_S2      GEAFAASGYARASGRVGVCVATSGPGATNLVSALADALLDSIPMVAITGQVPRRMIGTDA          180
ALS_S3      GEAFAASGYARASGRVGVCVATSGPGATNLVSALADALLDSIPMVAITGQVPRRMIGTDA          180
            ************************************************************

ALS_R1      FQETPIVEVTRSITKHNYLVLDVEDIPRVIQEAFFLASSGRPGPVLVDIPKDIQQQMAVP          240
ALS_R2      FQETPIVEVTRSITKHNYLVLDVEDIPRVIQEAFFLASSGRPGPVLVDIPKDIQQQMAVP          240
ALS_R3      FQETPIVEVTRSITKHNYLVLDVEDIPRVIQEAFFLASSGRPGPVLVDIPKDIQQQMAVP          240
ALS_S1      FQETPIVEVTRSITKHNYLVLDVEDIPRVIQEAFFLASSGRPGPVLVDIPKDIQQQMAVP          240
ALS_S2      FQETPIVEVTRSITKHNYLVLDVEDIPRVIQEAFFLASSGRPGPVLVDIPKDIQQQMAVP          240
ALS_S3      FQETPIVEVTRSITKHNYLVLDVEDIPRVIQEAFFLASSGRPGPVLVDIPKDIQQQMAVP          240
            ************************************************************

ALS_R1      VWDTPMSLPGYIARLPKPPSTESLEQVLRLVGESRRPILYVGGGCAASGEELRRFVELTG          300
ALS_R2      VWDTPMSLPGYIARLPKPPSTESLEQVLRLVGESRRPILYVGGGCAASGEELRRFVELTG          300
ALS_R3      VWDTPMSLPGYIARLPKPPSTESLEQVLRLVGESRRPILYVGGGCAASGEELRRFVELTG          300
ALS_S1      VWDTPMSLPGYIARLPKPPSTESLEQVLRLVGESRRPILYVGGGCAASGEELRRFVELTG          300
ALS_S2      VWDTPMSLPGYIARLPKPPSTESLEQVLRLVGESRRPILYVGGGCAASGEELRRFVELTG          300
ALS_S3      VWDTPMSLPGYIARLPKPPSTESLEQVLRLVGESRRPILYVGGGCAASGEELRRFVELTG          300
            ************************************************************

ALS_R1      IPVTTTLMGLGNFPSDDPLSLRMLGMHGTVYANYAVDKADLLLAFGVRFDDRVTGKIEAF          360
ALS_R2      IPVTTTLMGLGNFPSDDPLSLRMLGMHGTVYANYAVDKADLLLAFGVRFDDRVTGKIEAF          360
ALS_R3      IPVTTTLMGLGNFPSDDPLSLRMLGMHGTVYANYAVDKADLLLAFGVRFDDRVTGKIEAF          360
ALS_S1      IPVTTTLMGLGNFPSDDPLSLRMLGMHGTVYANYAVDKADLLLAFGVRFDDRVTGKIEAF          360
ALS_S2      IPVTTTLMGLGNFPSDDPLSLRMLGMHGTVYANYAVDKADLLLAFGVRFDDRVTGKIEAF          360
ALS_S3      IPVTTTLMGLGNFPSDDPLSLRMLGMHGTVYANYAVDKADLLLAFGVRFDDRVTGKIEAF          360
            ************************************************************

ALS_R1      ASRSKIVHIDIDPAEIGKNKQPHVSICADIKLALQGLNALLNGSKAQQGLDFGPWHKELD          420
ALS_R2      ASRSKIVHIDIDPAEIGKNKQPHVSICADIKLALQGLNALLNGSKAQQGLDFGPWHKELD          420
ALS_R3      ASRSKIVHIDIDPAEIGKNKQPHVSICADIKLALQGLNALLNGSKAQQGLDFGPWHKELD          420
ALS_S1      ASRSKIVHIDIDPAEIGKNKQPHVSICADIKLALQGLNALLNGSKAQQGLDFGPWHKELD          420
ALS_S2      ASRSKIVHIDIDPAEIGKNKQPHVSICADIKLALQGLNALLNGSKAQQGLDFGPWHKELD          420
ALS_S3      ASRSKIVHIDIDPAEIGKNKQPHVSICADIKLALQGLNALLNGSKAQQGLDFGPWHKELD          420
            ************************************************************

ALS_R1      QQKREFPLGFKTFGEAIPPQYAIQVLDELTKGEAIIATGVGQHQMWAAQYYTYKRPRQWL          480
ALS_R2      QQKREFPLGFKTFGEAIPPQYAIQVLDELTKGEAIIATGVGQHQMWAAQYYTYKRPRQWL          480
ALS_R3      QQKREFPLGFKTFGEAIPPQYAIQVLDELTKGEAIIATGVGQHQMWAAQYYTYKRPRQWL          480
ALS_S1      QQKREFPLGFKTFGEAIPPQYAIQVLDELTKGEAIIATGVGQHQMWAAQYYTYKRPRQWL          480
ALS_S2      QQKREFPLGFKTFGEAIPPQYAIQVLDELTKGEAIIATGVGQHQMWAAQYYTYKRPRQWL          480
ALS_S3      QQKREFPLGFKTFGEAIPPQYAIQVLDELTKGEAIIATGVGQHQMWAAQYYTYKRPRQWL          480
            ************************************************************

ALS_R1      SSSGLGAMGFGLPAAAGAAVANPGVTVVDIDGDGSFLMNIQELALIRIENLPVKVMILNN          540
ALS_R2      SSSGLGAMGFGLPAAAGAAVANPGVTVVDIDGDGSFLMNIQELALIRIENLPVKVMILNN          540
ALS_R3      SSSGLGAMGFGLPAAAGAAVANPGVTVVDIDGDGSFLMNIQELALIRIENLPVKVMILNN          540
ALS_S1      SSSGLGAMGFGLPAAAGAAVANPGVTVVDIDGDGSFLMNIQELALIRIENLPVKVMILNN          540
ALS_S2      SSSGLGAMGFGLPAAAGAAVANPGVTVVDIDGDGSFLMNIQELALIRIENLPVKVMILNN          540
ALS_S3      SSSGLGAMGFGLPAAAGAAVANPGVTVVDIDGDGSFLMNIQELALIRIENLPVKVMILNN          540
            ************************************************************

ALS_R1      QHLGMVVQWEDRFYKANRAHTYLGNPENESEIYPDFVTIAKGFNVPAVRVTKKSEVTAAI          600
```

```
ALS_R2      QHLGMVVQWEDRFYKANRAHTYLGNPENESEIYPDFVTIAKGFNVPAVRVTKKSEVTAAI          600
ALS_R3      QHLGMVVQWEDRFYKANRAHTYLGNPENESEIYPDFVTIAKGFNVPAVRVTKKSEVTAAI          600
ALS_S1      QHLGMVVQWEDRFYKANRAHTYLGNPENESEIYPDFVTIAKGFNVPAVRVTKKSEVTAAI          600
ALS_S2      QHLGMVVQWEDRFYKANRAHTYLGNPENESEIYPDFVTIAKGFNVPAVRVTKKSEVTAAI          600
ALS_S3      QHLGMVVQWEDRFYKANRAHTYLGNPENESEIYPDFVTIAKGFNVPAVRVTKKSEVTAAI          600
            ************************************************************

ALS_R1      KKMLETPGPYLLDIIVPHQEHVLPMIPSGGAFKDMIMEGDGRTAY    645
ALS_R2      KKMLETPGPYLLDIIVPHQEHVLPMIPSGGAFKDMIMEGDGRTAY    645
ALS_R3      KKMLETPGPYLLDIIVPHQEHVLPMIPSGGAFKDMIMEGDGRTAY    645
ALS_S1      KKMLETPGPYLLDIIVPHQEHVLPMIPSGGAFKDMIMEGDGRTAY    645
ALS_S2      KKMLETPGPYLLDIIVPHQEHVLPMIPSGGAFKDMIMEGDGRTAY    645
ALS_S3      KKMLETPGPYLLDIIVPHQEHVLPMIPSGGAFKDMIMEGDGRTAY    645
            *****************************************
```

Supplemental Figure 5. Protein sequence alignment comparing the ALS sequence between R and S samples

A CLUSTAL O (1.2.4) multiple sequence alignment of ALS amino acid sequences from resistant (R) and sensitive (S) feral rye samples showing no detectable sequence variation among all samples used for RNA-sequencing.

SAMPLE	TOTAL READS (FASTQ)	MAPPED READS	ASSIGNED	NO FEATURES	AMBIGUOUS	ASSIGNED %
R_0H_1	42,440,828	18,936,598	17,010,610	1,889,752	36,236	89.80%
R_0H_2	51,858,802	23,415,113	21,031,972	2,347,840	35,301	89.80%
R_0H_3	51,596,148	23,384,889	20,903,805	2,447,934	33,150	89.40%
R_0H_4	56,132,990	24,569,635	21,936,898	2,597,780	34,957	89.30%
R_8H_1	47,025,708	20,615,804	18,376,121	2,181,417	58,266	89.10%
R_8H_2	54,575,440	24,407,809	21,666,439	2,710,495	30,875	88.80%
R_8H_3	60,561,482	26,947,327	23,727,477	3,171,165	48,685	88.10%
R_8H_4	49,399,332	22,144,696	19,364,660	2,740,553	39,483	87.40%
S_0H_1	49,351,400	22,085,535	19,537,492	2,520,192	27,851	88.50%
S_0H_2	51,213,386	23,178,996	21,055,026	2,061,755	62,215	90.80%
S_0H_3	58,353,996	26,328,343	23,744,832	2,539,505	44,006	90.20%
S_0H_4	44,553,774	20,221,038	17,712,230	2,477,224	31,584	87.60%
S_8H_1	50,045,642	22,458,829	19,750,578	2,669,550	38,701	87.90%
S_8H_2	51,932,432	23,448,050	20,936,215	2,467,887	43,948	89.30%
S_8H_3	50,147,078	22,118,512	19,594,265	2,492,034	32,213	88.60%
S_8H_4	45,010,804	19,794,205	17,547,156	2,219,456	27,593	88.60%

Table S3. Read alignment and gene assignment summary for RNA-seq libraries.

Summary of sequencing RNA-seq samples representing resistant (R) and susceptible (S) plants at 0 h and 8 h after treatment. Total reads represent raw FASTQ sequence counts. Uniquely mapped reads reflect STAR genome alignment output. Assigned corresponds to reads successfully counted to annotated features using featureCounts, and No Features indicates reads aligning outside annotated gene models. Ambiguous reads represent multimatching or overlapping assignments.

Supplemental Material for Chapter 3 – DICAMBA RESISTANCE CONFERRED BY KOCHIA (*BASSIA SCOPARIA*) AUX/IAA16 MUTATION IN TOBACCO (*NICOTIANA TABACUM*)

Primer name	Sequence (5'-3')
BsIAA16_clone_1F	TTACCATGGGGCGCGATGTTGAGTAACGAGAGAGACAAG
BsIAA16_clone_843R	GACTCACCTAGGATCTCAGCTTCTGTTCTTGCACTTC

Table 1. PCR primers used to clone BsAUX/IAA16 into the pFGC5941 vector are listed in Table 1. Amplification was performed using the following thermocycler conditions: 95 °C for 5 min; 35 cycles of 95 °C for 15 s, 60 °C for 15 s, and 72 °C for 1 min; followed by a final extension at 72 °C for 5 min.